Aus dem Zentrum für Innere Medizin
der Universität zu Köln
Klinik und Poliklinik für Innere Medizin II der Universität zu Köln
Direktor: Universitätsprofessor Dr. med. Th. Benzing

Ciliary and Nuclear Characterization of NPHP9 (NEK8) and NPHP10 (SDCCAG8) Proteins in the Context of Nephronophthisis

Inaugural-Dissertation zur Erlangung der Doktorwürde
der Medizinischen Fakultät
der Universität zu Köln

vorgelegt von
Bijan Baten
aus Düsseldorf

promoviert am 11. September 2025

Gedruckt mit Genehmigung der Medizinischen Fakultät der Universität zu Köln
2025

Dekan: Universitätsprofessor Dr. G. R. Fink

1. Gutachter: Professor Dr. med. B. Schermer
2. Gutachter: Universitätsprofessor Dr. rer. nat. A. Wodarz

Erklärung

Ich erkläre hiermit, dass ich die vorliegende Dissertationsschrift ohne unzulässige Hilfe Dritter und ohne Benutzung anderer als der angegebenen Hilfsmittel angefertigt habe; die aus fremden Quellen direkt oder indirekt übernommenen Gedanken sind als solche kenntlich gemacht.

Bei der Auswahl und Auswertung des Materials sowie bei der Herstellung des Manuskriptes habe ich Unterstützungsleistungen von folgenden Personen erhalten:

Herr Prof. Dr. Bernhard Schermer
Frau Dr. Gisela Slaats

Weitere Personen waren an der Erstellung der vorliegenden Arbeit nicht beteiligt. Insbesondere habe ich nicht die Hilfe einer Promotionsberaterin/eines Promotionsberaters in Anspruch genommen. Dritte haben von mir weder unmittelbar noch mittelbar geldwerte Leistungen für Arbeiten erhalten, die im Zusammenhang mit dem Inhalt der vorgelegten Dissertationsschrift stehen.

Die Dissertationsschrift wurde von mir bisher weder im Inland noch im Ausland in gleicher oder ähnlicher Form einer anderen Prüfungsbehörde vorgelegt.

Die in dieser Arbeit angegebenen Experimente sind nach entsprechender Anleitung durch Frau Dr. Gisela Slaats von mir selbst ausgeführt worden.

Das dieser Arbeit zugrunde liegende Experiment der Massenspektrometrie (3.18) ist von mir mit Unterstützung von Frau Dr. Gisela Slaats und der medizinisch-technischen Assistentin Frau Ruth Herzog durchgeführt worden. In der Proteomics Facility des CECAD Cologne erfolgte die bioinformatische Prozessierung von Datensätzen durch Herrn Dr. rer. nat. Christian Freese.

Das dieser Arbeit zugrunde liegende Experiment „PamGene“ (3.20) wurde analysiert durch Dr. Savithri Rangarajan, PamGene International B.V. Die Datensätze wurden von mir interpretiert.

Erklärung zur guten wissenschaftlichen Praxis:

Ich erkläre hiermit, dass ich die Ordnung zur Sicherung guter wissenschaftlicher Praxis und zum Umgang mit wissenschaftlichem Fehlverhalten (Amtliche Mitteilung der Universität zu Köln AM 132/2020) der Universität zu Köln gelesen habe und verpflichte mich hiermit, die dort genannten Vorgaben bei allen wissenschaftlichen Tätigkeiten zu beachten und umzusetzen.

Köln, den 29.04.2025

Unterschrift: .....

Danksagung

Diese Arbeit wäre ohne die großzügige Bereitstellung der Räumlichkeiten und idealen Arbeitsbedingungen im Nephrologischen Forschungslabor der Uniklinik Köln durch Prof. Dr. Thomas Benzing nicht möglich gewesen. Hierfür möchte ich mich ausdrücklich bedanken.

Ein großer Dank gilt zudem meinem Doktorvater, Prof. Dr. Bernhard Schermer, für seine Begeisterung für sein Fach und die wertvollen Anregungen zu meiner Arbeit. Meiner Betreuerin, Dr. Gisela Slaats, danke ich für ihre kontinuierliche und motivierende Unterstützung. Durch sie konnte ich viele molekularbiologische Methoden erlernen, die mein wissenschaftliches Verständnis erweitert haben. Ebenso bedanke ich mich bei Dr. Lena Ebert, die mit ihren Anregungen meine Arbeit vorangebracht hat. Mein Dank gilt außerdem den immer hilfsbereiten Kollegen des Nephrologischen Forschungslabors. Besonders hervorheben möchte ich Dervla Reilly und Janna Bredow, mit denen sich über die Jahre eine enge Freundschaft entwickelt hat.

Von Herzen danke ich meiner Familie, besonders meiner Mutter, sowie meinen Freunden für ihre stetige Unterstützung während meines Studiums und der Doktorarbeit.

Meiner Familie.

Table of Contents

Abbreviation List

AcTub ..... *Acetylated tubulin*
ADPKD ..... *Autosomal dominant polycystic kidney disease*
ANKS6 ..... *Ankyrin repeat and sterile alpha motif domain containing 6*
aPKC ..... *atypical protein kinase C*
APS ..... *Ammonium persulfate*
ARL13B ..... *ADP-ribosylation factor-like protein 13B*
ARPKD ..... *Autosomal recessive polycystic kidney disease*
ATM ..... *Ataxia-telangiectasia mutated*
ATP ..... *Adenosine triphosphate*
ATR ..... *ATM- and Rad3-related*
AurA ..... *Aurora-A*
BBS ..... *Bardet-Biedl syndrome*
BCA ..... *Bicinchoninic acid*
BSA ..... *Bovine serum albumin*
cAMP ..... *Cyclic adenosine monophosphate*
CCD ..... *Cortical collecting duct*
cDNA ..... *Complementary DNA*
CDS ..... *Coding sequence*
CEP164 ..... *Centrosomal protein of 164 kDa*
CHK ..... *Checkpoint kinase*
CMV ..... *Cytomegalovirus*
CTGF ..... *Connective tissue growth factor*
DAPI ..... *4',6-diamidino-2-phenylindole*
DCT ..... *Distal convoluted tube*
DDR ..... *DNA damage response*
DMEM ..... *Dulbecco´s Modified Eagle Medium*
DNA ..... *Deoxyribonucleic acid*
DSB ..... *Double strand break*
DTT ..... *Dithiothreitol*
EGTA ..... *Ethylene glycol bis(2-aminoethyl)tetraacetic acid*
EMT ..... *Epithelial-mesenchymal transition*
ESRD ..... *End-stage renal disease*
EXO1 ..... *Exonuclease 1*
FACS ..... *Fluorescent activated cell sorting*
FBS ..... *Fetal bovine serum*
FITC ..... *Fluorescein isothiocyanate*
FRT ..... *Flippase recognition target*
GC content ..... *Guanine-cytosine content*
GFP ..... *Green fluorescent protein*
Gli ..... *Glioma-associated oncogene transcription factors*
GLIS2 ..... *GLIS Family Zinc Finger 2*
HDAC6 ..... *Histone deacetylase 6*
HEK ..... *Human embryonic kidney*
HEPES ..... *N-(2-Hydroxyethyl)piperazine-N'-(2-ethanesulfonic acid)*
HRP ..... *Horseradish peroxidase*
hTERT-RPE1 *human telomerase reverse transcriptase immortalized retinal pigment epithelial cells 1*
iBAQ ..... *intensity-based absolute quantification*
IFT ..... *Intraflagellar transport*
INVS ..... *Invasin*
IP *Immunoprecipitation*
JBS ..... *Joubert syndrome*
jck ..... *Juvenile cystic kidney*

JNK3 ..... *c-Jun N-terminal kinase 3*
LATS1 ..... *Large tumor suppressor kinase 1*
LB ..... *Lysogeny broth*
MAPK10 ..... *Mitogen-activated protein kinase 10*
MEF ..... *Mouse embryonic fibroblasts*
mIMCD3 ..... *Mouse inner medullary collecting duct-3*
MKS ..... *Meckel-Syndrome*
M-PER ..... *Mammalian protein extraction reagent*
mRNA ..... *Messenger ribonucleic acid*
MT ..... *Microtubule*
NDS ..... *Normal donkey serum*
NEB ..... *New England Biolabs*
NEK8 ..... *Never In Mitosis Gene A- Related Kinase 8*
NFκB ..... *Nuclear factor-κB*
NGS ..... *Next generation sequencing*
NPH, NPHP ..... *Nephronophthisis*
OFD ..... *Oro-facial-digital syndrome*
PAGE ..... *Polyacrylamide gel electrophoresis*
PAM ..... *Protospacer adjacent motif*
Pard6b ..... *Partitioning defective 6 homolog beta*, *Partitioning defective 6 homolog beta*
PBS ..... *Phosphate buffered saline*
PC ..... *Polycystin*
PCM1 ..... *Pericentriolar material 1*
PCR ..... *Polymerase chain reaction*
PDGF ..... *Platelet-derived growth factor*
Pen/Strep ..... *Penicillin-Streptomycin*
PFA ..... *Paraformaldehyde*
PI3K ..... *Phosphoinositide 3-kinase*
PIM ..... *Proteases inhibitor mix*
PKD ..... *Polycystic kidney disease*
PKG1 ..... *cGMP dependent protein kinase 1*
PKHD1 ..... *Polycystic kidney and hepatic disease 1*
PMSF ..... *Phenylmethylsulfonyl fluoride*
PNK ..... *Polynucleotide kinase*
PRKCI ..... *Protein kinase C iota type*, *Protein kinase C iota type*
PRKX ..... *Protein kinase X*
PVDF ..... *Polyvinylidene fluoride*
qPCR ..... *quantitative PCR*
RAB2 ..... *RAB GTPase binding effector protein 2*
Rab34 ..... *Ras-related protein Rab-34*
RBPJ ..... *Recombination signal binding protein for immunoglobulin kappa J region*
RCC1 ..... *Regulator of Chromosome Condensation 1*
RIPA ..... *Radioimmunoprecipitation Assay*
RNA ..... *Ribonucleic acid*
RT Buffer ..... *Reverse Transcription Buffer*
SAP ..... *Shrimp alkaline phosphatase*
SC35 ..... *Serine/arginine-rich splicing factor 2*
SDCCAG8 ..... *Sonic Hedgehog Signaling and Ciliogenesis Regulator 8*
SDS ..... *Sodium dodecyl sulfate*
sgRNA ..... *single guide RNA*
SLS ..... *Senior-Løken syndrome*
SNP ..... *single nucleotid polymorhpism*
SOC ..... *Super optimal broth*
STAT6 ..... *Signal transducer and activator 6*
STK ..... *Serine/threonine kinase*
TAE ..... *Tris-acetate-EDTA*

TAZ ..... *WW-domain-containing transcription regulator 1*
TEMED ..... *Tetramethylethylendiamine*
TGF-β..... *Transforming growth factor β*
TIP60 ..... *Tat-interactive protein 60*
Wnt..... *Wingless-related integration site*
WT ..... *Wild type*
YAP ..... *Yes-associated protein 1*
ZNF423 ..... *Zinc finger protein 423*

1 Summary

1.1 English Summary

Nephronophthisis (NPH) is an autosomal recessive kidney disease with renal cysts and fibrotic degeneration of the kidney as hallmarks. These changes lead to a progressive loss of kidney function. NPH is the most common monogenetic cause of end-stage kidney failure before the age of 30 with dialysis or kidney transplantation as the only therapeutic options. NPH belongs to the family of renal ciliopathies, as it is caused by pathogenetic variants in the NPHP genes (NPHP 1-20), which encode proteins localized to primary cilia. Cilia are antennae-like, sensory organelles present on the apical surface of tubular epithelial cells, from where they project into the tubular lumen.

In the present work, we studied the function of two NPH proteins, Serologically defined colon cancer antigen 8 (SDCCAG8; NPHP10) and Never in mitosis gene A (NIMA)-related kinase-8 (NEK8; NPHP9) and aimed to understand how their loss might affect the signaling of tubular cells. First, we aimed to overexpress the two proteins SDCCAG8 and NEK8 with a Flag or GFP tag in mouse kidney cells using a single-copy integration system. Both confocal microscopy and immunoblotting could not confirm localization and expression. In the second approach, we used Crispr/Cas9-mediated genome editing to create knockout cell lines (KO) of the *SDCCAG8* and *NEK8* genes, respectively. Four cell lines with *SDCCAG8*-KO and one cell line with *NEK8*-KO were successfully established. These KOs were validated by DNA sequencing and quantitative polymerase chain reaction (qPCR). Moreover, we successfully generated interactomes for NEK8 and SDCCAG8 by transiently transfecting the KO cells with the proteins of interest. Moreover, we performed a kinase activity screen, through which numerous differences in kinase activities and signaling pathways could be identified between wild-type and NEK8- or SDCCAG8- deficient cells.

Taken together, despite the fact that SDCCAG8 and NEK8 are very low-abundant proteins, their loss has significant effects on cellular signaling networks and pathways. Our findings might contribute to the understanding of signaling pathways and kinase activities altered in NPH. They could help to unravel not only the function of SDCCAG8 and NEK8 proteins in signaling networks but also the disease-causing pathophysiology underlying fibrosis, cyst formation, and cell death. A more detailed understanding of these mechanisms will be essential for establishing suitable future therapeutic strategies for kidney diseases.

1.2 German Summary

Nephronophthise (NPH) ist eine autosomal-rezessive Nierenerkrankung, die durch Zystennieren und fibrotische Degeneration der Niere gekennzeichnet ist. Die NPH ist die häufigste genetische Ursache für chronisches Nierenversagen vor dem 30. Lebensjahr. Dialyse oder Nierentransplantation stellen derzeit die einzigen verfügbaren therapeutischen Optionen dar. Die NPH gehört zur Familie der renalen Ziliopathien. Sie wird verursacht durch pathogenetische Varianten in den NPHP-Genen (NPHP 1-20), die für Proteine in primäre Zilien kodieren. Zilien sind sensorische Organellen an der apikalen Oberfläche von Tubulusepithelzellen, welche in der Chemo- und Mechanotransduktion der Zelle sowie im Zellzyklus eine maßgebliche Rolle spielen.

In der vorliegenden Arbeit wurde die Funktion zweier NPH-Proteine, des Serologically defined colon cancer antigen 8 (SDCCAG8; NPHP10) und der NIMA Related Kinase 8 (NEK8; NPHP9) studiert. Das Hauptaugenmerk lag darauf, zu untersuchen, wie sich der Verlust dieser Proteine auf die Biologie und Signaltransduktion von Tubuluszellen auswirkt.

Zunächst wurden SDCCAG8 und NEK8 mit einem Flag- oder GFP-Tag in Nierenzellen der Maus mit Hilfe eines Single-Copy-Integrationssystems überexprimiert. Sowohl konfokale Mikroskopie als auch Western Blotting konnten jedoch die korrekte Lokalisierung und Expression nicht bestätigen.

In einem zweiten Ansatz verwendeten wir die CRISPR/Cas9-Methode, um stabile Knockout-Zelllinien (KO) der Gene *SDCCAG8* und *NEK8* zu generieren. Vier Zelllinien mit *SDCCAG8*-KO und eine Zelllinie mit *NEK8*-KO wurden erfolgreich etabliert. Diese wurden durch DNA-Sequenzierung und quantitative Polymerase-Kettenreaktionen (qPCR) validiert. Darüber hinaus haben wir erfolgreich Interaktome für NEK8 und SDCCAG8 erstellt, indem wir KO-Zellen mit den jeweiligen Genen transfiziert haben. Weiterhin führten wir ein Kinase-Aktivitäts-Screening der KO-Zellen durch, bei dem zahlreiche Unterschiede in den Kinase-Aktivitäten und Signalwegen zwischen Wildtyp- und NEK8- oder SDCCAG8-defizienten Zellen identifiziert wurden.

Trotz der niedrigen Proteinexpression von SDCCAG8 und NEK8 zeigen deren Verluste signifikante Auswirkungen auf zelluläre Signalwege. Die in dieser Arbeit vorgelegten Ergebnisse tragen dazu bei, die Funktion von SDCCAG8 und NEK8 in Signalnetzwerken zu entschlüsseln und die krankheitsverursachende Pathophysiologie, die mit Fibrose, Zystenbildung und Zelltod in Zusammenhang steht, besser zu verstehen. Ein detailliertes Verständnis dieser Mechanismen wird für die Entwicklung geeigneter künftiger therapeutischer Strategien für Nierenkrankheiten von entscheidender Bedeutung sein.

2 Introduction

This thesis focusses on nephronophthisis (NPH), a genetic renal disease arising from dysfunction of primary cilia. Primary cilia are microtubule-based organelles that protrude from almost all cell types.[1] They are involved in several cellular processes, such as chemosensation, mechanotransduction, and cell cycle control. Cilia were largely neglected in biomedical science for many decades.[2] As primary cilia are non-motile organelles, scientists considered them less important than motile cilia. However, mutations of genes encoding proteins localizing to the primary cilium cause a group of diseases called “ciliopathies”. Scientists have not yet thoroughly understood how primary cilia function physiologically and what happens if the protein-encoding genes mutate. Internalizing this is crucial to understanding associated diseases, like NPH.

2.1 Ciliary structure and biology

Primary cilia emerge from almost all cell surfaces after exit from the mitotic cell cycle in G1 and G0 phase.[3] They consist of a basal body, which derives from the mother centriole and anchors a microtubule (MT) axoneme with a 9x2+0 structure of nine MT doublets without a central pair of MT (Fig. 1).[4] This complex is surrounded by the ciliary membrane, which is involved in cellular signaling pathways and is distinct from the normal cell membrane.[5,6] The transition zone, formed by transition fibers located between the basal body and the ciliary membrane, regulates the protein composition of cilia.[7] Ciliary protein trafficking is a highly regulated process facilitated by intraflagellar transport (IFT). This mechanism relies on specific motor proteins, namely kinesin-2 as the motor protein for anterograde transport to the tip of the axoneme and cytoplasmic dynein-2 for retrograde transport to the ciliary base (Fig. 1).[8]
Primary cilia are fundamental for cellular and organ development and cellular homeostasis.[9,10]
Ciliary functions can be subdivided into two main actions.
Firstly, primary cilia function as sensory organelles capable of detecting both mechanical and chemical stimuli originating from the extracellular environment and transducing these signals into the cell.[11] Ciliary receptors bind ligands and initiate signal cascades. They contain receptors and effectors for Hedgehog, platelet-derived growth factor (PDGF), wingless-related integration site (Wnt) and many other signaling cascades.[2] The Sonic Hedgehog pathway (Shh) plays a crucial role in the development of mammalian organs and tissues and exhibits pathogenic dysregulation in ciliopathies and various cancer types.[12] Primary cilia are also known to regulate planar cell polarity, which is important for tissue integrity in the kidney and related to Wnt signaling.[13] Some proteins associated with cilia or ciliopathies control cell proliferation and are involved in DNA damage repair signaling.[14,15]

Secondly, cilia are involved in cell cycle regulation, since the basal body needs to be released before mitotic cell division. Thus, before reentering the cell cycle, cilia have to be disassembled. This is mediated by Aurora-A kinase (AurA) which is activated upon Ca^{2+} signaling.[16] The enzyme histone deacetylase 6 (HDAC6) becomes phosphorylated and activated by AurA. HDAC6 then deacetylates axonemal α-tubulin which leads to destabilization of MTs and promotes the disassembly of the primary cilium.[17] After disassembly, centrioles are duplicated and form the spindle poles during cell division.[18] Upon cell division, each mother centriole of the daughter cells is again used to form a basal body and to promote ciliogenesis.

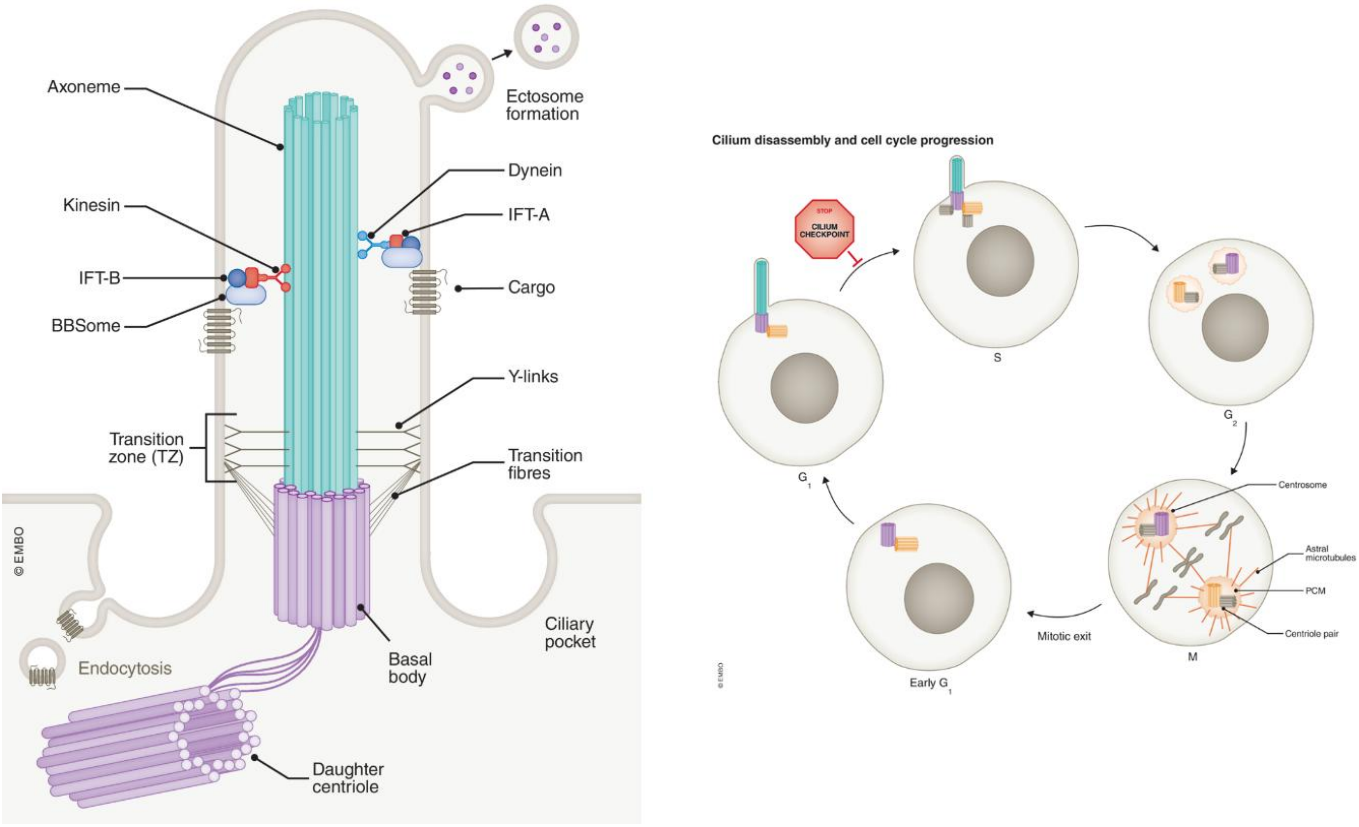

Figure 1: A) Ciliary structure and connection to the cell. (B) Cilia assembly and disassembly during cell cycle.

A) Cilia consist of a 9x2+0 microtubule axoneme, a ciliary membrane and are anchored to the cell by its basal body, made up by a mother centriole. In this graphic, ciliary transport by kinesin-2 (antegrade) and dynein-2 (retrograde) is illustrated. With this transport, cilia obtain proteins produced in the cell. B) Cilia are disassembled during mitosis and reassembled during G1 phase. Figure from [19].

Source: Reproduced with permission from Gopalakrishnan J, Feistel K, Friedrich BM, et al. *Emerging principles of primary cilia dynamics in controlling tissue organization and function.* EMBO J. © 2023

2.2 Ciliopathies

Cilia are essential sensory organelles that connect cells with their environment and regulate diverse cellular processes. Thus, it is conceivable that mutations leading to dysfunctional ciliary signaling affect multiple tissues. Indeed, defects in primary cilia cause clinically heterogenous disorders subsumed under the term "ciliopathies".[20]
Upon individual assessment of each ciliopathy, their classification as rare diseases becomes evident, e.g., Bardet-Biedl syndrome with an estimated incidence of 1:160 000 in northern Europe.[21] A more frequent ciliopathy is autosomal dominant polycystic kidney disease (ADPKD) with a prevalence between 1:500 and 1:2000.[22,23] Ciliopathies in general are associated with (poly)cystic kidney disease, retinal degeneration, liver fibrosis, mental impairment, infertility, bone changes, situs inversus, diabetes and obesity (Fig. 2).[24]
Ciliopathies can be classified by their modes of inheritance. Dominantforms include ADPKD and von-Hippel-Lindau disease, an inherited tumor syndrome.[25] ADPKD is one of the most common genetic diseases, caused by mutations in polycystic kidney disease 1 (*PKD1)* or 2 (*PKD2)* genes.[26]
On the other hand, there are several recessively inherited ciliopathies, including autosomal recessive polycystic kidney disease (ARPKD) with an incidence between 1:10.000 and 1:40.000.[27] NPH, Meckel-Gruber syndrome, Joubert syndrome, Jeune syndrome, Bardet-Biedl syndrome (BBS), Senior-Løken syndrome (SLS) or Oro-facial-digital syndrome (OFD) are also recessively inherited ciliopathies.
Some of these diseases show a multisystemic involvement, like cardiac pathologies, skeletal abnormalities, neurological disorders and retinal degeneration [e.g. Senior-Løken-Syndrome (Fig. 2)][28,29] with the kidney most commonly affected.
In all ciliopathies, mutations in the same genes can lead to a wide range of disease severity and organ involvement.[30] Mutations in NPH-associated genes mostly cause a fibrotic cystic phenotype, with small cysts in about 50% of the cases, while mutations in *PKD1* and *PKD2* predominantly cause a cystic phenotype.[24] A study by Bukanov et al., in which application of a cyclin-dependent kinase (CDK) inhibitor ameliorated kidney cysts, confirmed that impaired cell cycle regulation by ciliary proteins is causing cystogenesis.[31]

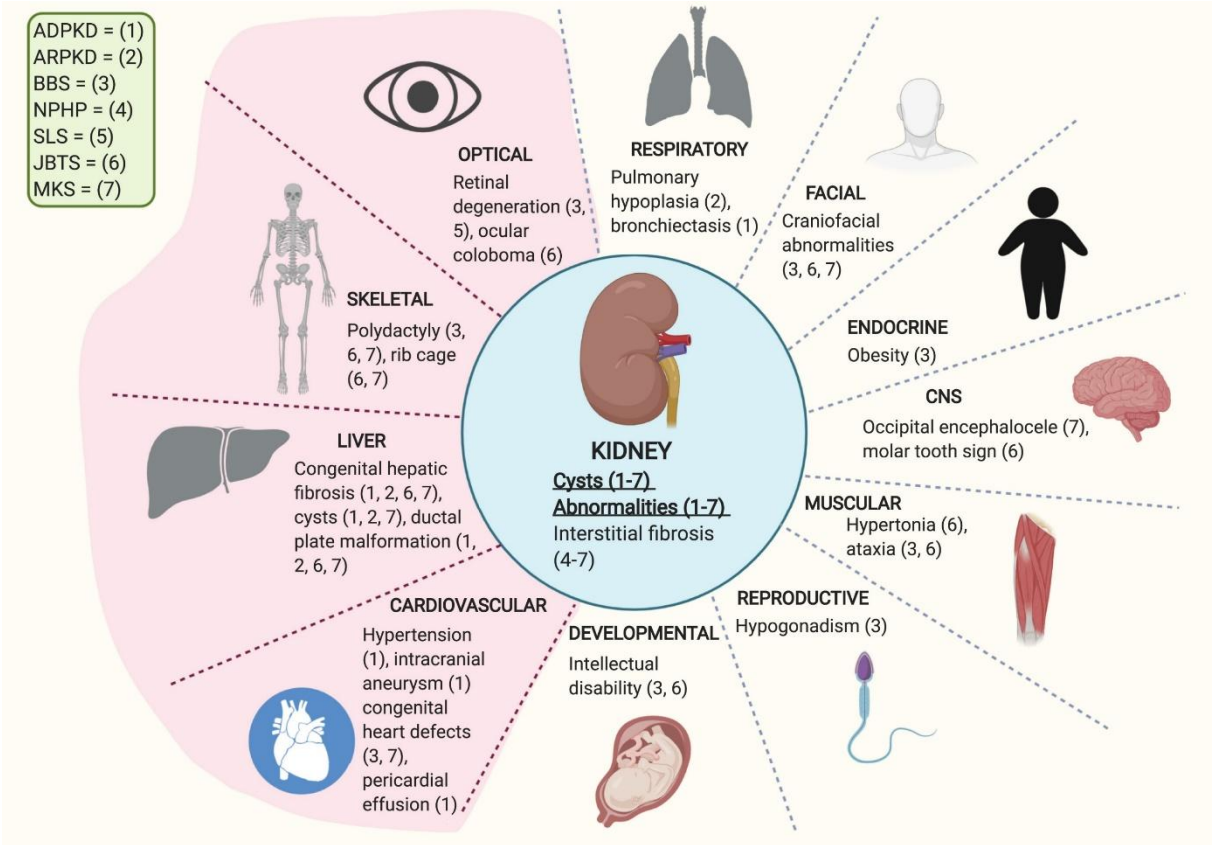

Figure 2: Overview of involvement of organ systems in NPH, NPH-related syndroms, ADPKD and ARPKD.

Primary involvement is shown in pink, secondary involvement is not highlighted. 1: autosomal dominant polycystic kidney disease (ADPKD), 2: autosomal recessive polycystic kidney disease (ARPKD), 3: Bardet-Biedl-Syndrome (BBS), 4: Nephronophthisis (NPHP), 5: Senior-Løken-Syndrome (SLS), 6: Joubert-Syndrome (JBS), 7: Meckel-Syndrome (MKS). A wide range of organ systems can be affected by ciliopathies because primary cilia emerge from almost all cell types in the living organism.

Source: McConnachie DJ, Stow JL, Mallett AJ. *Ciliopathies and the Kidney: A Review.* Am J Kidney License: © 2021 Elsevier. Published under the Creative Commons CC BY-NC-ND 4.0 License (https://creativecommons.org/licenses/by-nc-nd/4.0/).[32]

2.3 Nephronophthisis (NPH)

Nephronophthisis (NPH) is the most common genetic cause of end-stage renal failure until the age of 30 years.[33] The name originates from Greek: “nephron” – kidney, “phthisis” – loss = kidney/nephron loss.[34] NPH is caused by mutations in one of over 20 identified NPHP genes that encode proteins localizing to the primary cilium.[35] The most common mutation in about 20% of all NPH cases is found in the NPHP1 gene.[30] Around 70% of the disease-causing genes have not yet been discovered.[36] New sequencing methods, like Next Generation Sequencing (NGS), have accelerated the discovery of new genes.[35] Inconsistent data exist on the incidence of NPH, varying between 1:1.000.000 in the USA and 1:50.000 in Canada.[33] Differentiation is made between infantile, juvenile, adolescent, and the recently characterized adult onset of NPH.[37]

Clinically, the infantile form shows an oligohydramnion sequence in utero (limb contracture, pulmonary hypoplasia, facial dysmorphisms) or renal failure in the first years of life.[38,39] End-stage renal disease (ESRD) follows before the age of five.[40]The juvenile form is marked by polydipsia, polyuria (differential diagnostic: diabetes mellitus type 1), growth retardation and chronic iron-resistant anemia.[41] The median age of chronic kidney failure is 13 years.[42] In the adolescent form, similar to juvenile disease, ESRD occurs at a median age of 19 years.[43] Here, the interval between the onset of symptoms and ESRD is about four years.[44]

The most important diagnostic tool is the kidney ultrasound alongside classic findings and genetic testing.[41] The NPH kidney is macroscopically smaller than, or as big as, the healthy kidney.[45] It presents with renal cysts at the usually less differentiated corticomedullary border.[41] Histological findings are tubulointerstitial fibrosis and thickened, disrupted tubular basement membrane.[41] NPH is treated symptomatically, mainly by antihypertensive drugs and, in advanced stages, dialysis or kidney transplantation.[30] NPH geneticallly and phenotypically overlaps if a number of other ciliopathies, summarized as NPH-related ciliopathies (NPH-RC). These include, amongst others, SLS, Joubert syndrome, BBS and Meckel-Gruber syndrome which have been mentioned in 2.2.[30]

2.4 Kidney fibrosis & cystogenesis

Fibrosis is characterized by an increase of extracellular matrix leading to the loss of functional tissue. This pathology can occur in almost all organs. Kidney fibrosis is common in chronic kidney disease, kidney cancer, and hereditary kidney diseases, like ADPKD and NPH.[46,47]

Chronic tissue damage results in monocyte activation and liberation of cytokines, creating a pro-inflammatory environment and resulting in fibrosis.[48] Mechanistically, it comes to an augmentation of fibroblasts and to epithelial-to-mesenchymal transition (EMT). EMT is the transition from epithelial into mesenchymal cells, causing a loss of their physiological function.[49] Transforming growth factor β (TGF-β), a pivotal factor in the development of kidney fibrosis, incites EMT.[50] TGF-β is both an inflammatory and anti-inflammatory cytokine with important physiological functions.[51] Other profibrotic mediators are, among others, angiotensin II, connective tissue growth factor (CTGF) and interleukins (IL) like IL-1.[52,53] IL-4 contributes to fibrosis by increasing the production of collagen.[54] It activates signal transducer and activator of transcription 6 (STAT6) protein[55], which has been linked to fibrosis in liver and lung, and its loss reduces collagen accumulation in mice with obstructive nephropathy[56-58].

Recently, Li et al. linked mTORC2 signaling to kidney fibrosis by showing that mTORC2 becomes activated by TGF-β1.[59] This results in the activation of protein kinase B (Akt), which has a branch of downstream effects leading to cell survival and proliferation and is also associated with malignant transformation.[60] This was supported by the finding that Akt

activates nuclear factor-κB (NFκB), which is fundamentally involved in inflammatory cell responses, anti-apoptotic mechanisms, carcinogenesis and fibrosis.[61,62]

Stewart et al. found that Shh signaling is overactive in lung fibrosis, liver fibrosis and kidney fibrosis.[63-65] When this pathway is overactive, it causes increased levels of glioma-associated oncogene transcription factors (Gli), which result in the transcription of genes linked to proliferation and carcinogenesis.[66]

2.5 NEK8 (NPHP9)

The *NEK8* gene, also called *NPHP9,* is localized on chromosome 17q11.2 and encodes for a protein with a size of 692 amino acids and a weight of approximatey 75 kDa.[67] NEK8 is a serine-threonine kinase involved in various signaling pathways, DNA replication and cell-cycle regulation.

It consists of an N-terminal kinase domain and five C-terminal Regulator of Chromosome Condensation 1 (RCC1) repeat domains and is one of the eleven human Never in Mitosis gene A (NIMA) proteins.[68] NEK8 localizes both to the centrosomes and to the proximal region of the cilium.[69] Mutations in the *NEK8/NPHP9* gene mostly cause NPH following an autosomal recessive mode of inheritance.[68,70] Recently, a study by Claus et al. described an autosomal dominant form of PKD caused by specific heterozygous *NEK8* mutations.[71]

In the primary cilium, NEK8 is found at the proximal region at the inversin (INVS) compartment together with INVS/NPHP2, NPHP3 and Ankyrin repeat and sterile alpha motif domain (ANKS6)/NPHP16.[72,73] Mutations in genes encoding for these proteins lead to nephronophthisis. The INVS compartment and in particular inversin encoded by INVS/NPHP2 also plays an important role in the determination of the left-right axis.[74]

NEK8 modulates the expression of Polycystin-1 (PC1) and Polycystin-2 (PC2) and their ciliary localization. NEK8 mutant mice have increased expression of both PC1 and PC2 leading to enhanced cell proliferation.[75] In addition, Polycystin-1 and NEK8 regulate cystogenesis in a similar manner.[76] Compound heterozygous mutations in *NEK8 / PKD1* intriguingly lead to a more severe cystic phenotype than *NEK8 / PKD1* mutations alone.[76] In the juvenile cystic kidney disease (jck) mouse model, in which *NEK8* carries a point mutation, NEK8 protein localizes randomly to the entire cilium. Furthermore, NEK8 loss causes longer cilia and increased PC proteins, hinting to its regulative function for PC proteins inside the primary cilium.[72]

NEK8 has also been described as a genome maintenance factor that plays a pivotal role in replication stress and is involved in the ATM- and Rad3-related (ATR) kinase-mediated replication stress response.[77] Together with ATR and checkpoint kinase (CHK), it negatively influences CDK activity in healthy tissue. An indicator of higher CDK activity was the discovery that CDK inhibitors ameliorate cyst formation in juvenile cystic kidney (jck) mice.[78] Further, in

NEK8 depleted mouse embryonic fibroblasts (EF), DNA replication becomes notably less efficient in conditions of cellular stress, leading to DNA double-strand breaks. This arises from a combination of reduced replication fork speed and decreased fork stability.[77]

An additional noteworthy observation is that NEK8 interacts with Hippo effector WW-domain-containing transcription regulator 1 (also known as TAZ) and activates it.[79] In this pathway, large tumor suppressor kinase 1 (LATS1) physiologically phosphorylates YAP/TAZ and, thereby, inhibits nuclear translocation and action of YAP/TAZ as transcriptional factors.[80] In NEK8 deficient cells, yes-associated protein 1(YAP) seems to be imbalanced, accounting for pathological changes in morphogenesis.[68] Grampa et al. demonstrated that Verteporfin, a specific inhibitor of YAP transcriptional activity, could undo the morphogenesis effects in NEK8 knockdown mice.[68]

Recent studies have shown that NEK8 is overexpressed in some forms of breast cancer, emphasizing its proliferative effects when it is dysregulated.[67] Another function of NEK8 has been observed in the embryonic phase, where its loss perturbates left-right asymmetry development and leads to cardiac anomalies and glomerular kidney cysts.[70,81]

2.6 SDCCAG8 (NPHP10)

SDCCAG8 (serologically defined colon cancer antigen 8), also called *NPHP10*, is a gene located on chromosome 1q43-44 which contains 18 exons.[82] It encodes for the protein SDCCAG8, which has a size of 713 amino acids and a weight of approximately 82,5 kDa.[83] SDCCAG8 protein has an N-terminal globular domain and a C-terminal coiled-coil domain.[83] Cellular localizations of the protein are the centrosomes during the cell cycle and the basal body of cilia.[84] It can be detected in the kidney, lung epithelium, retina, and (rat) spermatocytes.[84] Colocalizations at the centrosome were described with ninein (a marker of the centrosomal appendage), oro-facial-digital syndrome 1 protein (OFD1) and NPHP5, of which the latter two are also ciliopathy-causing genes.[82]

Mutations in *SDCCAG8* are linked to NPH phenotypes. *SDCCAG8 gt/gt* mice display kidney cysts, predominantly in the cortical collecting duct (CCD) and in the distal convoluted tube (DCT), surrounded by fibrosis.[84] In the retina, SDCCAG8 is responsible for photoreceptor preservation.[84] Its loss leads to retinal degeneration and blindness primarily due to cone cell loss. There is a plethora of divergent observations concerning the formation of cilia in SDCCAG8-lacking cells. Airik et al. observed that *SDCCAG8 gt/gt* mice have cystic kidneys but not any global ciliary defects.[84] Cell culture studies with human telomerase reverse transcriptase immortalized retinal pigment epithelial cells (hTERT-RPE1 cells) treated with siSDCCAG8 meanwhile showed deficient ciliary formation.[85] Previous studies show that RAB GTPase binding effector protein 2 (RAB2)-lacking cells do not form cilia and that loss of SDCCAG8 results in the absence of RAB2.[85] Therefore, RAB2 regulates ciliogenesis and

SDCCAG8 is involved in the correct localization of RAB2 to the cilia.[85] As RAB2 is involved in protein trafficking from the cytoplasm into the cilia, the interaction of SDCCAG8 with RAB2 and other “vesicle transport components”[85] hints to a function of SDCCAG8 in protein trafficking.

Further investigations revealed that the pericentriolar material 1 (PCM1) protein involved in targeting proteins to the centrosome interacts with SDCCAG8.[86] SDCCAG8 is involved in the organization of microtubules (MT), which are crucial for the connection between nucleus and centrosome and important for neuronal migration.[86,87] SDCCAG8 is a regulator of migration in the developing mouse cortex and its loss hampers neuronal migration.[86] Some of the clinical manifestations, namely mental impairment and schizophrenia, are explained by neuronal migration defects.

Colocalizations of SDCCAG8 with DDR proteins tat-interactive protein 60 (TIP60), serine/arginine-rich splicing factor 2 (SC35), centrosomal protein of 164 kDa (CEP164), and zinc finger protein 423 (ZNF423) were demonstrated at the nucleus.[88] Registration of DNA damage is sensed by upstream components of the DDR complex, amongst others ataxia-telangiectasia mutated (ATM) and ATR. One of the cellular responses is the shift of a range of proteins into the nucleus, which repair the DNA or induce apoptosis.[88,89] The involvement in DDR was also illustrated by increased yH2AX-levels and ATM pathway activation in *Sdccag8*-KO cells.[84] yH2AX is a highly sensitive DNA damage marker, as it is phosphorylated upon double-strand breaks (DSB) by ATM and then initiates DDR, for example, by recruiting DSB repair proteins.[90] All in all, those studies show that SDCCAG8 plays a crucial role in DNA damage response (DDR).

Recently, SDCCAG8 mutations were discovered in individuals with SLS and BBS by whole exome sequencing.[82]

2.7 Aims of the thesis

The overarching goal of this project was to gain novel insights into the functions of the NPHP proteins NEK8/NPHP9 and SDCCAG8/NPHP10 to better understand the role of the proteins in tubular cells and NPH disease, especially in fibrosis and cyst formation. Furthermore, investigations were carried out to find and comprehend new signaling pathways and networks that might contribute to fibrosis, cystogenesis and apoptosis, considering that especially fibrosis is a pathophysiologic component in many known diseases.

To this end, one of the main aims was to generate cell lines with single copy integration of cDNA of both genes to characterize the ciliary localization of NEK8 and SDCCAG8 in mouse inner medullary collecting duct (mIMCD3) cells.

In addition, we aimed to establish stable *NEK8*- and *SDCAAG8*-KO cell lines through the CRISPR/Cas9 technology to investigate their function in tubular epithelial cells. The validation of the cell lines was done by Sanger sequencing and qPCR. The cells were used to screen for altered kinase activity and to perform protein interaction studies using MS/MS. We aimed to understand how cell signaling was altered upon loss of NEK8 or SDCCAG8 and to study the composition of protein complexes of both targets.

By investigating both the overexpression and the KO of the genes of interest *NEK8* and *SDCCAG8*, we hoped to reveal differences between WT and modified cells regarding ciliary environment, protein interactors, and cellular signaling. Ultimately, we aimed to discover potential new key pathways underlying the pathogenesis of NPH.

3 Material and Methods

3.1 Cell culture

All cell culture work was carried out under sterile conditions under a fume hood. Twenty minutes before splitting cells, the cell-type specific medium was placed into a 37°C water bath. Prior to every work in cell culture, the hood was cleaned with 70% ethanol and the vacuum pump was flushed with 1% Incidin. The medium bottle and the trypsin bottle were cleaned with 70% ethanol and placed under the hood. The confluency (ideally 80%) of the 10 cm cell dishes was observed under the microscope. Then, the medium was aspirated and the cells were washed with 10 mL phosphate buffered saline (PBS). After removal of PBS, 1 mL of Trypsin was added and the cells were incubated at 37°C for 3 to 5 minutes. During this time, a new 10 cm dish was labelled (name, date, cell type, passage number, splitting ratio) and filled with 8 to 10 mL of fresh medium (depending on the splitting ratio). After incubation of cells with trypsin, cell detachment from the dish was checked. Cells were then resuspended in fresh medium and transferred to the prepared new dish using a sterile stripette. The split cells were stored in the incubator and the old dishes were trashed and autoclaved. In the end, the working area was cleaned again with 70% ethanol and the vacuum pump was cleaned with 1% Incidin.

Table 1: Cell lines used

Cell type	Supplier	Cat. No.
Mouse IMCD3 WT	ATCC	CRL-2123
Human U2OS WT	ATCC	HTB-96
Human HEK 293T WT	ATCC	CRL-3216
mIMCD3 Flp-In	Kind gift of Peter Jackson	
mIMCD3 Flp-In SDCCAG8 pgLAP1	Generated for this work	
mIMCD3 Flp-In SDCCAG8 pgLAP2	“	
mIMCD3 Flp-In NEK8-pgLAP1	“	
mIMCD3 Flp-In NEK8-pgLAP2	“	
mIMCD3 Flp-In GFP-pgLAP1	“	
mIMCD3 Flp-In pgLAP1	“	

mIMCD3 Flp-In pgLAP2	“	
mIMCD3 WT Subclone #8 (nephrolab subclone)	“	
mIMCD3 CRISPR NEK8 KO D1II	“	
mIMCD3 CRISPR SDCCAG8 KO E8	“	
mIMCD3 CRISPR SDCCAG8 KO E9	“	

Table 2: Material for Cell Culture

Material	Supplier
Dulbecco’s Modified Eagle’s Medium / Nutrient Mixture F-12 Ham With 15 mM HEPES and sodium bicarbonate, without L-glutamine, liquid, sterile-filtered, suitable for cell culture; + 10% Fetal Bovine Serum (FBS) + 5 mL L-Glutamine added (+ 5 mL Penicillin-Streptomycin (Pen/Strep) added for CRISPR cells) (+ 5 mL Hygromycin added for Flp-In cells)	Sigma Cat. No.: D6421 Gibco Gibco Gibco InvivoGen
Dulbecco’s Modified Eagle Medium (DMEM**)** With 4,5 g/L Glucose, 110 mg sodium pyruvate, L-glutamine	Sigma Cat. No.: D6429

+ 10% FBS (Fetal Bovine Serum)	Gibco
Phosphate Buffered Saline (PBS) 136 mM NaCl, 2,7 mM KCl, 6,25 mM Na_2HPO_4, 1,5 nM KH_2PO_4 pH 7,4	 Sigma Carl Roth Sigma Sigma
Trypsin EDTA	Gibco
Cell culture dishes (10 cm), 6-well-, 12-well- plates	Corning
96-well-plates	GBO
Stripettes (5 mL, 10 mL, 25 mL)	Corning
TipOne sterile pipette tips (200 µl and 1000 µl)	Starlab

3.2 Transfection

3.2.1 Calcium phosphate transfection of HEK293T

The day before transfection (in a 1:6 dilution), we prepared a dish of human embryonic kidney (HEK) 293T cells. Before transfection, cells were checked under the microscope. A minimum of 30% confluency was required for successful transfection. Calcium chloride and 2x HEPES tubes were mixed well before using. First, 500 µl calcium chloride were mixed with 10 µg Plasmid-DNA. 500 µl of 2x HEPES were added dropwise on vortex and then added dropwise to the cells and the medium was mixed briefly. The cells took up the formed constructs by phagocytosis.[91] Medium (10 ml) was replaced after 7 hours using standard medium (DMEM + 10% FBS).

Table 3: Material for Calcium phosphate transfection

Material	Supplier
$CaCl_2$ (0,25 M)	Roth
2X HEBS-Buffer	Nephrolab

50 mM N-(2-Hydroxyethyl)piperazine-N′-(2-ethanesulfonic acid) (HEPES), 280 mM NaCl, 10 mM KCl, 22 mM Dextrose 1,5 mM Na_2HPO_4, ph 7,09, sterile filtered	Sigma Sigma Carl Roth Sigma

3.2.2 Lipofectamine® transfection

A 6-well plate was prepared with 2 ml of the medium-cell suspension. 1,5 ml of resuspended mouse inner medullary collecting duct-3 cells (mIMCD3) mix were transferred into a 15 ml Falcon containing 13,5 ml medium (resulting in a 1:10 dilution of cells), mixed and used for plating the wells. After 24 hours, cells were checked under the microscope. Required confluency was approximately 40%. Tubes containing Plasmid-DNA (2 µg), 200 µl Opti-MEM™ reduced serum media and pOG44-vector (2 µg) were prepared.
Then, a mix containing Opti-MEM™ and Lipofectamine® 2000 was prepared in a 200:6 ratio. 200 µl of the Lipofectamin mix were added to 200 µl DNA mix by pipetting up and down gently. The tubes were incubated for 20 minutes, so the positively charged liposomes could take up the negatively charged DNA.[92] 400 µl of the mix was transferred to each well and the medium was gently mixed. The cells were incubated for 48 hours at 37°C in an incubator.

Table 4: Material for Lipofectamine® transfection

Material	Supplier
15 ml Falcon	greiner-bio one
6 well plate	Corning
Opti-MEM™ Reduced Serum Media	Invitrogen
Lipofectamine® 2000 Transfection Reagent	Invitrogen

3.3 Polymerase Chain Reaction (PCR)

Polymerase Chain Reaction (PCR) was applied to amplify DNA. First, the DNA double strands were denatured at 98°C to break up the hydrogen bridge bonds. The temperature was reduced to 60-70°C so that starter molecules, called primers, were able to bind the DNA single strands (hybridization). Then, a heat-stable DNA-Polymerase (Q5® or RedTaq) synthesized a new DNA strand, starting at the primers. By using forward and reverse primers with specific sequences, it was possible to amplify the DNA regions of interest. Synthetic DNA-nucleotides were part of the reaction mix, which were joined in 3´ to 5´direction at 72°C (elongation). The cyclic repetition of denaturation, hybridization and elongation led to an exponential multiplication of the target DNA.[93] The DNA fragment could subsequently be used for cloning and sequencing.

Table 5: Red Taq PCR program (35 cycles)

Step	Temperature	Duration	
Initial Denaturation	94°C	3 min.	
Denaturation	94°C	30 sec.	
Hybridization	60°C	30 sec.	
Elongation	72°C	60 sec.	Go to "Denaturation", repeat 34 cycles
Termination	72°C	10 min.	
Cooling	10°C	forever	

Table 6: Material for RedTaq PCR

Material	Amount	Supplier
DNA polymerase mix (RedTaq)	10 µl	NEB / Sigma
Forward Primer (1:10)	1 µl	IDT (2.17 table 2)
Reverse Primer (1:10)	1 µl	IDT (2.17 table 2)
Water (PCR reagent)	7 µl	Sigma
DNA	1 µl	

Table 7: Q5® PCR Hot Start program (35 cycles)

Initial Denaturation	98 °C	30 sec.
Denaturation	98 °C	5-10 sec.
Hybridization	50-72 °C	30 sec.
Elongation	72 °C	20-30 sec. / kb
Termination	72 °C	2 min.
Cooling	15 °C	forever

Table 8: Material for PCR with Q5® Hot Start High-Fidelity DNA Polymerase

Material	Supplier
Template cDNA	/
SDCCAG8 Mlu1 fw	IDT
SDCCAG8 Not1 rv	IDT
5X Q5 Buffer	New England Biolabs (NEB)
5X Q5 Enhancer	New England Biolabs (NEB)
25 mM dNTPs	New England Biolabs (NEB)
Q5 DNA polymerase	New England Biolabs (NEB)
Nuclease free water	Invitrogen

3.4 Agarose gel-electrophoresis

We prepared an agarose gel-electrophoresis to confirm the correct performance of the PCR. The agarose gels varied in their agarose percentage, which influenced the separation of DNA molecules. In general, 1% gels build less dense polymers which allow bigger DNA fragments to pass through the electric field. Compared to this, 2% gels build close-meshed polymers, making it more difficult for larger fragments to move through the gel. 1 µl of 5x Green GoTaq® Flexi Buffer was added to the PCR products or digested Plasmid constructs to facilitate both loading on the gel and descending of the samples. The gel was placed into a gel chamber and the chamber was filled with 1x Tris-acetate-EDTA (TAE) electrophoresis running buffer. The electrophoresis buffer contained ethidium bromide, an intercalating agent that emits light after intercalating to DNA and being stimulated by UV light. By starting the current (e.g. 105 V), the DNA molecules moved through the polymerized gel (comparable to a grid) from cathode to

anod.[94] The gel was analysed under a UV-lamp, where DNA fragments became visible due to ethidium bromide intercalation.

Table 9: Material for native agarose gel-electrophoresis

Material	Supplier
Agarose	Sigma
Green GoTag® Flexi Buffer	Promega
TAE electrophoresis buffer 40 mM Tris 20mM Acetic Acid 1 mM EDTA pH 8,5	 Sigma Sigma Sigma
PCR product	

3.5 DNA Sequencing

Sequencing was applied to analyze cloning results and detect mutations. The method of choice was the dideoxynucleotide method by Sanger, as outlined in the BigDye protocol. DNA fragments could be analyzed by electrophoretic separation and laser detection and sorted in the correct sequence.[95] This last step was performed in the Cologne Center for Genomics. Sequencing results were analyzed using the Benchling web interface. To validate the target sequences, the experimental sequence was aligned with the wildtype sequence.

Table 10: Material for BigDye® Sequencing

Material	Amount	Supplier
BigDye® Terminator v3.1	0,25 µl	Thermo Fisher Scientific
5x BigDye®Sequencing Buffer	2,25 µl	Thermo Fisher Scientific
Primer (1µM)	2 µl	IDT (2.17 table 2)
Template DNA 200 ng	variable	
Fill up to 10 µl with Aqua dest.	variable	Nephrolab

3.6 Protein determination (BCA assay)

A Bicinchoninic acid (BCA) assay was performed prior to SDS-PAGE and Western Blot to quantitatively measure proteins and use equal protein amounts of all samples. Based on the classical biuret reaction in which Cu^{2+} is reduced to Cu^{+} by peptide bonds, the amount of reduced Cu^{2+} is proportional to the amount of protein in the sample. Two molecules of bicinchoninic acid bind to each Cu^{+} molecule. This complex absorbs light at a wavelength of 562 nm and forms a purple-colored complex. The amount of protein can then be quantified by measuring absorption spectra and compared with a spectra of proteins with known concentrations.[96]

The BCA Protein Assay Kit was used according to the manufacturer protocol. A serial dilution of a standard protein (albumin) with water was prepared, serving as a comparison standard for the measured samples. 5 µl of each standard were pipetted into one well of a flat bottom 96-well plate. Then, 5 µl of the samples (diluted 1:100) were pipetted in duplicates on the same plate. A master mix with 150 µl reagent A and 3 µl reagent B was prepared for all measured wells. Reagent A contained, among others, bicinchoninic acid, while reagent B contained 4% cupric acid. 150 µl of the master mix were added to each well. The plate was shaken for 15 seconds, 300 rpm on a plate shaker and then incubated for 15 minutes at 37 °C. Afterwards, the absorption at 562 nm was measured with the Envision Multimode Plate Reader. The standard curve (albumin) was compared with the absorption value of the measured sample to determine the protein concentration.

Table 11: Material for BCA assay

Material	Supplier
Pierce BCA Protein Assay Kit Albumin Standard Ampules, 2mg/mL Bovine Serum Albumin (BSA) at 2mg/mL in 0.9% saline and 0.05% sodium azide	Thermo Fisher Scientific REF: 23227
Transparent flat bottomed 96-well plate	greiner bio-one
Envision Multimode Plate Reader	Perkin Elmer
Radioimmunoprecipitation Assay (RIPA)-treated cell lysate	/

3.7 Sodium dodecyl sulfate gel-electrophoresis (SDS-PAGE) & Western Blot

Sodium dodecyl sulfate (SDS)-polyacrylamide gel-electrophoresis was performed to detect the proteins of interest and to validate the generated Flp-In and CRISPR cell lines. We prepared this experiment by harvesting cells from a 10 cm dish, lysing them with RIPA + phenylmethylsulfonyl fluoride (PMSF) + sodium orthovanadate, sonicating them and adding 2x Laemmli + Dithiothreitol (DTT). RIPA, with its components SDS and sodium deoxycholate, disrupts nuclear membranes. Sonication was applied to break intermolecular interactions and to shear DNA. Laemmli contains Tris, Glycine and SDS. SDS is a denaturing agent that additionally charges all proteins negatively. Tris works as a buffer while glycine serves for the collection of proteins in the stacking gel. The reducing agent DTT was added to break disulfide bonds between the amino acids leading to unfolded proteins. The proteins were then separated by their molecular size.[97,98]

The gels used in SDS-PAGE consisted of two parts, namely a stacking gel (5% Acrylamide, pH 6,8) and a separating gel (10-15% Acrylamide, pH 8,8). First, the separating gel was prepared with ultrapure water, 40% monomeric Acrylamide 37:1 Bisacrylamide, Buffer, 10% ammonium persulfate (APS) and Tetramethylethylendiamine (TEMED). APS is a polymerization initiator and TEMED is a polymerization catalysator, which together serve for the crosslinking of acrylamide. The stacking gel was then prepared exactly like the separating gel, only with a lower percentage of Acrylamide. As shortly described before, the stacking gel was necessary to collect proteins and concentrate them. The separation gel with smaller pores, higher salt concentration and a higher pH was then important for separating the proteins by their molecular size. The gels were placed in a gel electrophoresis chamber filled with protein running buffer. The Western Blot samples were cooked for 5 minutes on 95 °C and spun down for 2 minutes at full speed in a table-top centrifuge. A protein marker was loaded to later compare the sample bands with known protein sizes. Then, 10-20 µl of the samples were loaded. The first phase (stacking gel) ran for 30 minutes at 70 V and the second phase for 90 minutes at 30 mA (per gel). After the negatively charged proteins moved from cathode to anode, it was possible to perform a Coomassie staining of proteins or a Western Blot.

A Western Blot´s principle is the transfer of the proteins from the SDS-PAGE gel on a Polyvinylidene fluoride (PVDF) membrane followed by a staining with a protein-specific primary antibody[99]. This is followed by an incubation in a secondary antibody, which binds the primary one. It is labelled with a horseradish peroxidase (HRP). This peroxidase catalyzes the conversion of luminol into its oxidized form. This luminescene can then be shown in a fusion camera.

The transfer onto the membrane was done under semi-dry conditions, meaning that all components were wetted in a transfer buffer. A so called “sandwich” was assembled, consisting of (from bottom to top): paper – membrane – gel – paper. By starting a current of 12 V for 53 minutes, the proteins on the gel moved vertically from cathode to anode onto the PVDF membrane. Afterwards, the protein coated membrane was blocked in 5% BSA in purified water to block unspecific antibody binding sites. To prevent BSA contamination, we conducted three washing steps (10 minutes each) with protein wash buffer. The membrane was then incubated in the primary antibody over night at 4°C on a rotating shaker. The antibody was diluted in a specific dilution in 10 ml protein wash buffer. The next day, the membrane was washed three times for 10 minutes again to get rid of unspecific bound antibodies before it was incubated in the secondary antibody for 45 minutes at room temperature on a rotating shaker. The secondary antibody was also diluted in 5 ml wash buffer in a 1:30.000 dilution. Again, 3 washing steps were performed, each 10 minutes long. Then, it was possible to detect the proteins. We prepared a solution with 250 mM Luminol and 90 mM Coumaric acid. As shortly mentioned above, Luminol was converted into its oxidized form by the peroxidase linked to the secondary antibody, leading to a luminescent signal. Coumaric acid acted as a sensitizer for this reaction. The luminescent bands were detected by the Fusion Camera and showed the size of the proteins of interest.

Table 12: Material for SDS-Page & Western Blot

Stacking gel

Material	Supplier
5% Acrylamid	Carl Roth
0,2% SDS	AppliChem
2M Trizma Hydrochloride	Sigma
2M Trizma Base	Sigma
0,05% APS	AppliChem
0,1% TEMED	Carl Roth
Purified water	Nephrolab

Separating gel

Material	Supplier

10-15% Acrylamid	Carl Roth
0,2% SDS	AppliChem
2M Trizma Hydrochloride	Sigma
2M Trizma Base	Sigma
0,05% APS	AppliChem
0,1% TEMED	Carl Roth

Running Buffer

Material	**Supplier**
Glycine	Carl Roth
Tris	Sigma
SDS	AppliChem

Transfer Buffer

Material	**Supplier**
Glycine	Carl Roth
Tris	Sigma
Methanol	Carl Roth

Protein Wash Buffer

Material	**Supplier**
Tris	Sigma
Sodium chloride	Sigma
Tween (Polysorbat 20)	Caesar & Lorentz

ECL (Enhanced Chemiluminescence Solution)

Material	**Supplier**
Hydrogen peroxide	Carl Roth

Luminol	Fluka
Coumaric acid	Sigma
Tris	Sigma

Material	**Supplier**
Gel cassetes	Thermo Fisher
5% BSA (Bovine Serum Albumin)	Sigma
PVDF membranes	Millipore
Methanol	Carl Roth
Blotting paper	VWR

Table 13: Primary antibodies for Western Blot

Antibody	**Species**	**Dilution**	**Supplier**	**Cat. No.**	**Lot. No.**
GFP (B-2)	mouse	1:10.000	Santa Cruz	sc-9996	K2217
FLAG	mouse	1:10.000	Sigma Aldrich	F3165	SLBL1237V
FLAG	rabbit	1:5000	Sigma Aldrich	F7425	-
V5 Epitope Tag	rabbit	1:5000	Millipore	AB3792	633758
Fibrillarin	rabbit	1:500	Abcam	ab166630	-
β- Tubulin	mouse	1:500	Santa Cruz	sc-9104	F2504
SDCCAG8 (NPHP10)	rabbit	1:500	Proteintech	13471-1-AP	00023136
NEK8 (NPHP9) (N1N2) N-term	rabbit	1:500	GeneTex	GTX112027	40093

Table 14: Secondary antibodies for Western Blot

Antibody	Species	Dilution	Label	Supplier
Anti-mouse-IgG	goat	1:30.000	HRP	Dako
Anti-rabbit-IgG	goat	1:30.000	HRP	Dako

3.8 Immunoprecipitation (IP)

An immunoprecipitation was performed to pull down and enrich the low-abundant proteins of interest, which were then detected by Western Blot. We conducted two different IP approaches. First, our stably expressed proteins of interest linked to a FLAG tag were pulled down by M2 beads as these are coated with FLAG antibody. Another option was incubating Protein A sepharose beads with antibodies against the proteins of interest and pull them down.

Cells from ten 10 cm dishes were harvested in 1 ml cold 1x PBS and spun down at 1000 rpm for 5 minutes at 4 °C. The supernatant was aspirated and the cells were lysed on ice. In detail, mod. RIPA Buffer was supplemented with PIM (protease inhibitor mix) + EDTA and sodium orthovanadate. Each 10 cm cell dish received 500 µl of this mix.
Mod. RIPA disrupts cell membranes and is, therefore, efficient in cell lysis. Protease inhibitors prevent the proteins in the cell lysate from being degraded. It was combined with EDTA as this reagent complexes bivalent metal cations which are present in many enzymes, also proteases. The proteases are, thereby, inhibited. Sodium orthovanadate is a tyrosine phosphatase-, alkaline phosphatase-and ATPase-inhibitor.
After adding this mix, the cell pellets were lysed on ice for 30 minutes. The samples were sonicated for 60 pulses with 10% power (0,1 seconds pulse, 0,9 seconds off) to solubilize the cells and break intermolecular interactions by ultrasound. So-called “Input samples” were prepared for each IP sample by transferring 10% of the IP sample to a separate tube before adding the beads. This “Input sample” was also loaded on a Western Blot next to the IP sample to show the protein enrichment by immunoprecipitation.
In case of an anti-FLAG IP, 30 µl of M2 beads were added to each of the sonicated samples followed by overnight incubation on an overhead shaker at 4°C.
An Protein A sepharose beads-IP required an intermediate step. 500 µl mod. RIPA buffer was mixed in a 1,5 ml tube together with 30 µl Protein A sepharose beads and 2 µg of antibody. This mix was put on an overhead shaker for 1 hour at 4 °C to couple the antibodies to the beads. After that, the mix was spun down for 2 minutes at 2000 rpm and then the supernatant was removed. Subsequently, the sonicated samples were added to the beads.

The following day, the samples were spun down at 4000 rpm for 3 minutes at 4°C and the supernatant was removed. The IP samples were then washed 3 times with 700 µl mod. RIPA buffer to get rid of unspecific bound proteins. After the last washing step, 1x Laemmli + DTT was added to the samples, they were cooked for 5 minutes at 95°C and shortly spun down to prepare them for Western Blot.

Table 15: Material for Immunoprecipitation

Material	Supplier
M2 beads	Bimake
Protein A Sepharose beads	Life Technologies
Mod. RIPA Buffer: 10 mM Tris, ph 8 1 mM EDTA 0,5 mM Ethylene glycol bis(2-aminoethyl)tetraacetic acid (EGTA) 1% Triton-X 1,1% sodium deoxycholate	 Sigma Sigma Applichem Sigma
Proteases inhibitor mix (PIM) + EDTA	Roche
Sodium orthovanadate	
IP-Buffer 10% Triton-X-100 1M TrisHCl pH 7,5 2M sodium chloride (NaCl) 0,5M sodium fluoride (NaF) 0,125M $Na_4P_2O_7$	 Applichem Sigma Sigma Sigma Merck
Laemmli 2x 250 mM Tris 10% SDS 50% Gylcerol Bromophenol Blue	 Sigma AppliChem Carl Roth Carl Roth

100 mM DTT pH 6,8	Thermo Fisher

3.9 Immunostaining

Immunofluorescence staining was performed to investigate the localization of green fluorescent protein (GFP)- and FLAG- tagged proteins of the stable Flp-In cell lines. In the so-called secondary (indirect) immunofluorescence, the antigen (protein of interest) was bound by an antigen-specific primary antibody. Fluorophore-tagged secondary antibodies recognized the primary antibody and bound it. Imaging was performed at a Zeiss Confocal laser microscope. The fluorophores linked to the secondary antibody were excited with a specific laser wavelength, then the emitted light was detected[100].

IMCD3 cells were grown on coverslips on a 12 well plate in 1 ml medium. They were washed 2 times with 1x PBS and then fixed in 500 µl 4% Paraformaldehyde (PFA) for 10 minutes. Afterwards, PFA was removed and the cells were washed twice with 1x PBS. In the next step, 500 µl 0,1% Triton-X100 and 5% normal donkey serum (NDS) in PBS were added to each well for 60 minutes. Triton-X100 permeabilizes the cell membranes (antibodies can enter the cells and bind their antigen) and NDS blocks unspecific binding sites. Followed by this, we incubated the samples with primary antibodies in 0,1% Triton, 5% NDS and PBS overnight at 4 °C. For this purpose, the cover slips were transferred from the 12 well plate into a 100 µL antibody mix (example: 100 µL Triton-NDS-PBS, 1 µL NEK8-antibody, 0,1 µL acetylated tubulin-antibody) on a Parafilm in a humidity chamber. The cover slips were put back into the 12 well plate the next day and washed 3 times with 1x PBS. Incubation in secondary antibody was then performed in 0,1% Triton-PBS in a 1:500 dilution for 45 minutes at room temperature. The coverslips were washed three times with 1x PBS and finally mounted in 10 µl Prolong Gold + 4′,6-diamidino-2-phenylindole (DAPI), a fluorescent dye used to stain DNA. We put the samples on slides and analyzed them by Confocal Imaging.

Table 16: Material for Immunostaining

Material	Supplier
12 well plate	Corning
4% PFA (Paraformaldehyde)	Sigma
NDS (Normal Donkey Serum)	Jackson Immunoresearch
Triton-X100	Applichem

Prolong Gold + DAPI	Thermo Fisher
Zeiss LSM Confocal Microscope	Carl Zeiss
Coverslips	

Table 17: Primary antibodies for Immunostaining

Antibody	Species	Dilution	Supplier	Cat. No.	Lot. No.
acetylated Tubulin	Mouse	1:1000	Sigma	T6793	/
ARL13B	Rabbit	1:400	Proteintech	17711-1-AP	/
FLAG	Rabbit	1:1000	Sigma-Aldrich	F7425	/
NEK8/NPHP9	Rabbit	1:200	GeneTex	GTX106133	40135
SDCCAG8/NPHP10	Rabbit	1:200	Proteintech	13471-1-AP	000023136

Table 18: Secondary antibodies for Immunostaining

Antibody	Species	Dilution	Supplier
Cy3	Donkey anti mouse	1:500	Jackson ImmunoResearch
DyLight 649	Donkey anti rabbit	1:500	LI-COR
Alexa 488	goat anti rabbit	1:500	Life Technologies

3.10 RNA isolation

RNA isolation was done by applying the single-step method. First, the CRISPR clones (incl. WT as control) were plated on a 6 well plate the day before isolation of RNA. The medium was discarded the next day and the cells were washed one time with 1 mL Rnase free PBS. After discarding PBS, 0,7 mL TRI Reagent® were added under the RNA hood and pipetted up and down. TRI Reagent® contains Phenol, which is toxic and had to be treated extremely carefully under the RNA hood. It also contains Guanidinium thiocyanate, which lyses the cells and inactivates RNases. Phenol breaks down the cell material.

After adding the reagent, we incubated the cells for 5 minutes at RT. Then, they were transferred to a safe lock Eppendorf tube (alternative: store at -80°C). Immediately, 140 µL chloroform was added. This treatment led to a phase separation, building an aqueous phase (RNA), an intermediate phase (DNA) and an organic phase (proteins). The samples were vortexed for 15-30 seconds, incubated for 5 minutes on ice, and then vortexed again shortly. Centrifugation for 15 minutes at 14.000 rpm in a cold centrifuge at 4°C finally led to the final phase separation. 350 µL of the upper aquaeous phase (clear solution) was added to a new tube filled with 350 µL isopropanol. It was crucial not to transfer components of the intermediate phase (DNA) or the pink organic solution (proteins) to the new tube. The tubes were vortexed briefly and stored at -20 °C overnight. Isopropanol precipitated the ribonucleic acid (RNA). The next day, we carried out centrifugation for 10 minutes with 14.000 rpm at 4°. Afterwards, the supernatant was discarded. A small RNA pellet was visible. This pellet was washed with 0,2 mL 70% EtOH and centrifuged for 10 minutes, 11.000 rpm at 4°C. The supernatant was discarded and the pellet airdried for 30 minutes (open lid). Finally, the RNA was dissolved in 20 µL Rnase free water. Subsequently, the RNA sample was measured with NanoDrop to determine the RNA concentration.

Table 19: Material for RNA isolation

Material	Supplier
6 well plate	Corning
TRI-Reagent®	Sigma
Safe lock tube	Eppendorf
Chloroform	Merck
Isopropanol	Carl Roth
70% Ethanol	Carl Roth

3.11 Concentration measurement of RNA (NanoDrop)

In this spectrophotometric measurement, 1 µl of Aqua dest. was pipetted onto a pedestal to blank the NanoDrop machine (NanoDrop 1000 Spectrophotometer, Peqlab biotechnologies GmbH). The machine was set on “RNA”. Another 1 µl of Aqua dest. was added and measured. The surface of the pedestal was cleaned with a clean tissue. 1 µl of the RNA sample was then pipetted onto the pedestal and measured.

3.12 First-Strand library cDNA Synthesis for Reverse Transcriptase-PCR

In this procedure, mIMCD3 RNA was converted into first-strand complementary DNA (cDNA). 1,5 µg (8 µl) RNA, 1 µl 50 µM oligo (dT) Primer and 1 µl 10 mM DNTP mix (in total 10 µl) were mixed and centrifuged and then combined in an Eppendorf tube (RNA-primer-mix). Incubation took place for 5 minutes at 65°C and after that, the samples were placed on ice. The cDNA Synthesis Mix contained 5X reverse transcription buffer (RT Buffer), 0,1 M DTT, RNaseOUT™ (40 U/µl) and Super Script® III RT (200 U/ µl). 10 µl of cDNA Synthesis Mix were added to RNA primer mix, then mixed and spun down in a centrifuge for 2 minutes. The tubes were incubated at 50°C for 60 minutes. The reaction was terminated then at 70°C for 15 minutes. The samples were put on ice and the reaction product collected by brief centrifugation. We performed Q5 PCR immediately afterwards and stored the residual cDNA in – 20°C labelled as “cDNA library of mIMCD3 cells”.

Table 20: Material for cDNA Synthesis for RT-PCR

Material	Supplier
mIMCD3 RNA	Nephrolab
50 µM oligo (dT) Primer	Thermo Fisher Kit #18080-051
10 mM DNTP mix	Thermo Fisher
5X RT Buffer	Thermo Fisher
0,1 M DTT	Thermo Fisher
RNaseOUT™ (40 U/ µl)	Thermo Fisher
SuperScript® III RT (200 U/ µl) Reverse Transcriptase	Thermo Fisher

3.13 quantitative PCR (qPCR)

Quantitative PCR (qPCR) was applied to validate the CRISPR KO cell lines. By using a DNA-binding fluorescent dye (SYBRGreen I) it was possible to label the DNA while amplifying it. This technique was performed to validate the lower messenger RNA (mRNA) expression of NPHP9 & NPHP10 CRISPR clones compared to WT samples. We used CT-values to draw conclusions about the relative gene expression. A CT-value is defined as the cycle number in which a significantly higher fluorescent signal than the background fluorescent signal is measurable. The lower the CT value, the higher the amount of transcripts produced.

Cells were grown and harvested on 6 well plates, and the RNA was isolated. This was followed by cDNA synthesis. The 20 µL of cDNA synthesis mix were filled with 180 µL RNase free water, so that the concentration of cDNA was approximately 5 ng/ µL [starting with 1000ng, then diluted with water → 100 ng, then 10 µL Master Mix → 50 ng, then 1:10 diluted (180 µL water) → 5 ng / µL]. 12,5 µL SYBRGreen I, 0,15 µL Primer (50 µM) and 7,35 µL water were added per sample. As there were many samples to analyze, a Master Mix was prepared for each exon mix containing specific primers, e.g., for *SDCCAG8* Exon 2-3. 5 µL cDNA & 20 µL Master Mix were added to a 96 well plate (Fast optical, Applied) using Filter Tips. A plastic film was stuck with roller and tissue on top of the plate so the fluid could not evaporate. The plate was quickly spun for 1 minute, 8000 rpm to eliminate air bubbles. The qPCR machine was started and afterwards, the qPCR analysis was performed to validate the KO clones using the SDS 2.4 software.

Table 21: Material for qPCR

Material	Supplier
High-Capacity cDNA Reverse Transcription Kit	Applied Biosystems Kit #4368814
RNase free water	Invitrogen
SYBRGreen I	Applied Biosystems
Primer	IDT
96 well plate	Applied Biosystems
Centrifuge Multifuge 4 KR	Heraeus
qPCR machine (279002557)	Applied Biosystems

3.14 Cloning design

The mRNA coding sequences (CDS) of “mus musculus serologically defined colon cancer antigen 8 (*SDCCAG8*)” and “mus musculus NIMA (never in mitosis gena a) – related expressed kinase 8 (*NEK8*)” were found on “www.ensembl.org”. The forward primer sequence, including Mlu1 Clamp recognition site, and the reverse primer sequence, including Not1 Clamp recognition site, were designed. It was important that the Primers had a guanine-cytosine content (GC content) of 40 – 60%. The expected amplicon sizes of *SDCCAG8* and *NEK8* were 2154 bp and 2096 bp, respectively.

3.15 PCR using Q5® Hot Start High-Fidelity DNA Polymerase

Q5® PCR was applied to amplify the genes of interest, namely *Nek8* (NPHP9) and *Sdccag8* (NPHP 10), using the designed primers (see table 36 and 3.xx) All components were mixed prior to use. Forward and reverse primers were dissolved to 100 µM in nuclease free water and diluted 1:10 from stock in nuclease free water. Duplicate 25 µl Q5 tubes were prepared: 5 µl 5X Q5 Buffer, 5 µl 5X Q5 Enhancer, 0,2 µl 25 mM dNTPs, 1,25 µl of each forward and reverse primer, 5 µl DNA (300 ng), 0,25 µl Q5 DNA polymerase and 7 µl nuclease free water were mixed together. After mixing gently and pre-heating the lid of the cycler up to 98°C, the "Hot start" program was initiated (see 3.3).

3.15.1 Control Gel for identifying amplified PCR product

See 3.4.

3.15.2 Purification of PCR product

PCR product (*Sdccag8* / *Nek8*) was purified by using the GeneJet PCR Purification Kit (ThermoScientific) and following its purification protocol, elution was done in 26 µl Elution Buffer.

GeneJet PCR Purification Kit	Thermo Scientific #K0701

3.15.3 Digestion

Eluted DNA was mixed with 0,5 µl Mlu1, 0,5 µl Not1 and 3 µl Buffer 3.1. Mlu1 and Not1 are restriction enzymes which recognized the Mlu1 and Not1 sites in the genes of interest. They cut at these sites and form sticky ends. Digestion took place in a 37°C cycler for 6 hours. Concomitantly, the vector / backbone (pENTR1A), where the genes of interest became integrated, was digested as well. We followed with an incubation step for 2 hours at 37°C in the cycler. As human GLIS Family Zinc Finger 2 (hGLIS2) was cloned inside, digested human hGlis2 pENTR1A was loaded on a 1% Agarose gel, accomplishing a run for 35 minutes at 95V. After that, the band of pENTR1A (2717 bp) was cut out under UV-light using a scalpel. Another 1% control gel was prepared afterwards to check if cutting out of pENTR1A was successful. The digestion of the gene of interest-DNA was loaded on the same gel to prove the amplicon's correct size. This gel was run for 30' at 95V again.

Table 22: Material for Digestion

Material	Supplier
Mlu1	NEB x 5U/µL
Not1	NEB x 5U/µL
Buffer 3.1	NEB
Thermocycler	Bio-Rad S1000^{TM} Thermal Cycler

3.15.4 Ligation

The genes of interest were ligated into the digested pENTR1A / pSpCas9(BB) 2A-GFP backbone after digestion. 1µl of digestion product, 1,5 µl 10x T4 buffer, 0,3 µl T4 Ligase, 8,2 µl Water and 4 µl m*Sdccag8 / mNek8* digest were mixed together. Additionally, we prepared a control sample containing 4 µl Water. The mixes were incubated for 2 hours at room temperature. The gene of interest then was integrated into the backbone and formed a circular plasmid DNA.

Table 23: Material for Ligation

Material	Supplier
Backbone digest Insert digest	
10x T4 buffer	Thermo Fisher
T4 ligase	Thermo Fisher Cat.: EL0011, Lot: 00731391 5 U/µL
water	

3.15.5 Transformation

By transformation, the recombined plasmid DNA was amplified in chemo competent bacteria. First, 5 µl of both ligation sample and control sample were added to 50 µl DH10 bacteria. An incubation step of 10 minutes on ice was followed by heat shocking at 42°C for 45 seconds. Through heat shocking, the bacteria took up DNA efficiently. The bacteria were placed back on ice and 250 µl super optimal broth (SOC) medium was added to both Eppendorf tubes.

Next, it was incubated at 37°C, 800 rounds per minute on a thermomixer. After that, 50 µl bacteria were plated on one lysogeny broth (LB) plate containing Kanamycin or Ampicillin. Half of the plate was used for the DNA sample and the other half for the water control sample (water ligation). As the pENTR1A backbone contained a Kanamycin and pSpCas9(BB) 2A-GFP an Ampicillin resistance gene, only those bacteria that are efficiently transformed with the vector constructs survived. Colonies of bacteria with the target plasmid DNA were expanded in an incubator for 16 hours at 37 °C. Colonies only grew on the sample side, not on the control side.

Table 24: Material for Transformation

Material
Chemocompetent DH10 bacteria
42°C water bath
SOC medium
Eppendorf thermo mixer
LB plate (Kanamycin/Amipicillin) LB medium: Carl Roth

3.15.6 Plasmid preparation (Mini Prep)

First, 10 colonies were selected from the Kanamycin-plate by using a sterile pipette tip. LB medium with 0,1% Kanamycin was prepared. Then, the pipette tips with the picked colonies were transferred into a 15 ml Falcon containing 3 ml of Kanamycin-LB medium. The Falcons were incubated on a shaking incubator overnight at 37 °C. The lit stayed a bit loose for oxygen supply. On the next day, 1,5 ml of bacteria were transferred from the falcons to Eppendorf tubes and centrifuged at 8000 revolutions per minute (rpm) for 2 minutes and the supernatant was removed. By using the Thermo Scientific GeneJET Plasmid Miniprep Kit, plasmid DNA was purified. All bacteria were lysed during this procedure and the DNA was bound on a column. By using the Elution Buffer, the DNA was released from the column and collected at the bottom of the tube. After following the instructions, the DNA was eluted in 25 µl Elution Buffer.

Table 25: Material for plasmid preparation (Mini Prep)

Material	Supplier
LB medium	Carl Roth
Kanamycin	Sigma
GeneJET Plasmid Miniprep Kit	Thermo Scientific REF: K0503 Lot: 00789779

3.15.7 Plasmid digestion

Plasmid digestion was performed to restrict the pENTR1A vector containing the genes of interest in order to screen effective ligation on a gel (see 3.15.3). If the digestion was successful, we continued with Midi Prep.

3.15.8 Plasmid preparation (Midi Prep)

A Midi Prep was performed to purify cloned plasmid construct. 0,75 mL of bacterial culture was transferred to an Erlenmeyer flask containing 250 mL purified water, 5 g LB medium and 250 µl Kanamycin. The bacteria culture was expanded for 16 hours at 37°C. By following the instructions of the protocol in the Macherey-Nagel kit, the DNA was bound on an anion exchange spin column in several steps and spun in a 4°C cold centrifuge before it was eluted. Isopropanol and then 70% Ethanol were added to the eluted DNA to precipitate it as it was less soluble in alcohol. After removing the alcohol, the pellet was airdried and resuspended in 10mM Tris pH 7,5 and the DNA was stored in a safe-lock Eppendorf tube at 4°C.

Table 26: Material for plasmid preparation (Midi Prep)

Material	Supplier
Plasmid preparation Kit (Midi Prep)	Macherey-Nagel REF: 7404100.100, Lot: 1907/004
Avanti-J-26S XPI Centrifuge	Beckmann-Coulter

3.15.9 BigDye® Sequencing

See 3.5.

3.16 Flp-In system

Using mIMCD3 WT cells, we cloned the cDNA of *Nek8* and *Sdccag8* in pENTR1A vectors followed by a recombination into pgLAP1/2 vectors for stable expression of GFP- (pgLAP1) or FLAG-tagged (pgLAP2) proteins. These recombinations were enabled by restriction enzymes and ligases. The pgLAP vectors consist of a cytomegalovirus (CMV) promoter controlling the expression of EGFP/FLAG-TEV-S-peptide-tagged genes of interest flanked by flippase recognition target (FRT) sites. By co-transfection of the *Sdccag8 / Nek8*-pgLAP constructs with Flp recombinase expression vector (pOG44) into the Flp-in mIMCD3 cell line, stable integration of promoter, GFP/FLAG and genes of interest was accomplished.[101102]

Table 27: Material for Flp-In system

Material	Supplier
pgLAP1	pgLAP1 was a gift from Peter Jackson (Addgene plasmid # 19702; http://n2t.net/addgene:19702; RRID: Addgene_19702)
pgLAP2	pgLAP2 was a gift from Peter Jackson (Addgene plasmid #19703; http://n2t.net/addgene:19703; RRID: Addgene_19703)
Pog44	pOG44_FLP_recombinase (pEHA1338) was a gift from Vikram Khurana (Addgene plasmid # 209087 ; http://n2t.net/addgene:209087 ; RRID:Addgene_209087)

3.17 CRISPR/Cas9 cloning

We employed the CRISPR/Cas9 genome editing technique to knock out the genes of interest *Nek8* (*NPHP9*) and *Sdccag8* (*NPHP10*). The approach by Ran et. Al was applied here.[103]

3.17.1 Analysis of mIMCD3 WT Subclone #8 DNA

Before starting the CRISPR experiment, we ensured that the target DNA was mutation free. To prove this, the target exons were first amplified by PCR (see 3.13). Then, the PCR was cleaned up by EXO-SAP digestion and the amplicons were sequenced.

12 µl of the PCR product and 3 µl of 50 bp marker were loaded on a 2% agarose gel. This was followed by a gel run for 35 minutes at 120 V. The amplified exons (sizes between 250 and 350 bp) could be identified afterwards. Then, the remaining 8 µl PCR sample products were cleaned up with exonuclease I (EXO1) and shrimp alkaline phosphatase (SAP). This treatment was important prior to sequencing because EXO enzymatically removes non-incorporated primers and SAP dephosphorylates dNTPs. A mix of 1,625 µl water, 0,3 µl SAP and 0,075 µl EXO1 was prepared and added to 8 µl of each PCR product. This mix was incubated at 37°C for 20 minutes and at 72°C for 15 minutes in a thermocycler. The amplified exon sequences were sequenced by BigDye® Terminator V 3.1 Sequencing (see 3.5).

3.17.2 Preparation of sgRNA oligo plasmid inserts

A genomic target containing a protospacer adjacent motif (PAM) sequence “NGG” (N: not specified) was determined. The sequence of a single guide RNA (sgRNA) oligo complementary to the target sequence (top strand, 20 nucleotides) and its complementary sequence (bottom strand) were first phosphorylated and annealed. Phosphorylation was necessary for a successful ligation reaction. The top and bottom stands were resuspended to a concentration of 100 µM. Then, 1 µl sgRNA top strand, 1 µl sgRNA bottom strand, 1 µl 10x T4 ligation buffer, T4 polynucleotide kinase and 6 µl purified water were mixed.
The oligos were placed in a thermocycler for phosphorylation and annealing with the following program:

Table 28: Cycles for preparation of sgRNA oligo plasmid inserts (1)

Temperature	Duration
37°C	30 minutes
95°C	5 minutes
Ramp down to 25°C, 5°C per minute	

After that, the oligos were diluted 1:200 by adding 199 µl purified water to 1 µl of oligos.

Table 29: Material for preparation of sgRNA oligo plasmid inserts (2)

Component	Amount	Supplier
m*SDCCAG8* sgRNA Exon1 top (100 µM);	1 µl	IDT (2.17 table 2)

m*SDCCAG8* sgRNA Exon 1 bottom; m*SDCCAG8* sgRNA Exon 3 top; m*SDCCAG8* sgRNA Exon 3 bottom; m*NEK8* sRNA Exon 2 top; m*NEK8* sgRNA Exon 2 bottom; m*NEK8* sgRNA Exon 3 top; m*NEK8* sgRNA Exon 3 bottom		
T4 ligation buffer, 10x	1 µl	Fermentas
T4 polynucleotide kinase (PNK)	1 µl	Thermo Fisher
Purified water	6 µl	Nephrolab

3.17.3 Cloning sgRNA oligos into pSpCas9(BB) 2A-GFP

Next, we performed cloning of the sgRNA oligos into pSpCas9(BB) 2A-GFP vectors by collecting the material (Table 32) in a tube. The restriction enzyme digested the vector by cutting out the old insert. Phosphorylated and annealed oligos were then inserted into the vector by T7 ligase. Incubation of the ligation reaction was done for 1 hour in 6 cycles: 5 minutes at 37°C, 5 minutes at 21°C per cycle.

Table 30: Material for cloning sgRNA oligos into pSpCas9(BB) 2A-GFP

Component	Amount	Supplier
pSpCas9(BB) 2A-GFP	100 ng (0,5 µl)	Sigma
1:200 Diluted oligo duplex	2 µl	IDT
Tango buffer 10x	2 µl	Fermentas
DTT, 10 mM	1 µl	Thermo Fisher
ATP, 10 mM	1 µl	Sigma

FastDigest BpiI	1 µl	Thermo Fisher
T7 DNA ligase	0,5 µl	NEB
Purified water	12 µl	

Transformation was performed according to 3.5.
The plates were examined the next day and checked for bacterial colonies. We selected 5 colonies for every Exon targeted by CRISPR/Cas9 with a sterile 200 µl pipette tip. The tips were placed into a falcon with 3 ml of Ampicillin-LB medium (1:1000 ratio). The colonies were grown at 37°C overnight. A Mini Prep followed on the next day (see 3.12.8). Then, the concentration of purified DNA was measured by NanoDrop.

We proceeded with BigDye® Sequencing to detect mutations in the exon-targeting sequences. A primer recognizing and binding to the U6 promoter region was used because sgRNA sequence was integrated into the backbone right next to the U6 promoter region. The mutation-free plasmids were expanded via Midi prep (one Midi per exon). Validation of a successful Midi Prep was done by DNA analysis on a 1% agarose gel-electrophoresis. The most promising DNAs were selected and sequenced using the U6 promoter primer mentioned above.

3.17.4 Transfection

mIMCD3 WT subclone #8 cells were transfected with the assembled sgRNA-pSpCas9(BB) 2A-GFP plasmids (3.2.2)

3.17.5 Fluorescent activated cell sorting (FACS)

48 hours after transfection, cells were washed one time with 2 mL PBS and detached from the 6 well plate with 0,5 mL Trypsin. Five minutes of incubation at 37 °C and resuspension in 5 mL DMEM F12 medium followed. The cell suspension was transferred into 15 mL falcons and spun down at 1250 rpm at room temperature for five minutes. Then, the medium was aspirated and the falcons were kept on ice.
A 50 mL falcon containing FACS buffer (PBS + 2% FBS) was prepared and each pellet was resuspended in 0,5 mL of this buffer. Simultaneously, 96 well plates were prepared, from which each well received 80 µl of DMEM F12 + 1% Glutamax + 10 % FBS + 1% Penicillin-Streptavidin medium. Cells were sorted into these 96 well plates (MPI Age FACS facility). The falcons and 96 well plates were transported to FACS facility where the resuspended pellets were transferred to sterile FACS tubes. The tubes were placed into the FACSARIA IIIu Svea machine equipped with a 100um nozzle. One GFP positive cell was sorted in each well of the 96 well plates.

3.17.6 Analysis of clones

Colony expansion of the single-sorted cells took, on average, 10 to 14 days. When colonies were visible, one 10 cm dish was prepared for further culturing of the cells and one dish for DNA preparation. The medium was aspirated, the cells were washed with PBS and treated with some drops of Trypsin afterwards. After incubation for 10 minutes at 37 °C, the cells were resuspended in 200 µl medium. Some drops were added to a new 96 well plates, which already contained 80 µl of medium, and the rest was transferred to a 96 well plate used for DNA purification the next day.

To isolate the DNA, the medium was poured into the sink. Cells were washed in 1x PBS, which was also poured into the sink. 30 µl of lysis buffer + 100 µg/mL proteinase K were added to the wells using a multichannel pipette. The plates were rocked for 5 minutes at room temperature and the extracts were transferred to PCR tubes. Next, the extracts were incubated at 56 °C for 1 hour followed by 95 °C for 10 minutes. The purified DNA was stored at 4 °C.

By running a genotyping PCR of all prepared CRISPR DNAs, promising CRISPR clones (and mutations) were detected (see 3.13). After that, the PCR product was poured on an agarose gel (3.15.1) We performed EXO-SAP digestion as well as BigDye® Sequencing for every promising clone.

3.17.7 Validation

The CRISPR clones which showed mutations for the genes of interest were grown on 10 cm dishes. Before experiments, five to ten 10 cm dishes were pooled. The cells were harvested and an immunoprecipitation was performed. Afterwards, a Western Blot was done to detect differences between wild type (WT) and CRISPR clones.

3.18 Mass spectrometry

We conducted mass spectrometry to validate the CRISPR knockout cell lines. Preparation was done by harvesting, reduction, alkylation and trypsin digestion followed by the Nephrolab stage tip protocol (3.18.1, 2, 3 and 4).

3.18.1 Sample preparation & BCA measurement

We removed the medium and the transfected mIMCD 3 WT Subclone #8 cells were scraped from the in total five plates using 10 mL cold PBS. The cells were than centrifuged for 5 minutes at 1000 rpm at 4°C. Then, they were transferred into a 1,5 mL tube with 1 mL PBS. Another centrifugation step at 1000 rpm at 4°C for 5 minutes followed before the supernatant was aspirated. The pellets were snap frozen in liquid nitrogen and stored at -80°C.

Next, the cells were resuspended in 500 µl urea buffer in 50 mM ammonium bicarbonate with 5 µl phosphatase-protease inhibitor (10 µl PPI per mL urea buffer). The mixture was vortexed until the pellet was resolved. The samples were sonicated with 60 impulses (1 minute, 10% power) until a homogenous sample was obtained. Centrifugation at 4°C for 30 to 45 minutes at maximum speed followed. The supernatant was processed. For this purpose, new Eppendorf tubes were filled with 20 µl sample together with 20 µl purified water. A Pierce™ BCA Protein Assay was performed to determine the protein concentrations in the samples.

3.18.2 Reduction & Alkylation

We carried out reduction to break peptide bonds, whereas alkylation was done to prevent the free sulfhydryl groups on the cysteines to reform disulfide bonds.[104] The samples were reduced by adding 10 mM DTT for 45 minutes at room temperature. Alkylation was done by adding 200 mM iodoacetamide for one hour at room temperature in a dark room.

3.18.3 Trypsin digestion

Before the samples were digested, they had to be diluted to a concentration below 2 M urea with 50 mMl ammonium bicarbonate because trypsin only cut when the urea concentration was below 2 M and pH < 8. Dilution was done in a 1:10 ratio, meaning 8 µL sample together with 92 µL ammonium bicarbonate.

25 µg protein was used for a knockout validation experiment. Therefore, 1 µL of 1 µg/µL trypsin was added to the samples to hydrolytically break the peptide bonds. The digestion was done overnight for 14 hours.

3.18.4 Stop and go extraction tops for matrix-assisted laser desorption

Stage tipping was performed to clean the samples from salts and buffers.

After overnight digestion the samples were acidified to 0,5% formic acid. Vortex and pH check were done (ideal pH: < 3). Then, the samples were spun for 5-10 minutes with maximum speed at 4°C to get rid of the urea rests. The supernatants were used for stage tipping and tubes were changed.

The stage tips were equilibrated with 25 µL methanol and then spun for 1 minute at 500 g followed by another equilibration step with 25 µL buffer B and spinning step for 1 minute at 500 g. The stage tips were washed three times with 25 µL buffer A and spun for 1 min at 500 g after each washing step. The adapter and stage tips were put in new tubes. The samples were loaded (200 µL) and washed with 100 µL buffer A (3 minutes at 500 g). After that, the samples were bound on the C18 polymer. Again, a tube change was done for elution. 40 µL buffer B was slowly added to the new tubes and spun for 2 minutes at 300 g.

The samples were dried by speedvac at room temperature for 45 minutes. They were stored in the proteomics facility at -20 °C and analyzed by proteomics specialists.

Table 31: Material for Mass Spec preparation & Stage Tip

Material	Supplier	Catalog No.	Lot. No.
Urea	Sigma-Aldrich	U1250	SLBW0964
Ammonium Bicarbonate	Sigma-Aldrich	09830	BCBQ6426V
DTT	AppliChem	A1101, 0025	8R009950
Trypsin MS approved	Serva	37286.03	170741
Pierce™ BCA Protein Assay Kit	Thermo Fisher Scientific (REF: 23227)		
2-Iodoacetamide	Merck	8.04744.0025	L012040744 402
Methanol	VWR	83638.320	18Z2149
Buffer A: 0,1% formic acid 10 mL MS-grade water 10 µL formic acid	VWR	84867.290	DP641408
Buffer B: 80% ACN, 0,1% formic acid 1 mL MS-grade water 4 mL acetonitrile 5 µL formic acid	Fisher Scientific	LS122-500	192016
C18 polymer for stage tips	3M	34-8715-1013-6	320837D

3.19 Interactome preparation

To perform the interactome analysis for the KO cell lines, mIMCD3 cells lacking NPHP9 or NPHP10 were seeded. Lipofectamine transfection (see section 3.2.2) was carried out using V5.*hNPHP9*, V5.*hNPHP10*, and pcDNA6/V5.HisC as a control. After 48 hours of incubation at 37°C, the cells were harvested and washed with PBS. The cells were then scraped into 8 mL

of ice-cold PBS and transferred to a 15 mL tube. A 5-minute centrifugation step at 1500 rpm and 4°C followed, after which the supernatant was discarded. The cell pellets were resuspended in 300 µL of modified RIPA buffer (without SDS), and the cells were lysed on ice for 15 minutes. The lysates were then sonicated for 30 seconds. Following sonication, the cell lysates were centrifuged at full speed for 15 minutes at 4°C. The supernatant was carefully transferred to a fresh tube. A 50 µL aliquot of the lysate was mixed with 50 µL of Laemmli buffer and heated at 95°C for 5 minutes. The remaining lysate was stored at –20°C.

For immunoprecipitation, 1 µg of the V5 antibody was added to each tube, and the samples were incubated for 1 hour at 4°C with rotation. Next, 50 µL of Protein G beads were added to each sample, and the tubes were incubated overnight at 4°C with rotation.

The following day, the samples were subjected to elution for mass spectrometry. The cells were washed three times with modified RIPA buffer and centrifuged at 2000 rpm for 2 minutes at 4°C. The buffer was almost completely removed from the beads, and 60 µL of 5% SDS in PBS was added. The samples were heated at 95°C for 5 minutes, then centrifuged at full speed for 5 minutes. 60 µL of the supernatant was transferred to a fresh tube for further processing.

Reduction was performed by adding 200 mM DTT in 50 mM ammonium bicarbonate to the samples to achieve a final concentration of 10 mM. The samples were incubated at room temperature for 30 minutes. Alkylation was then carried out by adding 200 mM iodoacetamide (in 50 mM ammonium bicarbonate) to the samples , followed by a 30-minute incubation in the dark at room temperature. Finally, the samples were stored at –20°C until submission to the proteomics facility. Further processing of the samples and data analysis was then performed by the CECAD Proteomics Facility. iBAQ was used for the calculation of the t-test. Cilium-associated proteins were identified by applying keyword-focused filters to the dataset.

Table 32: Material for Interactome preparation

Material	Supplier
mIMCD3 Nphp9 -/- cells	-
mIMCD3 Nphp10 -/- cells	-
pcDNA6/V5.His cells	-
PBS	See Table 2
Mod. RIPA buffer	See Table 15

Laemmli	See Table 15
V5. antibody	Serotec
Protein G beads	Life Technologies
DTT	Thermo Fisher
Ammounium bicarbonate	Sigma-Aldrich
2-Iodoacetamide	Merck

3.20 PamGene

3.20.1 Principle

PamGene Serine / Threonine kinase assay was performed to determine kinase activity in the *NEK8* and *SDCCAG8* deficient cell samples which were created by CRISPR/Cas9. 144 serine / threonine kinase peptide substrates were immobilized on a chip and incubated with lysates containing kinases. The aim was to identify changes in phosphorylation in the two different knockout cell lines compared to the control wild type cell line. The experiment was run in four biological replicates of each mIMCD3 WT Subclone #8, CRISPR D1 II (*Nek8*) and E8 (*Sdccag8*).

3.20.2 Mix preparation

First, a BCA assay was done to determine protein concentration in each sample (see 3.6). Next, the “lysate dilution mix” and the “basic mix” were prepared. Shortly before adding to the arrays, these two mixes were combined, resulting in the “total mix” or sample mix. This was done to avoid contact between kinases and adenosine triphosphate (ATP) without a substrate being present.

The lysate dilution mix for each sample itself consisted of the sample and mammalian protein extraction reagent (M-PER) buffer with protease and phosphatase inhibitor. The basic mix consisted of ultrapure water (Mili Q), 10x PK buffer, 100x BSA, serine/threonine kinase (STK) antibody mix and 4mM ATP.

In the end, a detection mix, made of ultrapure water, 10x antibody buffer and STK antibody fluorescein isothiocyanate (FITC)-labelled, was prepared and applied.

3.20.3 Workflow

The program was started on the computer and the PamStation12 was filled with two syringes. Three PamChips with four arrays each were placed into the machine and the fluid barrier was

checked as well as the glasses. Then, 30 µL washing solution (1x PK wash buffer) were added. The blocking and washing steps followed, lasting 30 minutes.

The next step was to combine “lysate dilution mix” and “basic mix” and add 40 µL of this “sample mix” to each array. After incubation and washing for 110 minutes, 30 µL of the “detection mix” was added to each array and incubated. After 50 minutes, the arrays were once more washed. The final step was the BioNavigator analysis of kinase activity by Pamgene.

Table 33: Material for PamGene assay

Material	Supplier	Catalog No.
PamStation®12 System	PamGene	31500
Serin threonine Kinase PamChip®	PamGene	32501
STK reagent kit	PamGene	32201
M-PER™ Mammalian Extraction Buffer	Thermo Fisher Scientific	78503
Halt™ Phosphatase Inhibitor Cocktail (100x)	Thermo Fisher Scientific	78428
Halt™ Protease Inhibitor Cocktail, EDTA free (100x)	Thermo Fisher Scientific	78437
Ultrapure water	Nephrolab	

3.21 Vectors (Plasmids)

Table 34: Vectors (Plasmids)

Name	Purpose
hGlis2 pENTR1A Be -> cloning *SDCCAG8* & *NEK8*	Separate pENTR1A & hGlis2 and use pEntR1A as a backbone for *SDCCAG8* / *NEK8*
F9.m mNPHP9/*NEK8* WT FL pcDNA6	Clone *NEK8* into pcDNA6 backbone
pgLAP1 (N-term GFP)	GFP-tag for *SDCCAG8* / *NEK8*
pgLAP2 (N-term FLAG)	FLAG-tag for Sdccgag8 / *NEK8*

pOG44	Recombination
F9.GFP pcDNA6	Transfection control
SDCCAG8 pgLAP1	Created by Flp-In system
SDCCAG8 pgLAP2	Created by Flp-In system
NEK8 pgLAP1	Created by Flp-In system
NEK8 pgLAP2	Created by Flp-In system
pSpCas9(BB)-2A-GFP	Ordered for CRISPR-Cas9 cloning
SDCCAG8 sgRNA #1 pSpCas9(BB)-2A-GFP	Created by cloning sgRNA into the vector
SDCCAG8 sgRNA #3 pSpCas9(BB)-2A-GFP	Created by cloning sgRNA into the vector
NEK8 sgRNA #2 pSpCas9(BB)-2A-GFP	Created by cloning sgRNA into the vector
NEK8 sgRNA #3 pSpCas9(BB)-2A-GFP	Created by cloning sgRNA into the vector

3.22 Primer

Table 35: Primer

Name	Sequence	Purpose
m*SDCCAG8* MluI fw	5'-CCCGCGACGCGTATGGCGAAGTCCCCAGGGAAC –'3	Cloning *SDCCAG8* into pENTR1A backbone
m*SDCCAG8* Not1 rv	5'-CCCGCGGCGGCCGCTCAGCAATCAGATTGTGGCA -3'	Cloning *SDCCAG8* into pENTR1A backbone
m*SDCCAG8* Fw 1	5'-ATGGCGAAGTCCCCAGGGAA -3'	Sequencing *SDCCAG8*-pENTR1A
m*SDCCAG8* Fw 2	5'-CCAGTCTCAATATATCCACC -3'	Sequencing *SDCCAG8*-pENTR1A

m*SDCCAG8* Fw 3	5'-ATGCTTCTGAGGAAAGACTT-3'	Sequencing *SDCCAG8*-pENTR1A
m*SDCCAG8* Fw 4	5'-AGCTGGAGAGGCAGACAGAA -3'	Sequencing *SDCCAG8*-pENTR1A
m*SDCCAG8* Fw 5	5'-CCAGGAAATAGAGAAGTTGA-3'	Sequencing *SDCCAG8*-pENTR1A
m*SDCCAG8* Fw 6	5'-TCACTAAAGAGCAGATCGCA-3'	Sequencing *SDCCAG8*-pENTR1A
m*SDCCAG8* fw Primer 7	5'-CACCATGCACAACCTCGTTC-3'	Sequencing *SDCCAG8*-pENTR1A
mNPHP10 rv 8	5'-GCCATCGTCACATTCTGACG-3'	Sequencing *SDCCAG8*-pENTR1A
mNPHP10 fw 9	5'-GACAAGTGCCATGAGCAGGT -3'	Sequencing *SDCCAG8*-pENTR1A
mNPHP9 mlu 1 fp	5'-CGCGGGACGCGTATGGAGAAGTACGAGCGGAT -3'	Cloning *NEK8* into pENTR1A
mNPHP9 not 678 rp	5'-CGCGGGGCGGCCGCCTCAGGGGGGAACTGGTTCAT-3'	Cloning *NEK8* into pENTR1A
mNPHP9 rv	5´-CATAGTACTCGATGACGTTG-3	Sequencing *NEK8*-pENTR1A
mNPHP9 187 FP	5'-CTGCTACATCTCCCCTGAGC-3'	Sequencing *NEK8*-pENTR1A

mNPHP9 346 FP	5‘-TTAGCAGTCCCCTGAGGTTG-3‘	Sequencing *NEK8*-pENTR1A
mNPHP9 506 FP	5‘-TTAGCAGTCCCCTGAGGTTG-3‘	Sequencing *NEK8*-pENTR1A
mNPHP9 945 fp	5‘-GCCACTGTCTTCGGTCTACG-3‘	Sequencing *NEK8*-pENTR1A
mNPHP9 1281 fp	5‘-GTGTTTAGGTCACGGCAACC -3‘	Sequencing *NEK8*-pENTR1A
mNPHP9 1496 fp	5’-CAGGACAGGAAGCTCAGAGA -3’	Sequencing *NEK8*-pENTR1A
SDCCAG8 Exon 1 Fw	5’-GGCCTGTCCTCGGAGGGGTG -3’	PCR & Sequence *SDCCAG8* Exon 1 to show that it is mutation free
SDCCAG8 Exon 1 Rv	5’-GGCTGTGGAGGAAGACGACC -3’	PCR & Sequence *SDCCAG8* Exon 1 to show that it is mutation free
SDCCAG8 Exon 3 Fw	5’-GCTGTGTGGCCTTTGAGGGA -3’	PCR & Sequence *SDCCAG8* Exon 3 to show that it is mutation free
SDCCAG8 Exon 3 Rv	5’-CTGAAGCTAAGCTGGGAGGC -3’	PCR & Sequence *SDCCAG8* Exon 3 to show that it is mutation free
NEK8 Exon 2 Fw	5’-GGATTGTGCACCTGTGCCTG -3’	PCR & Sequence *NEK8* Exon 2 to show that it is mutation free
NEK8 Exon 2 Rv	5’-CTGGAGGGTGACGGCCCCTC -3’	PCR & Sequence *NEK8* Exon 2 to show that it is mutation free

NEK8 Exon 3 fw	5'-GCAGATCCTGCTGGCTCTGC -3'	PCR & Sequence *NEK8* Exon 3 to show that it is mutation free
NEK8 Exon 3 rv	5'-AGGGCCATCTAGACAGGGAC -3'	PCR & Sequence *NEK8* Exon 3 to show that it is mutation free
m*NEK8* Exon3 rv2	5'-AGGACTGTGGAGCAAGCCTC -3'	PCR & Sequence *NEK8* Exon 2 to show that it is mutation free
m*NEK8* Exon 3 fw2	5'-GCGCTGCAACTCTCTGCTAG -3'	PCR & Sequence *NEK8* Exon 2 to show that it is mutation free
m*SDCCAG8* sgRNA1 top	5'-CACCGAGATTCGGAGCAACTCACCC -3'	Creating oligos for sgRNA targeting *SDCCAG8* Exon 1
m*SDCCAG8* sgRNA1 bott	5'-AAACGGGTGAGTTGCTCCGAATCTC -3'	Creating oligos for sgRNA targeting *SDCCAG8* Exon 1
m*SDCCAG8* sgRNA3 top	5'-CACCGGTTGCGTCAACAAACAAATA -3'	Creating oligos for sgRNA targeting *SDCCAG8* Exon 3
m*SDCCAG8* sgRNA 3 bott	5'-AAACTATTTGTTTGTTGACGCAACC -3'	Creating oligos for sgRNA targeting *SDCCAG8* Exon 3
m*NEK8* sgRNA 2 top	5'-CACCGGGCGGCCCAGAACGAGTGCC -3'	Creating oligos for sgRNA targeting *NEK8* Exon 2
m*NEK8* sgRNA 2 bott	5'-AAACGGCACTCGTTCTGGGCCGCCC -3'	Creating oligos for sgRNA targeting *NEK8* Exon 2

m*NEK8* sgRNA 3 top	5'-CACCGTCTTGACAAACACCGCATGG -3'	Creating oligos for sgRNA targeting *NEK8* Exon 3
m*NEK8* sgRNA 3 bott	5'-AAACCCATGCGGTGTTTGTCAAGAC -3'	Creating oligos for sgRNA targeting *NEK8* Exon 3
SDCCAG8 Exon 2 qPCR fw	5'-TCCTTCCACCAGCATCAACG -3'	qPCR for Validation of CRISPR clones
SDCCAG8 Exon 3 qPCR rv	5'-CAACTTTCGTCTTCGCGGTG -3'	qPCR for Validation of CRISPR clones
SDCCAG8 Exon 4 qPCR fw	5'-CACCATGCACAACCTCGTTC -3'	qPCR for Validation of CRISPR clones
SDCCAG8 Exon 5 qPCR rv	5'-CCTCAATGTCTCCTCCGGTC -3'	qPCR for Validation of CRISPR clones
NEK8 Exon 2 qPCR fw	5'-TCAACCACCCCAACGTCATC -3'	qPCR for Validation of CRISPR clones
NEK8 Exon 3 qPCR rv	5'-TCTAGCAGAGAGTTGCAGCG -3'	qPCR for Validation of CRISPR clones
NEK8 Exon 4 qPCR fw	5'-TGCTACATCTCCCCTGAGCT -3'	qPCR for Validation of CRISPR clones
NEK8 Exon 5 qPCR rv	5'-TGTACCGGTCAGAGATGGGT -3'	qPCR for Validation of CRISPR clones
m-ACTB fp1	5'-AAGAGCTATGAGCTGCCTGA -3'	qPCR for Validation of CRISPR clones (housekeeping gene)

m-ACTB rp1	5'-TACGGATGTCAACGTCACAC-3'	qPCR for Validation of CRISPR clones (housekeeping gene)
m-HPRT1 fp	5'-GCTGACCTGCTGGATTACAT-3'	qPCR for Validation of CRISPR clones (housekeeping gene)
m-HPRT1 rp	5'-TTGGGGCTGTACTGCTTAAC-3'	qPCR for Validation of CRISPR clones (housekeeping gene)

3.23 Chemicals, Reagents & Solutions

Table 36: Chemicals, Reagents & Solutions

Chemicals	Catalog No.	Company
1M N-(2-Hydroxyethyl) piperazine-N'-(2-ethanesulfonic acid) (HEPES)	H0887	Sigma
37% Formaldehyde	4979.1	Th.Geyer
Agarose	A9539	Sigma
Ammonium persulfate (APS)	A1142, 0250	Applichem
Bovine Serum Albumin (BSA)	A9418	Sigma
Bromophenol blue	A512	Carl Roth
Chloroform	1.02445.1000	Merck
Coumaric acid	C9008	Sigma
Dimethyl sulfoxide (DMSO)	A3672, 0100	AppliChem
Dithiothreitol)	R0862	Thermo Fisher
DMEM plus Glutamax	31966-021	Gibco
dNTPs (100 mM)	R0182	Thermo Fisher

Dulbeccos's Modified Eagle Medium (DMEM)	D6429	Sigma
Ethanol 99%	A5007	Applichem
Ethanol absolute	9065	Carl Roth
Ethidiumbromide solution (1%)	2218	Carl Roth
Ethylenediaminetetraacetic acid disodium salt dihydrate (EDTA)	60-00-4	Sigma
Fetal Bovine Serum (FBS)	10270-106	Gibco
Gene Ruler 50bp DNA Ladder	35050-038	Thermo Fisher
Glutamax	35050-038	Gibco
Glycerol	3787	Carl Roth
Glycine	3908.3	Carl Roth
Hydrogen Peroxide 30%	8070.4	Carl Roth
Incidin Plus	225194	Igefa
Isopropanol	5752.3	Carl Roth
Lipofectamine®-2000	11668-027	Invitrogen
Luminol	9253	Fluka
Methanol	4627	Carl Roth
$MgCl_2$	1.05833.0250	Merck
Tetramethylethylenediamine (TEMED)	2367	Carl Roth
Na_2HPO_4	S9390	Sigma
Normal Donkey Serum (NDS)	017-000-121	Jackson
Opti-MEM®	31985-047	Invitrogen

PageRuler™ Plus Prestained Protein Ladder, 10 to 250 kDa	26619	Thermo Scientific
Paraformaldehyde (PFA)	P6148	Sigma
Penicillin-Streptomycin 10.000 U/mL	15140-122	Gibco
Polyacrylamide	T802	Carl Roth
Prolong Diamond + DAPI	P36971	Thermo Fisher
RNase-free water Ultra Pure	10977-035	Invitrogen
Sodium dodecyl sulfate SDS	A2263, 0500	AppliChem
Sodium chloride (NaCl)	S5886	Sigma
Sodium fluoride	S-1504	Sigma
Sodium (tetra-) diphosphate decahydrate	106591	Merck
SYBR Green		
TE buffer	60191	Invitrogen
Tris Hydrochloride (HCl)	9090.3	Sigma
Normal Donkey Serum	A4975, 1000	Applichem
Tris Base	T1503	Sigma
Trypsin-EDTA, 1x	25300	Gibco
Tween®20 (Polysorbat 20)	3472	Caesar & Lorentz
Water PCR Reagent	R2523	Sigma

4 Results

4.1 Stable cell lines with SDCCAG8 and NEK8 overexpression

We generated several stable mouse inner medullary collecting duct (mIMCD3) cell lines using the Flp-In system. This approach was applied as it allows a stable integration of a single copy of a transgene, typically resulting in low, almost physiological expression levels. In brief, mIMCD3 FLP-IN cells were co-transfected with the specific targeting vector and a plasmid encoding for the flp recombinase followed by selection with hygromycin. Immunofluorescence stainings and immunoblots were performed to validate both expression levels and localization of NEK8 and SDCCAG8. We first investigated whether stably expressed SDCCAG8-GFP protein localized to primary cilia (Fig. 3). The control cell line expressing GFP-GFP showed an unspecific GFP signal in the cytoplasm. The ciliary markers acetylated tubulin (AcTub) and ADP-ribosylation factor-like protein 13B (ARL13B) showed coherent signals at the primary cilium (Fig. 3). In line with a previous publication[85], SDCCAG8-GFP localized to the ciliary base represented by a GFP signal at the ciliary base (Fig. 3).

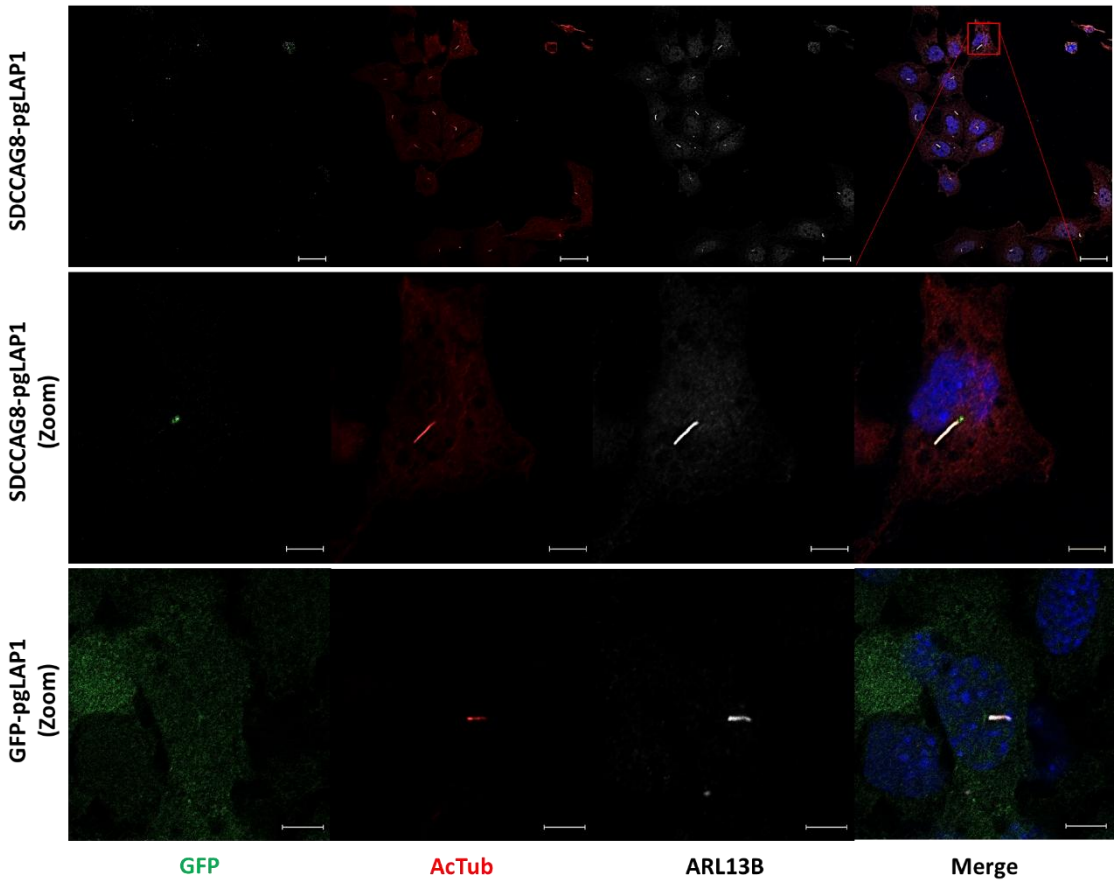

Figure 3: Subcellular localization of SDCCAG8.GFP in the stable mIMCD3 cell line.
Confocal microscopy of mIMCD3 cells stained for cilia with an antibody directed against acetylated tubulin (red) or against ARL13B (grey) and for GFP-tagged protein of interest SDCCAG8-GFP (green) with DAPI counterstaining (blue). The scale bars correspond to 20 µm in the non-zoomed images and 5 µm in the zoomed images.

We further analyzed the localization of NEK8.GFP which did not show any ciliary localization (Fig. 4). Both ciliary markers (acetylated tubulin and ARL13B) confirmed the presence of cilia, but a signal for NEK8.GFP could neither be identified in the cilium nor in the nucleus. It rather showed a cytoplasmic localization pattern.

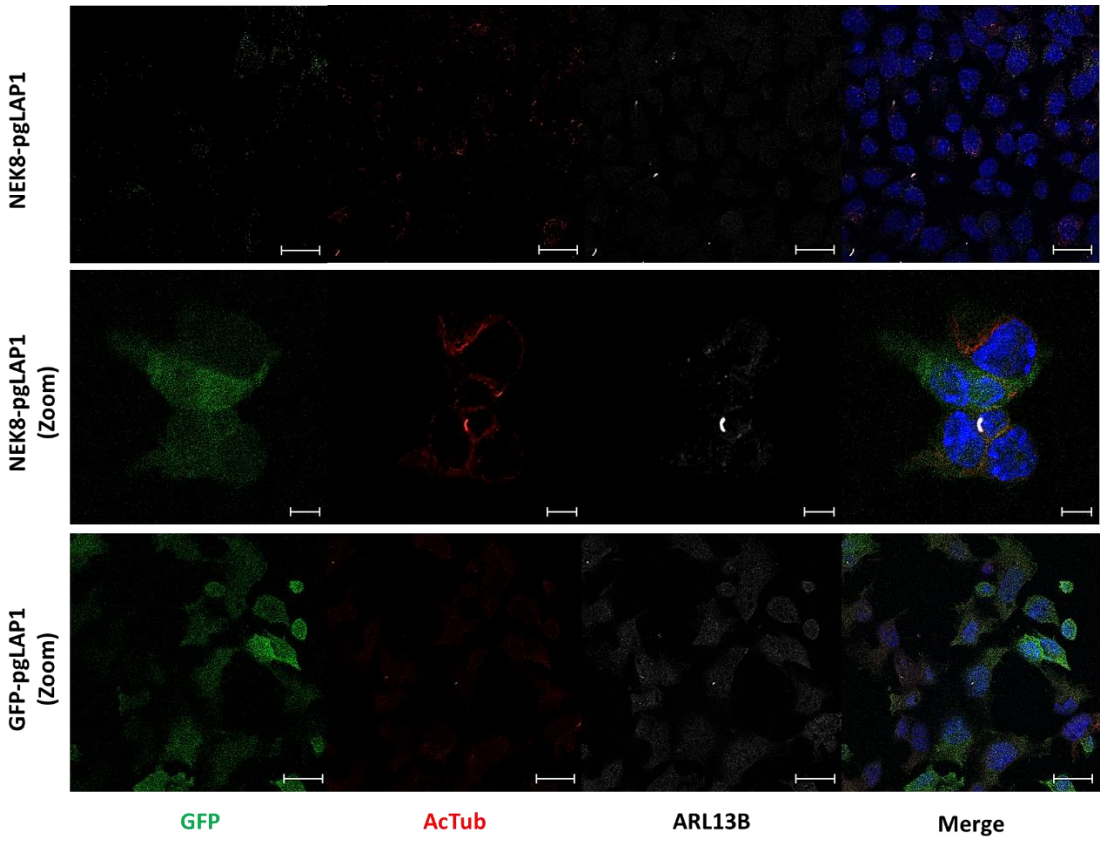

Figure 4: Subcellular localization of NEK8.GFP in the stable mIMCD3 cell line.

Confocal microscopy of mIMCD3 cells stained for cilia with an antibody directed against acetylated tubulin (red) or against ARL13B (grey) and for GFP-tagged protein of interest NEK8-GFP (green) with DAPI counterstaining (blue). The scale bars correspond to 20 µm in the non-zoomed images and 5 µm in the zoomed images.

For the FLAG-tagged SDCCAG8 cell lines we used anti-FLAG and anti-SDCCAG8 antibodies (Fig. 5A/B). A clear localization pattern for SDCCAG8-FLAG protein could not be confirmed. In fact, there was lower FLAG signal in the SDCCAG8-FLAG cells compared to the FLAG control cells. Alternatively, the signals in the SDCCAG8-FLAG cells and the FLAG cells were compared applying a human SDCCAG8 antibody (Fig. 5B). SDCCAG8 could be identified at the ciliary base in the SDCCAG8-FLAG cells, but not in the control cells, reflecting higher expression levels in the SDCCAG8-FLAG cell line. Additionally, untransfected human embryonic kidney cells (HEK293T) stained with an anti-human SDCCAG8 antibody showed ciliary localization of SDCCAG8 (Fig. 5C). Here, we could also demonstrate SDCCAG8 localization at the mitotic spindle pole in one of the cells, underlining its important function at

the centrosomes during cell cycle (mitosis). Anti-FLAG stainings of the stable NEK8.FLAG line did not confirm ciliary localization of NEK8 (Fig. 5D).

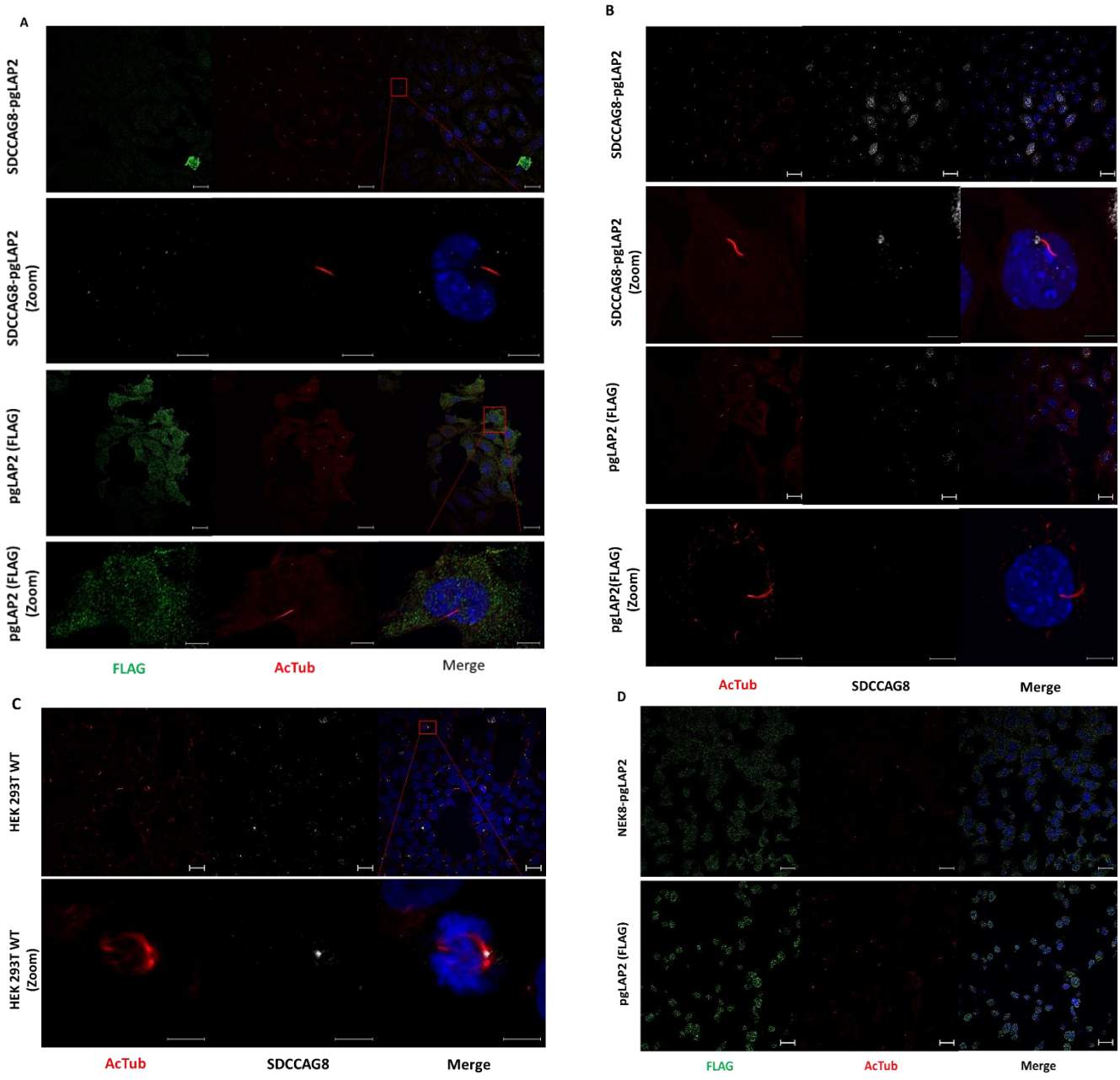

Figure 5: Subcellular localization of SDCCAG8.FLAG and NEK8.FLAG in stable mIMCD3 / HEK 293T cell lines.

Immunostaining of stable mIMCD3 cell lines expressing SDCCAG8.FLAG with anti-FLAG (green) and anti-acetylated tubulin (red). B. Immunostaining of stable mIMCD3 cell lines expressing SDCCAG8.FLAG with anti-SDCCAG8 (grey) and anti-acetylated tubulin (red). C. Immunostaining of HEK 293T cells expressing SDCCAG8.FLAG with anti-SDCCAG8 (grey) and anti-acetylated tubulin (red). D. Immunostaining of stable mIMCD3 cell lines expressing NEK8.FLAG with anti-FLAG (green) and anti-acetylated tubulin (red).

To validate the expression of SDCCAG8 and NEK8 in the cell lines, we performed immunoblots using protein lysates from the cells. An anti-GFP antibody detected GFP and GFP-GFP (GFP-pgLAP1) (Fig. 6A), both serving as positive controls. SDCCAG8-GFP protein with an expected molecular weight of 110 kDa (83 kDa SDCCAG8, 27 kDa GFP) was not detectable. NEK8-pgLAP1, however, was detectable with a molecular weight of 110 kDa (Fig. 6A). This is consistent with the expected molecular weight of NEK8-GFP protein (~75 kDa NEK8, ~27 kDa GFP). Anti-fibrillarin antibody served as a loading control. The amount of fibrillarin was almost equal in all samples with consistent bands at 34 kDa. The Western blot performed with the anti-FLAG antibody did not detect any of the proteins, neither NEK8-FLAG nor SDCCAG8-FLAG. F9.GFP, the positive control, was detectable at 27 kDa. The anti-fibrillarin loading control proved an equal amount of all samples (Fig. 6B).

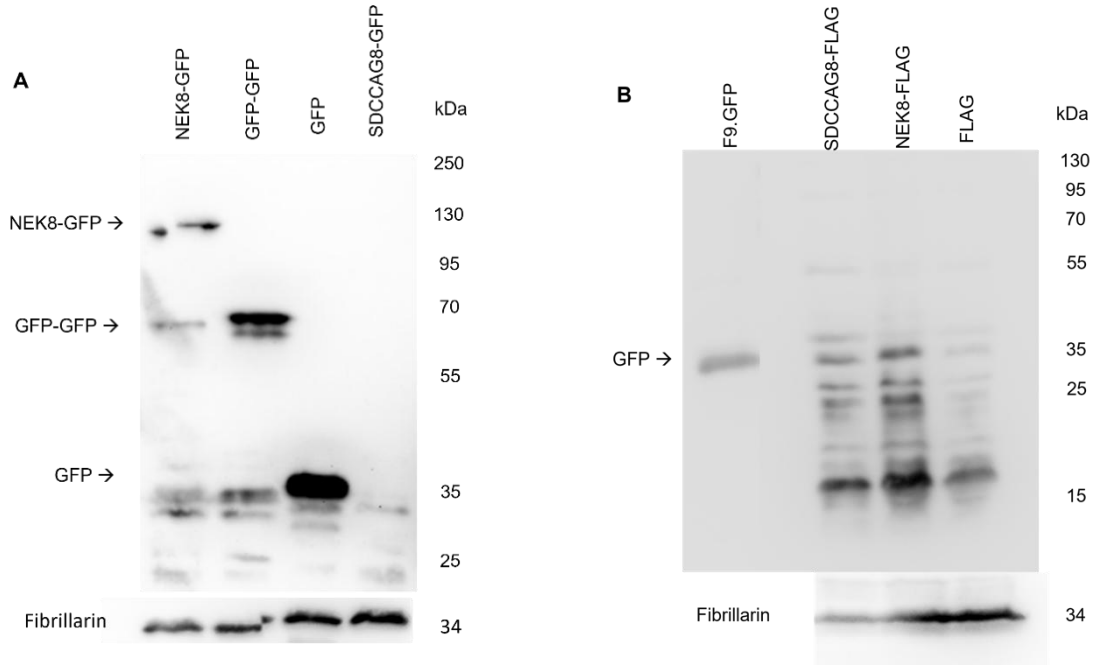

Figure 6: Validation of stable cell lines overexpressing SDCCAG8-GFP and SDCCAG8-FLAG / NEK8-GFP and NEK8-FLAG by immune blotting.

Due to the lack of protein detection in the immunoblots, overexpressed and endogenous NEK8 and SDCCAG8 were enriched by immunoprecipitation (IP) using anti-FLAG and anti-NEK8/SDCCAG8 antibodies. However, neither immunoprecipitated FLAG-tagged proteins from the cell lines nor endogenous NEK8 or SDCCAG8 from mouse IMCD3 wild-type cells could be detected (data not shown). Because of these technical constraints, we refrained from performing additional investigations, including mass spectrometry analysis.

4.2 Generation of *NPHP9* and *NPHP10* KO cell lines by CRISPR/Cas9 genome-editing

Subsequently, we aimed to establish knockout cell lines using CRISPR/Cas9 to investigate the effects of depleting NEK8 and SDCCAG8 proteins. Workflow and clone numbers are summarized in Figure 7.

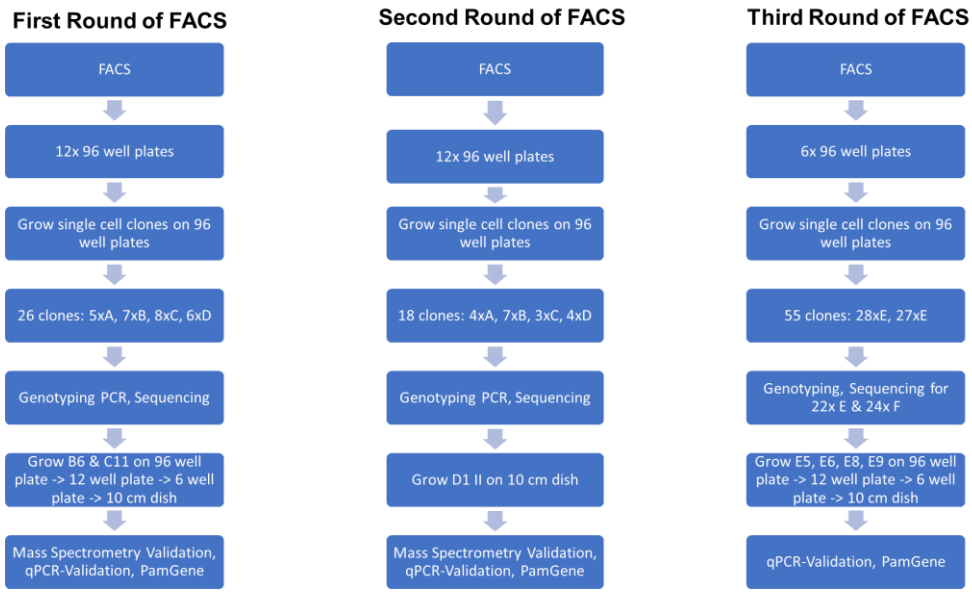

Figure 7: Summary of three rounds generating KO cell lines and number of clones obtained.

The workflow for three rounds of FACS is presented. Single-cell clones were cultured on twelve 96-well plates and subsequently analyzed. Promising clones—B6 and C11 (from round one), D1 II (from round two), and E5, E6, E8, and E9 (from round three)—were expanded on 10 cm dishes and later harvested for qPCR validation and PamGene experiment.

First:	3x 96 well plates with Sdccag8 sgRNA Exon 1 (A), 3x sgRNA Exon 3 (B)
	3x 96 well plates with Nek8 sgRNA Exon 2 (C), 3x sgRNA Exon 3 (D)
Second:	3x 96 well plates with Sdccag8 sgRNA Exon 1 (AII), 3x sgRNA Exon 3 (BII)
	3x 96 well plates with Nek8 sgRNA Exon 2 (CII), 3x sgRNA Exon 3 (D1 II)
Third:	3x 96 well plates with Sdccag8 sgRNA Exon 1 (E)
	3x 96 well plates with Sdccag8 sgRNA Exon 3 (F)

We first analyzed the target sequences in the mouse mIMCD3 wildtype cells to rule out preexisting mutations in the regions where the sgRNAs were supposed to bind. These regions were *SDCCAG8* exon 1 and exon 3 as well as *NEK8* exon 2 and exon 3. Once the absence of mutations or single nucleotid polymorhpisms (SNP) was confirmed, cells were transfected

with the pSpCas9(BB) 2A-GFP vectors, and GFP-positive cells were sorted by FACS to obtain single clones.

A total of twenty-six vital clones were genotyped and sequenced in the first round. In the end, two heterozygous *SDCCAG8*$^{-/-}$ clones (B6, C11) were identified. As the main goal was to receive homozygous KO clones, a second and a third attempt were performed. Here,18 clones out of 1152 and 55 clones out of 556 single clones were further analyzed. In summary, four SDCCAG8 clones which all showed frameshift mutations in the intronic region immediately behind exon 1 were identified [E5, E6; E8, E9 (Fig. 10)]. Clone E8 has a frameshift mutation leading to the deletion of four base pairs (GTGA). Because of the deletion of the first two base pairs (guanine and thymine), the splice donor site is disrupted (green arrow, Fig. 8). Clone E9 has a deletion of the last two base pairs (guanine and thymine), also here the splice donor site is disrupted (green sequence annotation). For *NEK8*, one clone with a homozygous one base pair insertion (D1II) leading to a frameshift and stop codon in exon 3 of *NEK8 was* identified (Fig. 8). This mutation leads to the premature termination of the amino acid chain after a span of 34 amino acids (Fig. 9). Moreover, the qPCR of all here described clones showed a significant downregulation on the mRNA level (Fig. 10).

Figure 8: Sequencing results for *SDCCAG8* clones E8 and E9 and *NEK8* clone D1 II.

In E8 and E9, the intronic splice site located behind *SDCCAG8* Exon 1 was targeted. In clone D1 II, Exon 3 of *NEK8* was targeted. This resulted in an insertion of adenine leading to a frameshift mutation and a stop-codon after seven triplets in exon 3. **c.(166_167insA) p.M29Nfs*35.**

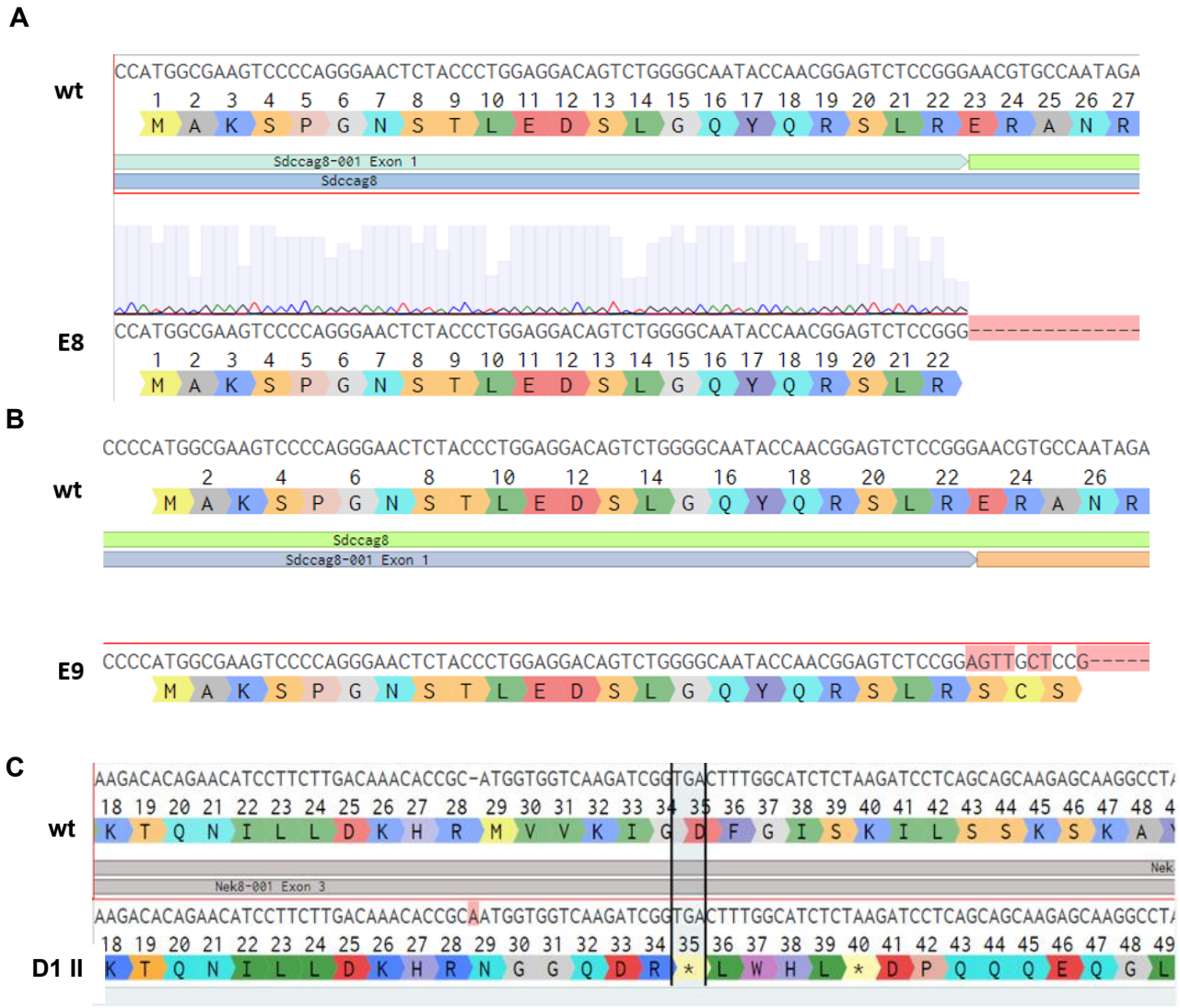

Figure 9: Point mutations of homozygous clones generated for SDAACG8 (A/B) and NEK8 (C) affecting the translated proteins.

Clones E8 and E9 exhibit a shortened amino acid chain due to the disruption of splice donor sites. Clone D1II shows a frameshift after the codon for R28 leading to a stop codon after 6 extra residues.

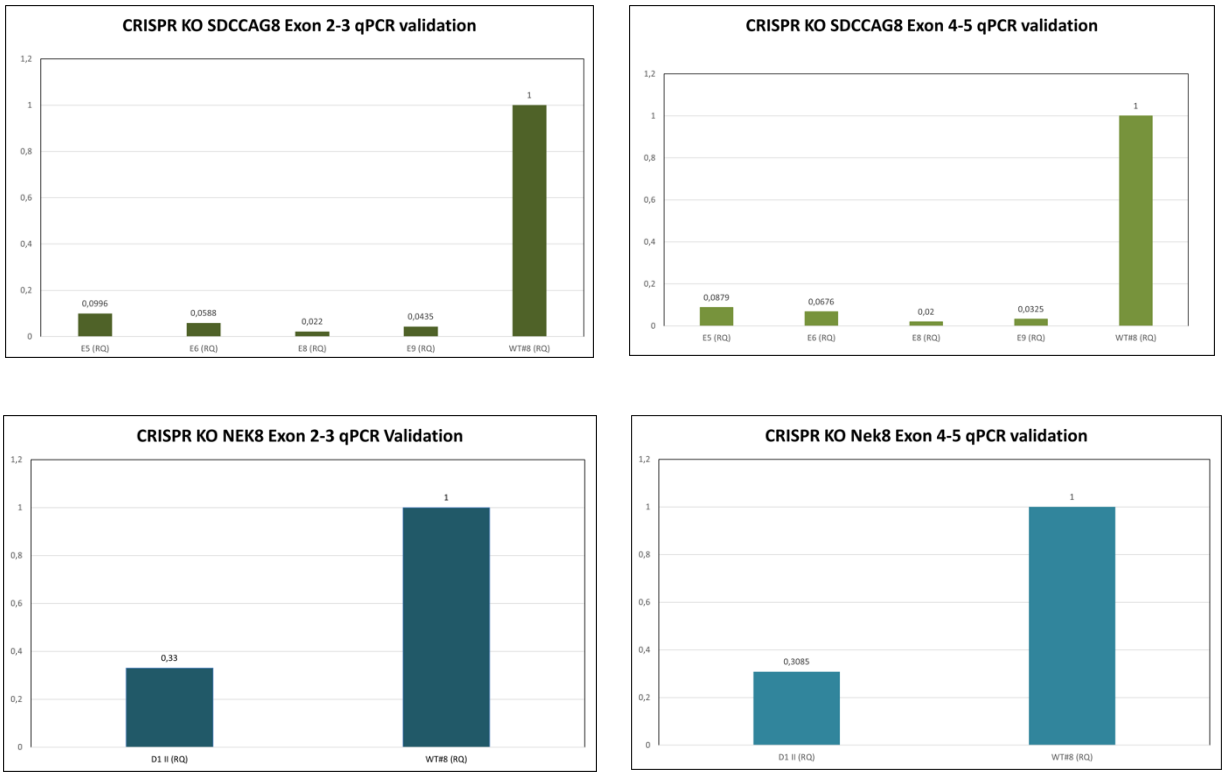

Figure 10: Analysis of homozygous SDCCAG8 and NEK8 KO clones by qPCR

Analyzed *SDCCAG8* clones E5, E6, E8 and E9 are shown in relation to WT cells. E5, E6, E8 and E9 which all targeted the intronic region around exon 1 show a significant downregulation of mRNA expression both with primers for exons 2 to 3 and for exons 4 to 5. Analyzed *NEK8* KO clone D1 II is shown in relation to WT cells, demonstrating loss of Nek8 expression of almost 70%.

4.3 Validation of knockout cell lines via mass spectrometry

We validated the knockout cell lines by mass spectrometry. Mass spectrometry samples were prepared for wild type cells as well as for clones B6 (targeted *SDCCAG8* Exon 3, heterozygous mutation; not shown), C11 (targeted *NEK8* Exon 2, heterozygous KO; also not shown) and D1 II (targeted *NEK8* Exon 3, homozygous mutation leading to a stop codon). Positive controls were HEK 293T cells transfected with SDCCAG8-pgLAP2 (FLAG) and NEK8-pgLAP2 (FLAG) vectors.

Overexpressed mSDCCAG8-FLAG and mNEK8-FLAG in 293T cells served as controls and were detectable. However, neither SDCCAG8 (protein ID Q80UF4) / NEK8 (protein ID Q91ZR4) wild type proteins nor SDCCAG8-KO (clone B6) / NEK8-KO (clone C11, D1 II) were detectable.

Table 37: Mass Spectrometry

					NEK8	SDCCAG8	B6	C11	D1 II	WT	
T: id	T: Protein	Majority pr	T: Protein	T: Gene na	IBAQ 293T mNEK	IBAQ 293T mSDCCA	IBAQ B6	IBAQ C1	IBAQ D1	IBAQ WT 8	N: Mol. Weight [kDa]
							IBAQ (log 10)				
1668	Q80UF4	Q80UF4	Serologically	Sdccag8	NaN	9,86603	NaN	NaN	NaN	NaN	82,978
2334	Q91ZR4	Q91ZR4	nine-protein	Nek8	9,24797	NaN	NaN	NaN	NaN	NaN	75,264

4.4 Interactome of NEK8 and SDCCAG8

Next, we used the KO cells to investigate the interactomes for NEK8 and SDCCAG8, respectively, by transient overexpression of V5.*Sdccag8* and V5.*Nek8.* Subsequently, co-immunoprecipitation with anti-V5-antibodies allowed the purification of the target proteins along with their protein complexes and their potential protein interactors, as depicted in Figure 11. We found 49 putative interactors of NEK8 (supplemental table one showing the strongest 30 interactors) and 79 interactors of SDCCAG8 (supplemental table two showing the strongest 30 interactors). The most enriched proteins are NEK8 and SDCCAG8, indicating a successful pulldown.

Relevant interactors of NEK8 were RBPJ and Rab34. RBPJ is associated with the establishment of physiological left-right asymmetry[105], while Rab34 is involved in ciliogenesis.[106]. Important interactors of SDCCAG8 were, amongst others, Pard6b and PRKCI, which are both associated with the regulation of cell polarity.[107,108]

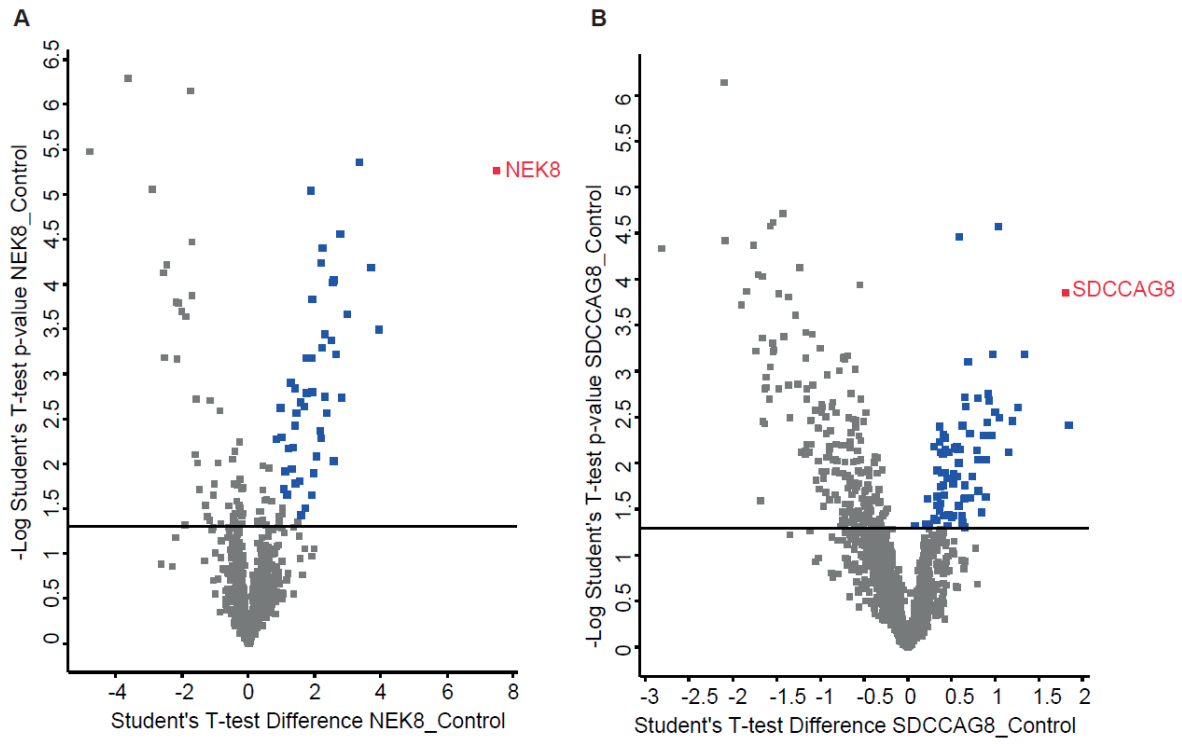

Figure 11: Interactome of NEK8 and SDCCAG8.

V5-tagged NEK8 or SDCCAG8 were expressed in the respective KO cell line. Immunoprecipitation was performed with anti-V5 antibody and Protein G beads followed by MS/MS analysis of the precipitates. The bait is highlighted in red. The horizontal axis represents the Student's T-test Difference, while the vertical axis shows the -log10 (p-value) from the Student's t-test, indicating the statistical significance of the results. Significantly enriched proteins are highlighted in blue. (A) Volcano plot of NEK8 interactors. (B) Volcano plot of SDCCAG8 interactors.

4.5 Exploring associated pathways and networks through PamGene kinase assay

In pursuit of delineating the pathways and networks associated with SDCCAG8 and NEK8, as well as assessing the activity of multiple kinases in the KO samples, we conducted a Serine-Threonine Kinase (STK)-Pam Gene kinase assay for the two most auspicious clones: D1 II (*NEK8* Exon 3) and E8 (*SDCCAG8* Exon 1).

Changes in kinase activities were anticipated in both *NEK8* and *SDCCAG8* KO cell lines. This expectation originated from NEK8's intrinsic kinase activity, and from the hypothesis that the KO of *SDCCAG8* could potentially impact the activity of kinases connected within SDCCAG8 protein networks. The Pam Gene assay uses peptides representing substrates of different serine/threonine and tyrosine kinases spotted on a chip. This chip is incubated with cell lysates and, subsequently, phosphorylation of the peptides is determined by fluorescence stainings.

Protein clustering gave an overview about phosphorylations by kinases in wild type #8, NEK8 D1 II and SDCCAG E8 cell line lysates, respectively (Fig. 12A). When comparing CRISPR clone E8 with WT, there was less kinase activity in the E8 sample, representing a possible downregulation. This is also shown in the volcano plot (Figure 12B) and the normalized kinase statistics (Fig. 12D). In these statistics, many proteins like protein kinase A (PKA), cGMP dependent protein kinase 1 (PKG1) and PKD1 showed inhibition. In the volcano plot of the *SDCCAG8* KO (E8), an inhibition of various kinases was detected, being consistent with a changed kinase activity and interaction profile. Inhibited pathways in the E8 samples were amongst others mTORC2 downstream signaling and immune response IL-4 signaling pathways, which both are associated with fibrosis development [[59,109], Fig. 12C]. Process networks affected by the knockouts were associated with cell cycle G1-S growth factor regulation, anti-apoptosis mediated by external signals by estrogen and inflammation via IL-2 signaling (Fig. 12C). Another finding was the change of specific molecular signaling events in cytosolic NF-κB signaling.

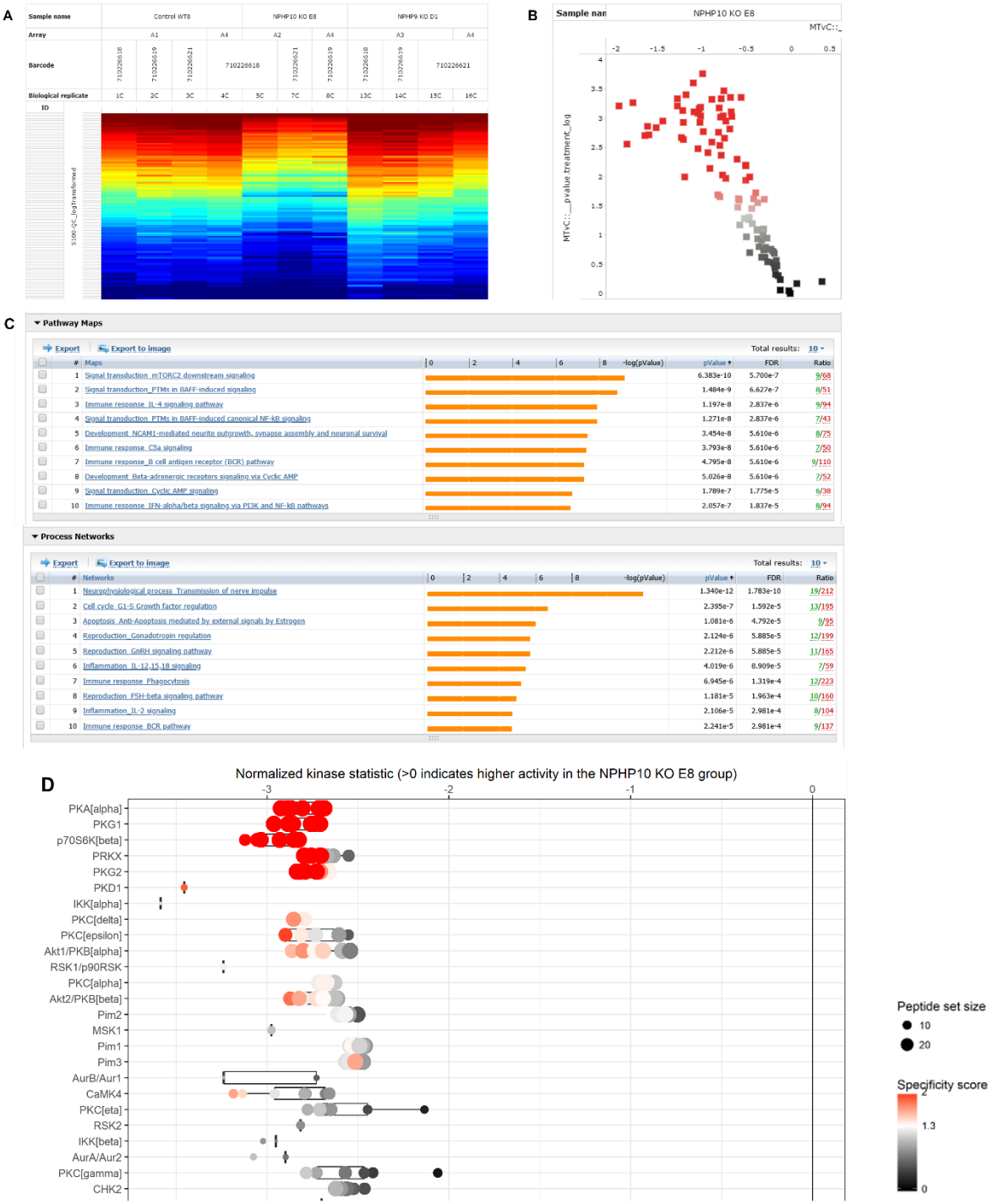

Figure 12: PamGene assay of *SDCCAG8*-KO lysates.

A. Clustering of the proteins in WT sample, E8 and D1 II sample. Red = phosphor site activated, Blue = phosphor site not activated. D1II samples exhibited increased activation, while E8 samples displayed greater inhibition. B. Volcano plot for E8. Statistically significant from log (0,05) = -1,3. Red squares in this area represent inhibited proteins (negative values). C. Pathway maps and process networks for sample E8. Orange bars represent inhibited pathways / networks. D. Normalized kinase statistics for E8 show less kinase activity of certain kinases in E8 group. Depiction of the 25 most inhibited kinases.

The clustering of sample D1 II diverged from the WT in exhibiting more activation of phosphorylation sites, as illustrated in Figure 13A. An increase of phosphorylated peptides could be shown in the volcano plot for *NEK8* knockdown sample (D1 II) (Fig. 13A). Several pathways were upregulated in a significant manner (Figure 13B): protein kinase B (AKT) signaling pathway, mTORC2 downstream signaling and immune response IL-3 signaling via ERK and Phosphoinositide 3-kinases (PI3K) pathways were more active. Especially AKT plays a crucial role in cell cycle progression and cell proliferation.[110] The associated process networks also emphasized the findings by showing upregulation of “positive regulation of cell proliferation” and “anti-apoptosis mediated by external signals via PI3KT/Akt” (Figure 13B). Akt pathway seemed to be an important upregulation in the KO as its networks are also changed. Also, mTORC2, which activates Akt signaling, is upregulated.

This was consistent with the normalized kinase statistics in which many kinases were upregulated, e.g. extracellular signal-regulated kinase 5 (ERK5), Cyclin-dependent kinase 2 (CDK2) and mitogen-activated protein kinase 10 (MAPK10), also known as c-Jun N-terminal kinase 3 (JNK3) (Figure 13C).

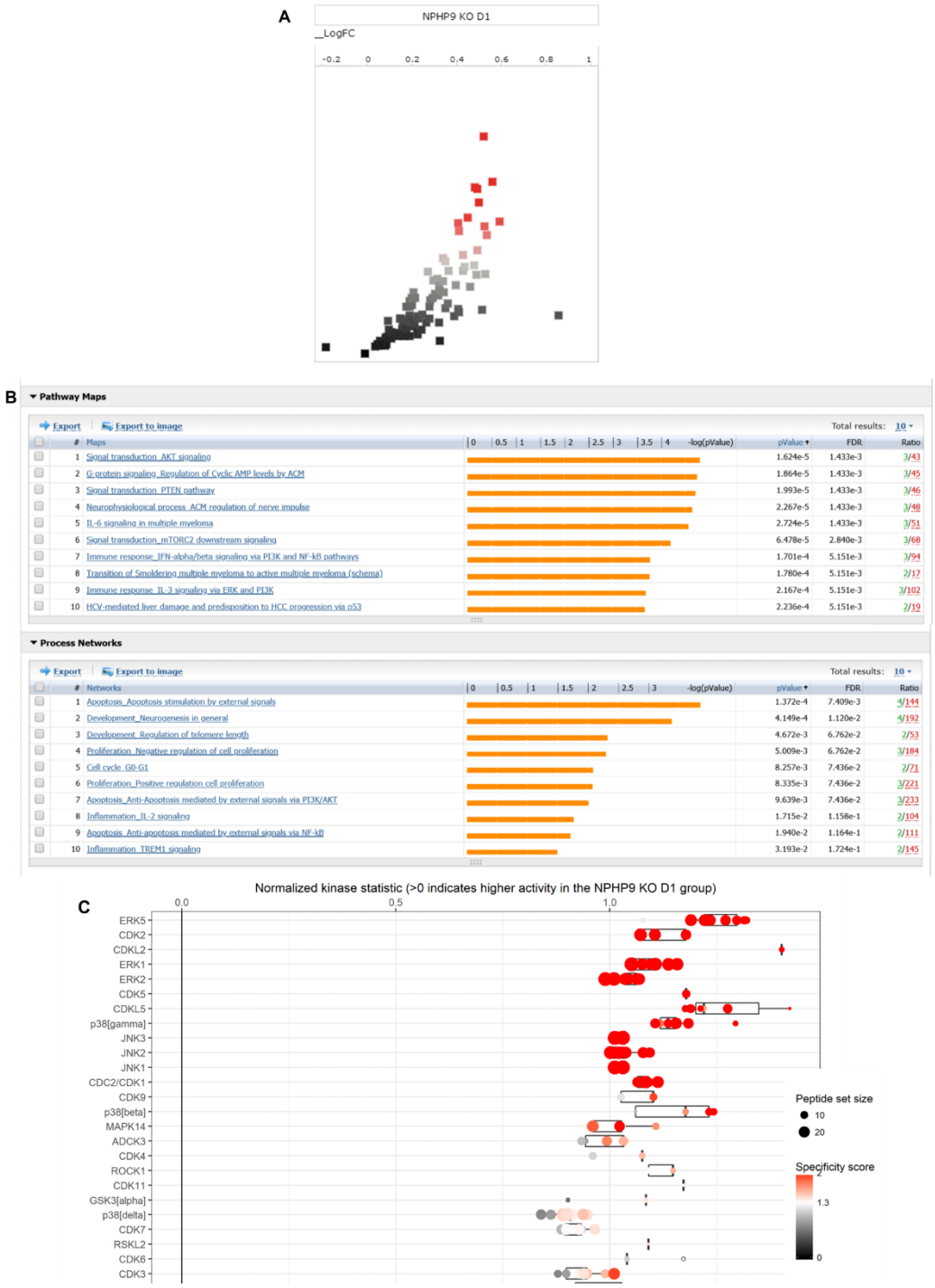

Figure 13: PamGene analysis of *NEK8*-KO lysates

A. Volcano plot for D1 II. Statistically significant from log (0,05) = -1,3. Red squares represent activated proteins. B. Pathway maps and process networks for sample D1 II. Orange bars represent activated pathways / networks. C. Normalized kinase statistics for D1 II show higher kinase activity of different kinases in D1 II group. Depiction of the 25 most upregulated kinases.

5 Discussion

In this thesis, we aimed to characterize the role of NEK8 and SDCCAG8 in cellular processes and to link the role of these proteins to the pathogenesis of NPH. For this purpose, both the Flp-In and CRISPR/Cas9 methodologies were employed to investigate the impact of both overexpression and protein depletion on kidney epithelial cells.

5.1 Challenges of NEK8 and SDCCAG8 detection in Flp-In & WT cell lines

While the technical aspects of the Flp-In approach were successful, protein detection in immunostaining proved challenging due to weak signals (Fig. 3, 4, 5). Possibly, the proteins were not abundant or stable enough to be detectable or the cells did not tolerate the addition of a third copy of the genes. This could have led to apoptosis of the cells overexpressing SDCCAG8 / NEK8 proteins. The results of the Western Blots contributed to this hypothesis, as SDCCAG8 was not detectable (Fig. 6). However, NEK8-GFP could be detected in immunoblots (Fig. 6). Intriguingly, both NEK8-GFP and NEK8-FLAG showed exclusively cytoplasmic localization in immunostainings and did not localize to the nucleus (Fig. 4,5). NEK8 as a DNA damage repair regulator is expected to be found in the nucleus.[78] Nevertheless, Liu et al. had also described the cytoplasmic localization of NEK8.[111] One could consider, that the GFP / FLAG tag or even a conformational change prevented the protein´s translocation through the nucleoporins into the nucleus, which would also affect ciliary localization. One plausible hypothesis for the ineffectual immunostainings could be attributed to the employed antibodies, which may not have recognized the epitopes of the proteins or may not be sensitive enough. The rabbit antibody against NEK8 used by us was described as exclusively human-reactive in its datasheet (https://www.genetex.com/Product/Detail/*NEK8*-antibody-N1N2-N-term/GTX112027) and had been tested for Western Blots only. In a publication by Mahjoub et al., detection of NEK8 in mIMCD3 cells was possible using a rabbit anti-mouse antibody, which underlines the hypothesis that the failing detection of mouse-NEK8 could be based in a non-species-specific antibody.[112] There is a possibility that applying the anti-mouse antibody may enhance NEK8 protein detectability. For the future, due to the lack of detection of NEK8 and SDCCAG8 by commercial antibodies, monoclonal antibodies against these proteins could be produced by the hybridoma technique.[113] Although being a complex approach, this could be a way to finally detect the proteins of interest and to perform further studies on their properties.

The lack of detection of NEK8 and SDCCAG8 could be explained by declined expression of both overexpressed and wild-type SDCCAG8 and NEK8 proteins due to passaging of the cells. Since these proteins are of low abundance, their detection may have become impossible over

time due to promotor silencing or an advantage of wildtype cells over the transgene expressing cells.

5.2 Evaluation and potential of established KO cell lines

5.2.1 Reflection on the CRISPR approach

Regarding the CRISPR/Cas9 methodology, we can summarize that three successive FACS-experiments yielded five homozygous knockout (KO) clones: *SDCCAG8* clones E5, E6, E8, E9 and *NEK8* clone D1II (Fig. 9). This relatively low number of KO could be the consequence of an increased level of cellular stress or of inefficient genome editing. However, given that a single cell clone had to expand to large colonies, it is conceivable that a considerable number of clones lacking NEK8 and SDCCAG8 had suboptimal growth conditions. At least it is imaginably that, due to increased replication stress [NEK8 loss[77]] or increased DDR [SDCCAG8 loss[85]], cell colonies did not proliferate optimally.

One of the primary objectives of our research was to establish an interactome and thus to characterize the protein complexes containing NEK8 and SDCCAG8. However, using the commercially available antibodies did not allow efficient immunoprecipitation of endogenous NEK8 or SDCCAG8. When exogenously expressing a tagged protein, this is always competing with the endogenous protein, in particular if it comes to integration in protein complexes. To address this issue, KO cells of the respective protein were transiently transfected with V5.*Sdccag8* and V5.*Nek8*, respectively (Fig. 11). This facilitated the elucidation of protein interactors. Future studies should focus on the significance of the here found potential interactors and their possible roles in ciliary biology.

5.2.2 Link to other studies and observations

In an upcoming experiment, the here applied CRISPR approach could be executed *in vivo*, for example in a mouse model, offering the possibility to perform phenotype and kidney tissue analysis.

In recent *in vivo* experiments conducted by Airik et al., *Sdccag8* gene trap mice were found to display retinal degeneration and later-onset nephronophthisis (NPH), all without showing global ciliary defects. Intriguingly, the study revealed an overactive DNA damage response signaling, indicating potential challenges in DNA stability within cells lacking *SDCCAG8.*[84] It would be highly interesting to study this in our knockout cell lines in the future.

In a study led by Liu et al., an in-depth investigation focused on jck mice unveiled the presence of a *Nek8* mutation. Examination of kidney tissues from these mice revealed cysts in the

cortical collecting ducts, with minimal involvement of the glomeruli and proximal tubules. Additionally, disturbed cell organization was noted. To establish a direct link between the observed changes and the *Nek8* mutation, morpholino antisense oligonucleotides targeting *Nek8* were introduced into zebrafish embryos. Following thorough analysis, these embryos exhibited the formation of pronephric cysts, closely resembling the observed phenotype in jck mice.[111] It is essential to clarify whether comparable observations can be discerned in tissue analyses of the here applied *NEK8*-KO cells or similar experimental conditions.

Another study by Manning et al. conducted in jck mice demonstrated a disrupted left-right asymmetry in *Nek8*-depleted cells. This finding is correlated with the observations from the interactome analysis we conducted, in which an interactor of NEK8 plays a significant role in the establishment of physiological asymmetry (see 5.3.1).[114]

5.2.3 Kinase activity in cells depleted for *SDCCAG8* or *NEK8*

The kinase activity measurement of *SDCCAG8*-KO cells revealed the inhibition of mTORC2 downstream signaling (Fig. 12C), probably resulting in less activation of Akt/PKB by mTORC2 (Fig. 12D). Akt1/PKB [alpha] and Akt2/PKB [beta] inhibition is expected to lead to less activation of NFκB by Akt, which results in more apoptosis as NFκB has anti-apoptotic effects.[115] Moreover, the tendency of the KO cells to exhibit limited growth could be explained by high apoptosis rates. NF-κB seems to play a role in the *SDCCAG8* KO cells and a suitable attempt to determine its exact significance would be specific cell death assays.

PKA activity was downregulated in the SDCCAG8-/- E8 samples (Fig. 12D). PKA is a negative regulator of the Shh pathway as it is involved in the proteolysis of Ci and Gli2.[116] After their cleavage, these transcription factors translocate into the nucleus and suppress target genes.[117] Lower PKA activity results in a more active Shh pathway due to less proteolysis and increased activity of Ci and Gli, leading to more transcription and proliferation. Many of the components of the Shh pathway localize to the primary cilium whose functionality is probably disturbed in *SDCCAG8* KO cells.[5,85] Shh is essential for mammalian development and growth: its overactivity leads to proliferation and has been described in various cancer types, while reduced activity causes developmental problems such as holoprosencephaly, craniofacial and skeletal malformations.[12,118,119] Shh-signaling has also been linked to the pathogenesis of kidney fibrosis through stimulation of myofibroblast transformation and proliferation of fibroblasts.[120] Another association exists with cyst formation in ADPKD (see 5.3).[121] Linking the data from the PamGene assay with Shh signaling, an overactive Shh signaling pathway is a possible result of a *SDCCAG8* KO and could contribute to fibroblast proliferation and NPH development. This could be investigated using a luciferase assay, in which the luciferase gene is inserted downstream of a promoter regulated by the Hedgehog signaling pathway. The more active the promoter — and thus the Hedgehog pathway — the more luciferase is produced.

When adding the subtrate luciferin, light is emitted. This resulting light emission correlates positively with the activity of the pathway.[122].

Protein Kinase G1 (PKG1) and protein kinase G2 (PKG2), also called cGMP regulated protein kinases, were also inhibited in the *SDCCAG8* KO (Fig. 12D) and their reduced activity has been associated with higher levels of pro-inflammatory and pro-fibrotic cytokines, contributing to kidney fibrosis.[123] Some of the changed pathways and kinase profiles in *SDCCAG8* KO cells were coherent with the initial hypothesis that loss of SDCCAG8 protein might result in a profibrotic environment and in NPH. However, an increase in pro-apoptotic pathways leading to cell death had not been described before in NPHP10 deficiency. This observation should be further analyzed, for example in cell death assays using the KO cells or by analysis of cell death in KO tissues. Moreover, the associated diseases which were of neurological origin should be kept in mind. As it is known that symptoms of NPH-related ciliopathies are not limited to the kidneys but also include neurocognitive and developmental disorders, this finding would be consistent with the SDCCAG8 loss.[124] It should be analyzed whether neurological impairments can be reproduced *in vivo* as well.

The *NEK8* KO intriguingly showed upregulated protein kinase B (Akt)-signaling which is linked to augmented mTORC2 activity and cell proliferation (Fig. 13B). In this pathway, PI3K is activated upon receptor binding which consequently leads to recruitment and activation of Akt. Akt activates a range of effectors, amongst others mTORC1 and mTORC2. Between mTORC2 and Akt also exists the co-activation of Akt through mTORC2.[125] Higher Akt activity is associated with DNA damage accumulation and cell proliferation, both being involved in the pathogenesis of polycystic kidney disease and NPH.[30,126] Especially NEK8 loss was associated with increased DNA damage, which makes it conceivable that high Akt-activity leading to DNA damage and uncontrolled proliferation is one of the mechanisms in the *NEK8* KO cells.[77]

Other important findings were the increased CDK, ERK and JNK activities (Figure 13C). Up to this point it was already known that NEK8 inhibits Cyclin A-CDK2 activity directly and indirectly via ATR kinase and Chk1 activation which reduces origin firing and rapid fork movement[127]. Consistently, CDK2 activity was increased in *NEK8* KO cells, being an indicator of the missing regulatory function of NEK8. Moreover, CDKL2, CDK5 and CDKL5, CDKC2/CDK1, CDK9 and CDK4 were upregulated indicating that NEK8 not only regulates CDK2 but might be regulating several cyclin-dependent kinases.

Regarding the activation of ERK5, ERK1 and ERK2, several hypotheses can be proposed. One of the more active pathways was G-protein signaling via cAMP (regulation of cyclic AMP

levels by ACM, Figure 13B). It had already been described that higher cAMP levels lead to activation of PKA which results in increased ERK signaling, being proliferative, cystogenic and mitogenic.[128,129] Recently, overactive ERK has also been linked to kidney damage by Wang et al., where it was suspected to play a role in cisplatin-induced apoptosis in cilia-deficient cells.[130] ERK was also linked to increased apoptosis in sodium channel and clathrin linker 1 (SCLT1) deficient cells.[128] The possibility of ERK serving as another effector being suppressed by NEK8 and potentially being overactive in NEK8-deficient cells requires further investigation.

An intriguing observation was that JNK3, JNK2 and JNK1 exhibited higher activity. Moreover, rise of PC1 activity, as it might occur due to NEK8 loss, was linked to increased JNK activity.[72,131] The JNK pathway is not only associated with higher rates of apoptosis, but also with cell cycle regulation, inflammation and differentiation.[131] JNK could be one of the effectors in *NEK8* KO cells responsible for hampered cell cycle regulation and increased apoptosis rates. It is also important to mention that both ERK and JNK are members of the MAP kinase family (mitogen-activated protein) whose signaling cascades are amongst others involved in proliferation and apoptosis.[132] The finding of MAPK-overactivity is also consistent with the literature on ADPKD.[133] It is known that NEK8 is involved in the pathogenesis of cystic kidney disease and NPH, and these findings might link these diseases. Intriguingly, *NEK8* nonsense mutation goes along with a cystic phenotype similar to other cystic kidney diseases, hinting to a similar pathogenesis.[68] Taking together the PamGene results, the findings for *NEK8* KO strengthened the concept that both DNA damage, disturbed cell cycle regulation and cystic kidney development are part of the pathophysiology caused by *NEK8* KO.

5.3 Interactome Analysis

NEK8 and SDCCAG8 are predominantly detected in the interactome because they were specifically immunoprecipitated using Protein G beads. The following analysis elaborates on some important interactors.

5.3.1 NEK8 and RBPJ: Role in Left-Right Asymmetry

Recombination signal binding protein for immunoglobulin kappa J region (RBPJ), a critical transcriptional mediator of Notch signaling, plays a central role in establishing physiological left-right asymmetry during development and is part of the NEK8 interactome.[134] Another protein connected to left-right asymmetry is Polaris which localizes to the primary cilium, emphasizing the significance of this organelle in orchestrating developmental processes.[135] As a ciliary kinase, NEK8 might be involved in similar mechanisms, potentially contributing to the establishment of left-right asymmetry through its role in ciliary signaling. These results are

consistent with the observations that NEK8-loss leads to pertubated left-right asymmetry development (section 2.5).

5.3.2 Rab34 and NEK8: Interplay in Ciliogenesis

Ras-related protein Rab-34 (Rab34), a centrosome-localized protein, has been identified as an interactor of NEK8. It is essential for the fusion of preciliary vesicles with the plasma membrane, a crucial step in ciliogenesis that facilitates the formation and function of primary cilia.[106] Rab34-deficient cells demonstrate impaired ciliogenesis at early stages, highlighting its importance in this process.[136] Preciliary vesicles likely deliver cargo essential for cilia formation. This underscores a potential mechanistic link in ciliary assembly and maintenance. Disruptions in this pathway could lead to defective ciliogenesis and associated signaling deficits.

5.3.3 SDCCAG8 and Its Role in Cell Polarity

SDCCAG8 interacts with several key regulators of cell polarity, including Partitioning defective 6 homolog beta (Pard6b) and Protein kinase C iota type (PRKCI). Pard6b plays a pivotal role in ensuring the proper orientation of the mitotic spindle pole, a process critical for maintaining tissue architecture. Its interaction with atypical protein kinase C (aPKC) is particularly important, as disruptions in this interdependency can lead to the formation of renal cysts.[137] aPKC is also involved in the assembly of the zonula adherens in zebrafish, a structure essential for cell polarity and organogenesis.[107] Additionally, Pard6b contributes to neurulation by guiding spindle pole orientation during mitosis.[138] SDCCAG8 has also been implicated in maintaining epithelial cell polarity. Otto et al. (2010) demonstrated that the absence of SDCCAG8 results in polarity defects in 3D renal cell cultures, emphasizing its critical role in tissue organization.[82]

PRKCI, another SDCCAG8 interactor, is also integral to the regulation of cell polarity. Deficiencies in PRKCI lead to mislocalization of adhesion molecules, resulting in disorganized polarity during epithelial cavitation.[108] This highlights the role of PRKCI in establishing and maintaining polarized cellular structures essential for organogenesis.

Further investigation is warranted to elucidate the molecular mechanisms underlying these interactions and their contributions to developmental disorders and ciliopathies.

5.4 Commonalities between NPH and PKD

It is noticeable that some of the observations made for NPH type 9 and type 10 in this thesis are consistent with other cystic kidney diseases, namely ADPKD and ARPKD. ADPKD, as it is one of the most common genetic diseases, has been extensively investigated. In ADPKD,

increased Shh signaling was associated with cyst development and inhibition of Shh reduced cyst formation.[121] The increased tendency to apoptosis in the *SDCCAG8* KO cells can be associated with early stages of ADPKD where apoptosis has a significant role in cyst development.[139] In accordance with our results for the *NEK8* KO, higher CDK activity was also linked to cyst formation in ADPKD by Zhang et al.[140] Increased activity of the Gα12/JNK apoptosis pathway, as found for the *NEK8* KO, is also present in ADPKD.[141] Moreover, higher cAMP levels leading to increase of ERK activity had been associated with cyst development in ADPKD cells.[129] The so called *jck* mice also exhibit cystic phenotypes.[72] In contrast to ARPKD which is caused by autosomal recessive mutations in the *PHKD1* gene, jck is caused by a point mutation in the *NEK8* gene.[72,142,143] As described above, mutated *NEK8* causes overexpression of PC-1 and PC-2, contributing to ciliary imbalance and cystogenesis.[72] Thus, altered signaling in our cell lines might reflect some common mechanisms of cystogenesis and fibrosis in renal ciliopathies.

5.5 Final conclusion and outlook

In this thesis, we aimed to improve our understanding of the nuclear and ciliary functions of SDCCAG8 (NPHP10) and NEK8 (NPHP9). Nephronophthisis might be a rather rare disease but the pathophysiology leading to kidney fibrosis is crucial to understand renal diseases, above all chronic kidney disease with a prevalence of approximately 13,4%.[144] To date, it has already been reported that mutations in *NPHP10* cause nephronophthisis-related ciliopathies including not only renal cysts and fibrosis but also mental impairment, retinal degeneration and schizophrenia.[85,86] NPHP9 as a ciliary kinase serves as a genome maintainer, and its loss leads to the accumulation of DNA damage, nephronophthisis, and polycystic kidney disease.[77] The results obtained in this thesis allow us to link NPH to apoptosis, increased Shh signaling, increased proliferation, and to the pathophysiology of other cystic kidney diseases, like ADPKD. As described before, individuals suffering from NPH develop chronic tubulointerstitial nephritis, corticomedullary kidney cysts, fibrosis and reduced renal concentrating ability.[41] Our analysis on the *SDCCG8*-KO pointed out pro-apoptotic and pro-fibrotic mechanisms while analyses of *NEK8*-KO revealed a proliferative and potentially cystic environment, along with an increase in DNA damage in NPH.

Finally, in vivo studies and human tissue analyses are needed to confirm and filter our observations, to characterize the phenotypes resulting from *NEK8*- and *SDCCAG8*-KO precisely and to understand more about fibrotic and cyst-causing mechanisms in order to develop therapeutic strategies.

6 Attachments

6.1 List of Figures

6.2 List of Tables

6.3 Supplemental Tables

NPHP9

Protein IDs	Majority protein IDs	Protein names	Gene names	-Log Student's T-tes	Student's T-test
Q99KF1	Q99KF1	Transmembrane emp24 domain-cc	Tmed9	5,355192173	3,353630543
Q91ZR4	Q91ZR4	Serine/threonine-protein kinase Ne	Nek8	5,259036506	7,503636837
Q1HFZ0	Q1HFZ0	tRNA (cytosine(34)-C(5))-methyltra	Nsun2	5,039745862	1,892211437
O09061	O09061	Proteasome subunit beta type-1	Psmb1	4,553591418	2,764645576
P99026	P99026	Proteasome subunit beta type-4	Psmb4	4,402412881	2,253311634
Q6PDQ2;A2A8L1	Q6PDQ2	Chromodomain-helicase-DNA-binc	Chd4	4,240627813	2,207413673
Q925H1	Q925H1	Zinc finger transcription factor Trp	Trps1	4,181359744	3,703534603
Q9D7X3	Q9D7X3	Dual specificity protein phosphata	Dusp3	4,047182943	2,586412907
P40240	P40240	CD9 antigen	Cd9	4,018230023	2,56768322
Q8CGF7	Q8CGF7	Transcription elongation regulator	Tcerg1	3,833698792	1,93766737
P47955	P47955	60S acidic ribosomal protein P1	Rplp1	3,663213018	2,986757278
O54984	O54984	ATPase Asna1	Asna1	3,491091066	3,94749403
P31266	P31266	Recombining binding protein supp	Rbpj	3,446630939	2,319552422
P45878	P45878	Peptidyl-prolyl cis-trans isomerase	Fkbp2	3,368032463	2,506743908
P60904	P60904	DnaJ homolog subfamily C membe	Dnajc5	3,293797605	2,213362694
Q8R2Q8	Q8R2Q8	Bone marrow stromal antigen 2	Bst2	3,217071229	2,653058529
O70404	O70404	Vesicle-associated membrane prot	Vamp8	3,177207901	1,91769886
Q99LD8	Q99LD8	N(G),N(G)-dimethylarginine dimeth	Ddah2	3,17528733	1,766896725
Q9Z1Z0	Q9Z1Z0	General vesicular transport factor p	Uso1	2,901680428	1,292714119
P98078	P98078	Disabled homolog 2	Dab2	2,841244163	1,409580708
P01899;P14428;P01897;	P01899;P14428;P01897;P019	H-2 class I histocompatibility antig	H2-D1;H2-K1;H2-L	2,797489074	1,944545746
Q9JMG1	Q9JMG1	Endothelial differentiation-related	Edf1	2,791310253	1,779100418
P97792	P97792	Coxsackievirus and adenovirus rec	Cxadr	2,742041894	2,308362484
Q9D1L0	Q9D1L0	Coiled-coil-helix-coiled-coil-helix c	Chchd2	2,736556843	2,82050848
Q64008	Q64008	Ras-related protein Rab-34	Rab34	2,684477989	1,567059517
Q8K2K6	Q8K2K6	Arf-GAP domain and FG repeat-con	Agfg1	2,641214478	1,698164463
Q9R1P3	Q9R1P3	Proteasome subunit beta type-2	Psmb2	2,624765993	0,973828793
O54833	O54833	Casein kinase II subunit alpha	Csnk2a2	2,572024875	1,4460783
Q93092	Q93092	Transaldolase	Taldo1	2,5654067	2,377632618

Table S1. Top 30 interactors of NPHP9 determined by mass spectrometry.

NPHP10

Protein IDs	Majority protein IDs	Protein names	Gene names	-Log Student's T-test p-value iBA	Student's T-test Diffe
P23249	P23249	Putative helicase MOV-	Mov10	4,570317769	1,03654635
O54946	O54946	DnaJ homolog subfamil	Dnajb6	4,465223578	0,591599226
Q80UF4	Q80UF4	Serologically defined cc	Sdccag8	3,858225022	1,808852077
Q8K273	Q8K273	Membrane magnesium	Mmgt1	3,188943988	1,342910051
P17897	P17897	Lysozyme C-1	Lyz1	3,18307859	0,973570347
Q9D7W5	Q9D7W5	Mediator of RNA polym	Med8	3,104156131	0,69283855
Q9D0M1	Q9D0M1	Phosphoribosyl pyropho	Prpsap1	2,750358978	0,918439269
Q8CI11	Q8CI11	Guanine nucleotide-bin	Gnl3	2,719894538	0,660102367
Q3V1V3	Q3V1V3	ESF1 homolog	Esf1	2,708637899	0,803834915
O70579	O70579	Peroxisomal membran	Slc25a17	2,683411874	0,933101416
P24788	P24788	Cyclin-dependent kinas	Cdk11b	2,616437813	0,670087337
Q60848	Q60848	Lymphocyte-specific he	Hells	2,610093209	1,265222788
P05977;P09542	P05977;P09542	Myosin light chain 1/3,	Myl1;Myl3	2,554111607	1,004065037
Q5NCR9	Q5NCR9	Nuclear speckle splicing	Nsrp1	2,496089409	1,048529029
Q9R0U0	Q9R0U0	Serine/arginine-rich spl	Srsf10	2,460024291	1,20042181
Q4VA53	Q4VA53	Sister chromatid cohesi	Pds5b	2,447216979	0,914537787
Q4FK66	Q4FK66	Pre-mRNA-splicing fact	Prpf38a	2,417358048	1,849792004
Q8R323	Q8R323	Replication factor C sut	Rfc3	2,406450538	0,633243918
Q9D0D4	Q9D0D4	Probable dimethyladen	Dimt1	2,404479408	0,366112351
Q60710	Q60710	Deoxynucleoside tripho	Samhd1	2,326919354	0,715671301
P31266	P31266	Recombining binding p	Rbpj	2,315628699	0,415455341
Q3U5H5	Q3U5H5	Splicing factor, suppres	Sfswap	2,308065111	0,966511607
Q0VGB7	Q0VGB7	Serine/threonine-prote	Ppp4r2	2,30733205	0,874258518
Q9CXL3	Q9CXL3	Uncharacterized protein	C7orf50 homolog	2,277224574	0,428416133
Q3UFS4	Q3UFS4	G patch domain-contair	Gpatch11	2,235286844	0,363269687
Q8BQZ5	Q8BQZ5	Cleavage and polyadem	Cpsf4	2,186533157	0,300251722
Q6ZWQ7	Q6ZWQ7		Spcs3	2,185349313	0,565660357
Q66GT5	Q66GT5	Phosphatidylglycerophc	Ptpmt1	2,171536194	0,542915821
Q91VT1	Q91VT1	E3 SUMO-protein ligas	Nsmce2	2,152712219	0,572125554
Q6Q477;G5E829	Q6Q477;G5E829	Calcium-transporting A	Atp2b4;Atp2b1	2,148744291	0,605044246
P97762	P97762	Retinitis pigmentosa 9	rp9	2,146745098	0,431922078
P27612	P27612	Phospholipase A-2-acti	Plaa	2,140675269	0,792401552
Q9JK83	Q9JK83	Partitioning defective 6	Pard6b	2,128641923	0,474354625
P97376	P97376	Protein FRG1	Frg1	2,123918589	0,375671148
P68181;P05132	P68181;P05132	cAMP-dependent prote	Prkacb;Prkaca	2,122508583	1,161024928
P83882	P83882	60S ribosomal protein l	Rpl36a	2,108317569	0,398783803
Q8K0C9	Q8K0C9	GDP-mannose 4,6 dehy	Gmds	2,042413734	0,813661456
Q9DCR2	Q9DCR2	AP-3 complex subunit s	Ap3s1	2,041519466	0,896444678
Q9CXI0	Q9CXI0	2-methoxy-6-polypreny	Coq5	2,006804052	0,583083868
Q8C7D2	Q8C7D2	Protein cereblon	Crbn	1,927009845	0,341663241
Q62074	Q62074	Protein kinase C iota ty	Prkci	1,903731953	0,426927805

Table S2. Top 42 interactors of NPHP10 determined by mass spectrometry.

7 References

1. Izawa I GH, Kasahara K, Inagaki M. Current topics of functional links between primary cilia and cell cycle. Cilia. 2015.
2. Veland IR, Awan, A., Pedersen, L.B., et al. Primary cilia and signaling pathways in mammalian development, health and disease. Nephron Physiology. 2009:39-53.
3. Fu J, Hagan, I.M., Glover, D.M. The Centrosome and Its Duplication Cycle. Cold Spring Harbor Perspectives in Biology. 2015.
4. Breslow DK HA. Mechanism and Regulation of Centriole and Cilium Biogenesis. *Annu Rev Biochem* 2019; **88**: 691-724.
5. Goetz SC AK. The primary cilium: a signalling centre during vertebrate development. Nat Rev Genet. 2010:331-44.
6. Garcia G, Raleigh, D.R., Reiter, J.F. How the ciliary membrane is organized inside-out to communicate outside-in. Current Biology. 2019:R421-R34.
7. Gonçalves J, Pelletier, L. The Ciliary Transition Zone: Finding the Pieces and Assembling the Gate. Molecules and Cells. 2017:243-53.
8. Abraham Z, Hawley, E., Hayosh, D., Webster-Wood, V. A., & Akkus, O. Kinesin and Dynein Mechanics: Measurement Methods and Research Applications. Journal of biomechanical engineering. 2018.
9. Fry AM, Leaper, M.J., Bayliss, R. The primary cilium: guardian of organ development and homeostasis. Organogenesis. 2014:62-8.
10. Singla V, Reiter, J.F. The Primary Cilium as the Cell's Antenna: Signaling at a Sensory Organelle. Science. 2016:629-33.
11. Abou Alaiwi WA, Lo, S.T., Nauli, S.M. Primary Cilia: Highly Sophisticated Biological Sensors. Sensors. 2009:7003-20.
12. Bangs F, Anderson, K.V. Primary Cilia and Mammalian Hedgehog Signaling. Cold Spring Harbor Perspectives in Biology. 2017.
13. Jones C, Roper, V., Foucher, I. et al. . Ciliary proteins link basal body polarization to planar cell polarity regulation. *Nat Genet* 2008; **40**: 69-77.
14. Quarmby LM PJ. Cilia and the cell cycle? *J Cell Biol* 2005; **169**(5): 707-10.
15. Walz G. Role of primary cilia in non-dividing and post-mitotic cells. Cell and Tissue Research. 2017:11-25.
16. Plotnikova OV, Pugacheva, E.N., Golemis, E.A. Aurora A Kinase Activity Influences Calcium Signaling in Kidney Cells. The Journal of Cell Biology. 2011:1021-32.
17. Goto H, Inoko, A., Inagaki, M. Cell cycle progression by the repression of primary cilia formation in proliferating cells. Cellular and Molecular Life Sciences. 2013:3893-905.
18. Woodruff JB, Wueseke, O., Hyman, A.A. Pericentriolar material structure and dynamics. Philosophical Transactions of the Royal Society B - Biological Sciences. 2014.
19. Gopalakrishnan J, Feistel K, Friedrich BM, et al. Emerging principles of primary cilia dynamics in controlling tissue organization and function. *The EMBO Journal* 2023; **42**(21): e113891.
20. Shaheen R, Szymanska, K., Basu, B., et al. Characterizing the Morbid Genome of Ciliopathies. Genome Biology. 2016:242.
21. Forsythe E, Beales, P.L. Bardet-Biedl syndrome. European Journal of Human Genetics. 2013:8-13.
22. Bergmann C, Guay-Woodford, L.M., Harris, P.C. et al. Polycystic kidney disease. Nat Rev Dis Primers. 2018.
23. Waters AM, Beales, P.L. Ciliopathies: an expanding disease spectrum. Pediatric Nephrology. 2011:1039-56.
24. Hildebrandt F, Benzing, T. Ciliopathies. 2011:1533-43.
25. van Asselt SJ, de Vries, E.G., van Dullemen, H.M., et al. Pancreatic cyst development: insights from von Hippel-Lindau disease. Cilia. 2013.
26. Igarashi P SS. Genetics and pathogenesis of polycystic kidney disease. J Am Soc Nephrol. 2002:2384-98.

27. Büscher R BA, Weber S, Mohr J, Hegen B, Vester U, Hoyer PF. Clinical manifestations of autosomal recessive polycystic kidney disease (ARPKD): kidney-related and non-kidney-related phenotypes. *Pediatr Nephrol* 2014; **29**(10): 1915-25.
28. Tay SA VA. Senior-Løken syndrome and intracranial hypertension. Ophthalmic Genet. 2020:354-7.
29. Wolf MTF. Nephronophthisis and related syndromes. Current Opinion in Pediatrics. 2016:201-11.
30. Srivastava S. ME, Raman S. and Sayer J.A. Many Genes - One Disease? Genetics of Nephronophthisis (NPHP) and NPHP-Associated Disorders. Front Pediatr. 2018.
31. Bukanov NO, Smith, L.A., Klinger, K.W., et al. Long-lasting Arrest of Murine Polycystic Kidney Disease With CDK Inhibitor Roscovitine. Nature. 2006:949-52.
32. McConnachie DJ SJ, Mallett AJ. Ciliopathies and the Kidney: A Review. Am J Kidney Dis. 2021:410-9.
33. Wolf MTF, Hildebrandt, F. Nephronophthisis. Pediatric Nephrology. 2014:181-94.
34. Simms RJ, Hynes, A.M., Eley, L., Sayer, J.A. Nephronophthisis: A Genetically Diverse Ciliopathy. International Journal of Nephrology. 2011.
35. Gupta S O-KJ, Phillips JK. Nephronophthisis-Pathobiology and Molecular Pathogenesis of a Rare Kidney Genetic Disease. Genes (Basel). 2021.
36. Hildebrandt F, Attanasio, M., Otto, E. Nephronophthisis: Disease Mechanisms of a Ciliopathy. J Am Soc Nephrol JASN. 2009:23-35.
37. Hudson R PC, Hawley CM, O'Shea S, Snelling P, Ho G, Holman K, Bennetts B, Crawford J, Francis L, Simons C, Mallett A. Adult-Diagnosed Nonsyndromic Nephronophthisis in Australian Families Caused by Biallelic NPHP4 Variants. Am J Kidney Dis. 2020.
38. Simms RJ, Eley, R., Sayer, J.A. Nephronophthisis. European Journal of Human Genetics. 2009:406-16.
39. Shastry SM, Kolte, S.S., Sanagapati, P.R. Potter's Sequence. Journal of Clinical Neonatology. 2012:157-9.
40. Salomon R, Saunier, S., Niaudet, P. Nephronophthisis. Pediatric Nephrology. 2009:2333-44.
41. Stokman M, Lilien, M., Knoers, N., et al. Nephronophthisis. GeneReviews. 2016:1993-2020.
42. Hildebrandt F SB, Nothwang HG, Gretz N, Schnieders B, Singh-Sawhney I, Kutt R, Vollmer M, Brandis M. Molecular genetic identification of families with juvenile nephronophthisis type 1: rate of progression to renal failure. APN Study Group. Arbeitsgemeinschaft für Pädiatrische Nephrologie. *Kidney Int* 1997; **51**(1): 261-9.
43. Omran H, Häffner, K., Burth, S., et al. Evidence for Further Genetic Heterogeneity in Nephronophthisis. Nephrology Dialysis Transplant. 2001:755-8.
44. Slaats GG, Lilien, M.R., Giles, R.H. Nephronophthisis: should we target cysts or fibrosis? Pediatric Nephrology. 2016:545-54.
45. Blowey DL, Querfeld, U., Geary, D., et al. Ultrasound findings in juvenile nephronophthisis. Pediatric Nephrology. 1996:22-4.
46. J N. Fibrosis and progression of autosomal dominant polycystic kidney disease (ADPKD). *Biochimica et biophysica acta* 2011; **1812**(10): 1327–36.
47. Joung JW OH, Lee SJ, Kim YA, Jung HJ. Significance of Intratumoral Fibrosis in Clear Cell Renal Cell Carcinoma. *J Pathol Transl Med* 2018; **52**(5): 323-30.
48. Wynn TA VK. Macrophages in Tissue Repair, Regeneration, and Fibrosis. *Immunity* 2016; **44**(3): 450-62.
49. Stone RC PI, Ojeh N, Chen V, Liu S, Garzon KI, Tomic-Canic M. Epithelial-mesenchymal transition in tissue repair and fibrosis. *Cell Tissue Res* 2016; **365**(3): 495-506.
50. Xu J LS, Derynck R. TGF-beta-induced epithelial to mesenchymal transition. *Cell Res* 2009; **19**(2): 156-72.
51. Sanjabi S, Zenewicz, L. A., Kamanaka, M., & Flavell, R. A. Anti-inflammatory and pro-inflammatory roles of TGF-beta, IL-10, and IL-22 in immunity and autoimmunity. *Current opinion in pharmacology* 2009; **9**(4): 447–53.

52. Ruiz-Ortega M RM, Lorenzo O, Esteban V, Blanco J, Mezzano S, Egido J. Angiotensin II: a key factor in the inflammatory and fibrotic response in kidney diseases. *Nephrology Dialysis Transplantation* 2006; **21**(1): 16-20.
53. Lemos DR MM, Karaca G, Wilflingseder J, Leaf IA, Gupta N, Miyoshi T, Susa K, Johnson BG, Soliman K, Wang G, Morizane R, Bonventre JV, Duffield JS. Interleukin-1β Activates a MYC-Dependent Metabolic Switch in Kidney Stromal Cells Necessary for Progressive Tubulointerstitial Fibrosis. *J Am Soc Nephrol* 2018; **29**(6): 1690-705.
54. Fertin C NJ, Gillery P, Kalis B, Banchereau J, Maquart FX. Interleukin-4 stimulates collagen synthesis by normal and scleroderma fibroblasts in dermal equivalents. *Cell Mol Biol* 1991; **37**(8): 823-9.
55. Takeda K TT, Shi W, Matsumoto M, Minami M, Kashiwamura S, Nakanishi K, Yoshida N, Kishimoto T, Akira S. Essential role of Stat6 in IL-4 signalling. *Nature* 1996; **380**(6575): 627-30.
56. Walford HH DT. STAT6 and lung inflammation. *JAKSTAT* 2013; **2**(4).
57. Kong X HN, Mori M, Gao B. Cytokines and STATs in Liver Fibrosis. *Front Physiol* 2012; **3**.
58. Yukawa K KM, Goda M, Liang XM, Kimura A, Tanaka T, Bai T, Owada-Makabe K, Tsubota Y, Ueyama T, Ichinose M, Maeda M, Takeda K, Akira S. STAT6 deficiency inhibits tubulointerstitial fibrosis in obstructive nephropathy. *Int J Mol Med* 2005; **15**(2): 225-30.
59. Li J, Ren, J., Liu, X., et al. Rictor/mTORC2 signaling mediates TGFβ1-induced fibroblast activation and kidney fibrosis. Kidney Int. 2015:515-27.
60. Nicholson KM AN. The protein kinase B/Akt signalling pathway in human malignancy. *Cell Signal* 2002; **14**(5): 381-95.
61. Bai D UL, Vogt PK. Akt-mediated regulation of NFkappaB and the essentialness of NFkappaB for the oncogenicity of PI3K and Akt. *Int J Cancer* 2009; **125**(12): 2863-70.
62. Xia Y SS, Verma IM. NF-κB, an active player in human cancers. *Cancer Immunol Res* 2014; **2**(9): 823-30.
63. Stewart GA HG, Ahmad SA, Jarman E, Wallace WA, Harrison DJ, Haslett C, Lamb JR, Howie SE. Expression of the developmental Sonic hedgehog (Shh) signalling pathway is up-regulated in chronic lung fibrosis and the Shh receptor patched 1 is present in circulating T lymphocytes. *J Pathol* 2003; **199**(4): 488-95.
64. Syn WK CS, Liaskou E, Karaca GF, Agboola KM, Oo YH, Mi Z, Pereira TA, Zdanowicz M, Malladi P, Chen Y, Moylan C, Jung Y, Bhattacharya SD, Teaberry V, Omenetti A, Abdelmalek MF, Guy CD, Adams DH, Kuo PC, Michelotti GA, Whitington PF, Diehl AM. Osteopontin is induced by hedgehog pathway activation and promotes fibrosis progression in nonalcoholic steatohepatitis. *Hepatology* 2011; **53**(1): 106-15.
65. Kramann R. Hedgehog Gli signalling in kidney fibrosis. *Nephrology Dialysis Transplantation*; **31**(12): 1989–95.
66. Rowitch DH S-JB, Lee SM, Flax JD, Snyder EY, McMahon AP. Sonic hedgehog regulates proliferation and inhibits differentiation of CNS precursor cells. *J Neurosci* 1999; **19**(20): 8954-65.
67. Bowers AJ, Boylan, J.F. Nek8, a NIMA Family Kinase Member, Is Overexpressed in Primary Human Breast Tumors. Gene. 2004:135-42.
68. Grampa V, Delous, M., Zaidan, M, et al. Novel NEK8 Mutations Cause Severe Syndromic Renal Cystic Dysplasia through YAP Dysregulation. PLOS Genetics. 2016.
69. Zalli D, Bayliss, R., Fry, A.M. The Nek8 Protein Kinase, Mutated in the Human Cystic Kidney Disease Nephronophthisis, Is Both Activated and Degraded During Ciliogenesis. Human Molecular Genetics. 2012:1155-71.
70. Frank V, Habbig, S., Bartram, M.P., et al. Mutations in NEK8 Link Multiple Organ Dysplasia With Altered Hippo Signalling and Increased c-MYC Expression. Human Molecular Genetics. 2013:2177-85.
71. Claus LRea. Certain heterozygous variants in the kinase domain of the serine/threonine kinase NEK8 can cause an autosomal dominant form of polycystic kidney disease. *Kidney international* 2023; **104**(5): 995-1007.
72. Sohara E, Luo, Y., Zhan, J., et al. Nek8 Regulates the Expression and Localization of Polycystin-1 and Polycystin-2. J Am Soc Nephrol JASN. 2008:469-76.

73. Hoff S, Halbritter, J., Epting, D., et al. ANKS6 is a central component of a nephronophthisis module linking NEK8 to INVS and NPHP3. Nature Genetics. 2013:951-6.
74. Otto E, Schermer, B., Obara, T. et al. Mutations in INVS encoding inversin cause nephronophthisis type 2, linking renal cystic disease to the function of primary cilia and left-right axis determination. Nat Genet. 2003:413-20.
75. Cai Y, Somlo, S. Too Much of a Good Thing: Does Nek8 Link Polycystic Kidney Disease and Nephronophthisis? J Am Soc Nephrol JASN. 2008:418-20.
76. Natoli TA, Gareski, T.C., Dackowski, W.R., et al. Pkd1 and Nek8 Mutations Affect Cell-Cell Adhesion and Cilia in Cysts Formed in Kidney Organ Cultures. American Journal of Physiology Renal Physiology. 2008:F73-83.
77. Choi HJC, Lin, J.R., Vannier, J.B., Slaats, G.G., et al. NEK8 Links the ATR-regulated Replication Stress Response and S-phase CDK Activity to Renal Ciliopathies. Molecular Cell. 2013:423-39.
78. Abeyta A, Castella, M., Jacquemont, C. et al. NEK8 Regulates DNA Damage-Induced RAD51 Foci Formation and Replication Fork Protection. *Cell Cycle* 2017; **16**(4): 335-47.
79. Habbig S, Bartram, M.P., Sägmüller, J.G., et al. The ciliopathy disease protein NPHP9 promotes nuclear delivery and activation of the oncogenic transcriptional regulator TAZ. Human Molecular Genetics. 2012:5528-38.
80. Moroishi T, Park, H.W., Qin, B., et al. A YAP/TAZ-induced feedback mechanism regulates Hippo pathway homeostasis. Genes & Development. 2015:1271-84.
81. Manning DK, Sergeev, M., van Heesbeen, R.G., et al. You have access. J Am Soc Nephrol JASN. 2013:100-12.
82. Otto EA HT, Airik R, Chaki M, Zhou W, Stoetzel C, Patil SB, Levy S, Ghosh AK, Murga-Zamalloa CA, van Reeuwijk J, Letteboer SJ, Sang L, Giles RH, Liu Q, Coene KL, Estrada-Cuzcano A, Collin RW, McLaughlin HM, Held S, Kasanuki JM, Hildebrandt F, et al. Candidate exome capture identifies mutation of SDCCAG8 as the cause of a retinal-renal ciliopathy. Nat Genet. 2010:840-50.
83. Kenedy AA CK, Loveys DA, Kato GJ, Dang CV. Identification and characterization of the novel centrosome-associated protein CCCAP. 2003:35-46.
84. Airik R SG, Guo Z, et al. Renal-retinal cilipathy gene Sdccag8 regulates DNA damage response signaling. J Am Soc Nephrol JASN. 2014:2573-83.
85. Airik R, Schueler, M., Airik, M., et al. SDCCAG8 Interacts with RAB Effector Proteins RABEP2 and ERC1 and Is Required for Hedgehog Signaling. PLoS One. 2016.
86. Insolera R, Shao, W., Airik, R. Hildebrandt, F., et al. SDCCAG8 Regulates Pericentriolar Material Recruitment and Neuronal Migration in the Developing Cortex. Neuron. 2014:805-22.
87. Sakakibara A AR, Sapir T, Tanaka T. Microtubule dynamics in neuronal morphogenesis. Open Biol. 2013.
88. Chaki M AR, Ghosh AK, Giles RH, Chen R, Slaats GG, Wang H, Hurd TW, Zhou W, Cluckey A, Gee HY, Ramaswami G, Hong CJ, Hamilton BA, Cervenka I, Ganji RS, Bryja V, Arts HH, van Reeuwijk J, Oud MM, Letteboer SJ, Roepman R, Otto EA, Hildebrandt F. Exome capture reveals ZNF423 and CEP164 mutations, linking renal ciliopathies to DNA damage response signaling. Cell. 2021:533-48.
89. Jackson SP BJ. The DNA-damage response in human biology and disease. Nature. 2009:1071-8.
90. Mah L, El-Osta, A. & Karagiannis, T. γH2AX: a sensitive molecular marker of DNA damage and repair. Leukemia. 2010:679-86.
91. Loyter A SG, Juricek D, Keene D, Ruddle FH. Mechanisms of DNA entry into mammalian cells. II. Phagocytosis of calcium phosphate DNA co-precipitate visualized by electron microscopy. *Exp Cell Res* 1982; **139**(1): 223-34.
92. Felgner PL GT, Holm M, Roman R, Chan HW, Wenz M, Northrop JP, Ringold GM, Danielsen M. Lipofection: a highly efficient, lipid-mediated DNA-transfection procedure. *Proc Natl Acad Sci U S A* 1987; **84**(21): 7413-7.
93. KB M. The unusual origin of the polymerase chain reaction. *Sci Am* 1990; **262**(4): 56-66.

94. McDonell MW SM, Studier FW. Analysis of restriction fragments of T7 DNA and determination of molecular weights by electrophoresis in neutral and alkaline gels. *J Mol Biol* 1977; **110**(1): 119-46.
95. Sanger F NS, Coulson AR. DNA sequencing with chain-terminating inhibitors. *Proc Natl Acad Sci U S A* 1977; **74**(12): 5463-7.
96. Smith PK KR, Hermanson GT, Mallia AK, Gartner FH, Provenzano MD, Fujimoto EK, Goeke NM, Olson BJ, Klenk DC. Measurement of protein using bicinchoninic acid. *Anal Biochem* 1985; **150**(1): 76-85.
97. UK L. Cleavage of structural proteins during the assembly of the head of bacteriophage T4. *Nature* 1970; **227**(5259): 680-5.
98. Schegger H. Tricine-SDS-PAGE. *Nat Protoc* 2006; **1**(1): 16-22.
99. Gültekin H HK. The use of polyvinylidenedifluoride membranes as a general blotting matrix. *Anal Biochem* 1988; **172**(2): 320-9.
100. Im K MS, Diaz MFP, Yong WH. Im K, Mareninov S, Diaz MFP, Yong WH. An Introduction to Performing Immunofluorescence Staining. *Methods Mol Biol* 2019; **1897**: 299-311.
101. Torres JZ, Miller, J.J., Jackson, P.K. High-throughput Generation of Tagged Stable Cell Lines for Proteomic Analysis. Proteomics. 2009:2888-91.
102. Hartley JL TG, Brasch MA. DNA cloning using in vitro site-specific recombination. *Genome Res* 2000; **10**(11): 1788-95.
103. Ran F, Hsu, P.D., Wright, J. et al. Genome engineering using the CRISPR-Cas9 system. Nature Protocols. 2013:2281-308.
104. Gundry RL WM, Murray CI, Kane LA, Fu Q, Stanley BA, Van Eyk JE. Preparation of proteins and peptides for mass spectrometry analysis in a bottom-up proteomics workflow. *Curr Protoc Mol Biol* 2009.
105. Krebs LT, Iwai, N., Nonaka, S., Welsh, I. C., Lan, Y., Jiang, R., Saijoh, Y., O'Brien, T. P., Hamada, H., & Gridley, T. Krebs, L. T., Iwai, N., Nonaka, S., Welsh, I. C., Lan, Y., Jiang, R., Saijoh, Y., O'Brien, T. P., Hamada, H., & Gridley, T. (2003). Notch signaling regulates left-right asymmetry determination by inducing Nodal expression. Genes & development, 17(10), 1207–1212. https://doi.org/10.1101/gad.1084703. 2003.
106. Xu S LY, Meng Q, Wang B. Rab34 small GTPase is required for Hedgehog signaling and an early step of ciliary vesicle formation in mouse. *J Cell Sci* 2018; **131**(21).
107. Horne-Badovinac S, Lin, D., Waldron, S., Schwarz, M., Mbamalu, G., Pawson, T., Jan, Y., Stainier, D. Y., & Abdelilah-Seyfried, S. Positional cloning of heart and soul reveals multiple roles for PKC lambda in zebrafish organogenesis. *Current biology: CB* 2001; **11**(19).
108. Mah IK SR, Izuhara AK, Lakeland DL, Wang C, Mariani FV. Prkci is required for a non-autonomous signal that coordinates cell polarity during cavitation. *Dev Biol* 2016; **16**(1).
109. Huaux F, Liu, T., McGarry, B., et al. Dual Roles of IL-4 in Lung Injury and Fibrosis. Journal of Immunology. 2003:2083-92.
110. Xu N, Lao, Y., Zhang, Y., Gillespie, D.A. Akt: A Double-Edged Sword in Cell Proliferation and Genome Stability. Journal of Oncology. 2012.
111. Liu S LW, Obara T, Kuida S, Lehoczky J, Dewar K, Drummond IA, Beier DR. A defect in a novel Nek-family kinase causes cystic kidney disease in the mouse and in zebrafish. *Development* 2002; **129**(24): 5839-46.
112. Mahjoub MR TM, Quarmby LM. NIMA-related kinases defective in murine models of polycystic kidney diseases localize to primary cilia and centrosomes. *J Am Soc Nephrol* 2005; **16**(12): 3485-9.
113. Köhler G MC. Continuous cultures of fused cells secreting antibody of predefined specificity. *Nature* 1975; **256**(5517): 495-7.
114. Manning DK SM, van Heesbeen RG, Wong MD, Oh JH, Liu Y, Henkelman RM, Drummond I, Shah JV, Beier DR. Loss of the ciliary kinase Nek8 causes left-right asymmetry defects. 2013; **24**(1).
115. Romashkova JA MSN. NF-kappaB is a target of AKT in anti-apoptotic PDGF signalling. *Nature* 1999; **401**(6748).
116. Chen Y GN, Goodman RH, Smolik SM. Protein kinase A directly regulates the activity and proteolysis of cubitus interruptus. Proc Natl Acad Sci U S A. 1998:2349-54.

117. Tuson M, He, M., Anderson, K.V. Protein kinase A acts at the basal body of the primary cilium to prevent Gli2 activation and ventralization of the mouse neural tube. Development for advances in developmental biology and stem cells. 2011:4921-30.
118. Nanni L MJ, Bocian M, Steinhaus K, Bianchi DW, Die-Smulders C, Giannotti A, Imaizumi K, Jones KL, Campo MD, Martin RA, Meinecke P, Pierpont ME, Robin NH, Young ID, Roessler E, Muenke M. The mutational spectrum of the sonic hedgehog gene in holoprosencaphaly: SHH mutations cause a significant proportion of autosomal dominant holoprosencephaly. Hum Mol Genet. 1999:2479-88.
119. Varjosalo M TJ. Hedgehog: functions and mechanisms. Genes Dev. 2008:2454-72.
120. Edeling M, Ragi, G., Huang, S., et al. Developmental signalling pathways in renal fibrosis: the roles of Notch, Wnt and Hedgehog. Nature Reviews Nephrology. 2016:426-39.
121. Silva LM, Jacobs, D.T., Allard, B.A., et al. Inhibition of Hedgehog Signaling Suppresses Proliferation and Microcyst Formation of Human Autosomal Dominant Polycystic Kidney Disease Cells. Scientific Reports. 2018.
122. McNabb DS RR, Marciniak RA. Dual luciferase assay system for rapid assessment of gene expression in Saccharomyces cerevisiae. *Eukaryot Cell* 2005; **4**(9): 1539-49.
123. Das S NK, Peters WN, Periyasamy R, Pandey KN. Depletion of cyclic-GMP levels and inhibition of cGMP-dependent protein kinase activate p21Cip1 /p27Kip1 pathways and lead to renal fibrosis and dysfunction. *FASEB J* 2020; **34**(9): 11925-43.
124. Schaefer E, Zaloszyc, A., Lauer, J., et al. Mutations in SDCCAG8/NPHP10 Cause Bardet-Biedl Syndrome and Are Associated With Penetrant Renal Disease and Absent Polydactyly. Molecular Syndromology. 2011 September:273-81.
125. Yang G, James, D.E. A Positive Feedback Loop between Akt and mTORC2 via SIN1 Phosphorylation. Cell Reports. 2015:937-43.
126. Conduit SE, Davies, E.M., Ooms, L.M, et al. AKT signaling promotes DNA damage accumulation and proliferation in polycystic kidney disease. Human Molecular Genetics. 2020:31-48.
127. Jackson PK. Nek8 Couples Renal Ciliopathies to DNA Damage and Checkpoint Control. Molecular Cell. 2013:407-8.
128. Li J, Lu, D., Liu, H., et al. Sclt1 deficiency causes cystic kidney by activating ERK and STAT3 signaling. Human Molecular Genetics. 2017:2949-60.
129. Yamaguchi T NS, Wallace DP, Belibi FA, Cowley BD, Pelling JC, Grantham JJ. Cyclic AMP activates B-Raf and ERK in cyst epithelial cells from autosomal-dominant polycystic kidneys. Kidney Int. 2003:1983-94.
130. Wang S, Wei, Q., Dong, G., Dong, Z. ERK-mediated Suppression of Cilia in Cisplatin-Induced Tubular Cell Apoptosis and Acute Kidney Injury. Biochimica et Biophysica Acta (BBA). 2013:1582-90.
131. Parnell SC MB, Maser RL, Zien CA, Frischauf AM, Calvet JP. Polycystin-1 activation of c-Jun N-terminal kinase and AP-1 is mediated by heterotrimeric G proteins. *J Biol Chem* 2002; **277**(22): 19566-72.
132. Pearson G, Robinson, F., Gibson, T.B. Mitogen-Activated Protein (MAP) Kinase Pathways: Regulation and Physiological Functions. Endocrine Reviews. 2001:153-83.
133. Yu W, Kong, T., Beaudrey, S. et al. Polycystin-1 Protein Level Determines Activity of the Gα12/JNK Apoptosis Pathway. Journal of Biological Chemistry. 2010:10243-51.
134. Krebs LT, Iwai N, Nonaka S, et al. Notch signaling regulates left-right asymmetry determination by inducing Nodal expression. *Genes Dev* 2003; **17**(10): 1207-12.
135. Taulman PD HC, Balkovetz DF, Yoder BK. Polaris, a protein involved in left-right axis patterning, localizes to basal bodies and cilia. *Mol Biol Cell* 2001; **3**(12): 589-99.
136. Stuck MW, Chong, W. M., Liao, J. C., & Pazour, G. J. Rab34 is necessary for early stages of intracellular ciliogenesis. *Current biology: CB* 2021; **31**(13).
137. Durgan J KN, Jin D, Hall A. Par6B and atypical PKC regulate mitotic spindle orientation during epithelial morphogenesis. *J Biol Chem* 2011; **286**(14).
138. Munson C, Huisken, J., Bit-Avragim, N., Kuo, T., Dong, P. D., Ober, E. A., Verkade, H., Abdelilah-Seyfried, S., & Stainier, D. Y. Regulation of neurocoel morphogenesis by Pard6 gamma b. *Developmental biology* 2008; **324**(1).

139. S I. Increased apoptosis and proliferative capacity are early events in cyst formation in autosomal-dominant, polycystic kidney disease. *ScientificWorldJournal* 2007: 1757-67.
140. Zhang C BB, Ma M, Zhao J, Tian X, Kluger Y, Somlo S. Cyclin-Dependent Kinase 1 Activity Is a Driver of Cyst Growth in Polycystic Kidney Diseas. *J Am Soc Nephrol* 2021; **31**(1): 41-51.
141. Smith AO JJ, Preval KM, Davis RJ, Pazour GJ. c-Jun N-terminal kinase (JNK) signaling contributes to cystic burden in polycystic kidney disease. *PLoS Genet* 2021; **17**(12).
142. Onuchic LF FL, Nagasawa Y, Hou X, Eggermann T, Ren Z, Bergmann C, Senderek J, Esquivel E, Zeltner R, Rudnik-Schöneborn S, Mrug M, Sweeney W, Avner ED, Zerres K, Guay-Woodford LM, Somlo S, Germino GG. PKHD1, the polycystic kidney and hepatic disease 1 gene, encodes a novel large protein containing multiple immunoglobulin-like plexin-transcription-factor domains and parallel beta-helix 1 repeats. *Am J Hum Genet* 2002; **70**(5): 1305-17.
143. Atala A FM, Mandell J, Beier DR. Juvenile cystic kidneys (jck): a new mouse mutation which causes polycystic kidneys. *Kidney Int* 1993; **43**(5): 1081-5.
144. Hill NR, Fatoba, S.T., Oke, J.L., et al. Global Prevalence of Chronic Kidney Disease – A Systematic Review and Meta-Analysis. PLoS One. 2016.